AD-A137 019 A STUDY OF ANNULAR DIFFUSER FLOW USING A PHOTON-CORRELATING LASER DOPPLER..(U) AIR FORCE INST OF TECH WRIGHT-PATTERSON AFB OH SCHOOL OF ENGI.. 1/2

UNCLASSIFIED J M DIERKSEN DEC 83 AFIT/GAE/AA/83D-6 F/G 20/4 NL

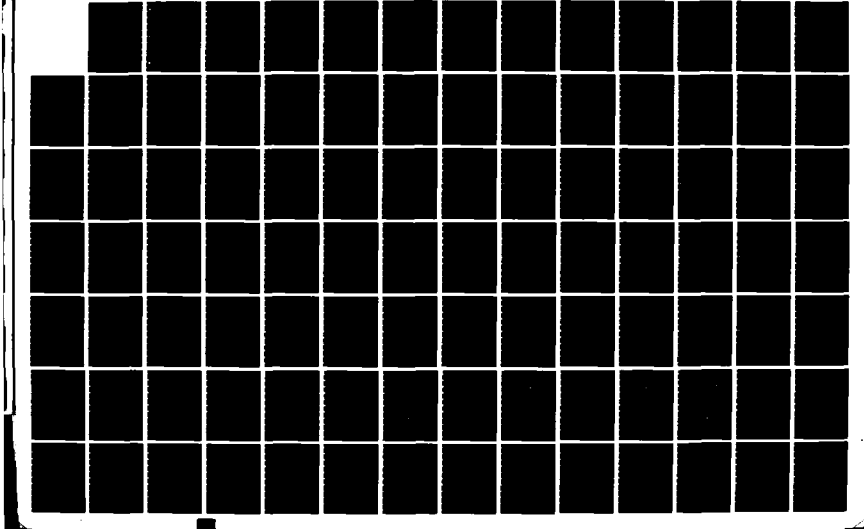

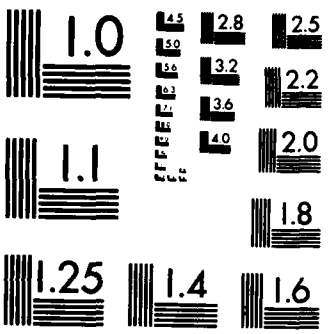


# A STUDY OF ANNULAR DIFFUSER FLOW USING A PHOTON-CORRELATING LASER DOPPLER ANEMOMETER

THESIS

Jeffrey M. Dierksen
Captain, USAF

AFIT/GAE/AA/83D-6



DEPARTMENT OF THE AIR FORCE
AIR UNIVERSITY
AIR FORCE INSTITUTE OF TECHNOLOGY

Wright-Patterson Air Force Base, Ohio

AFIT/GAE/AA/83D-6

# A STUDY OF ANNULAR DIFFUSER FLOW USING A PHOTON-CORRELATING LASER DOPPLER ANEMOMETER

THESIS

Jeffrey M. Dierksen
Captain, USAF

AFIT/GAE/AA/83D-6

AFIT/GAE/AA/83D-6

# A STUDY OF ANNULAR DIFFUSER FLOW

# USING

# A PHOTON-CORRELATING LASER DOPPLER ANEMOMETER

THESIS

Presented to the Faculty of the School of Engineering
of the Air Force Institute of Technology
Air University
In Partial Fulfillment of the
Requirements for the Degree of
Master of Science in Aeronautical Engineering

Jeffrey M. Dierksen, B.S.
Captain, USAF



December 1983

## Acknowledgements

My study of annular diffuser flow has been a challenging one. Over the past year, a number of people have made important contributions to my project for which they will always have my deepest appreciation. Dr. William C. Elrod, my thesis advisor, was an immense help in this study and the most important contributor to my educational endeavors at AFIT. I also wish to thank the other members of my thesis committee, Major Michael Wallace and Captain Wesley Cox, for their assistance. The people at the AFIT Fabrication Shop were indispensible. The hardware they made for me worked beautifully and was an invaluable aid in my research. I especially wish to thank Carl Shortt, Dave Paine, Ron Ruley, John Brohas, and Jack Tiffany. I also extend my thanks to the AFIT Aero Lab technicians: Nick Yardich, Leroy Cannon, Steve Coates, and Harley Linville. Always willing to help, their assistance made the project run smoothly. I thank Mr. Joe Ferguson of the Air Force Aero Propulsion Laboratory, who helped me obtain the cable to connect the laser anemometer and mini-computer. While it may seem like a small contribution, its benefits were enormous.

There were a number of ups and downs during the course of my studies at AFIT. My wife, Kate, deserves all my love for her understanding and help through the rough times. I couldn't have made it without her.

Jeffrey M. Dierksen

## Table of Contents

## List of Figures

## List of Symbols

| | | |
|---|---|---|
| A | area | ($m^2$) |
| ADRF | Annular Diffuser Research Facility | |
| AFIT | Air Foce Institute of Technology | |
| D | laser beam separation | (mm) |
| d | pipe diameter | (cm) |
| $d_a$ | aperture diameter | (μm) |
| $d_f$ | fringe spacing | (μm) |
| $d_m$ | measuring volume diameter | (μm) |
| $d_m'$ | effective measuring volume height | (μm) |
| $d_m''$ | effective measuring volume width | (μm) |
| F | scattered light frequency | (Hz) |
| ΔF | phase modulator frequency shift | (Hz) |
| f | focusing lens focal length | (mm) |
| f' | collecting lens focal length | (mm) |
| $G^{(2)}(\tau)$ | intensity autocorrelation function | |
| $g_1$ | value of the correlation function at the first valley | |
| $g_2$ | value of the correlation function at the second peak | |
| $g_3$ | value of the correlation function at the second valley | |
| HP | Hewlett-Packard | |
| I(t) | intensity function | |
| IGV | inlet guide vane | |
| $\bar{K}_0$ | vector sum of two incident light vectors | |
| $\bar{k}_0$, $\bar{k}_{01}$, $\bar{k}_{02}$ | incident light vector | |
| $\bar{k}_s$ | scattered light vector | |
| L | pipe length | (m) |
| LDA | Laser Doppler Anemometer | |
| LDV | Laser Doppler Velocimeter | |
| $l_i$ | inlet length | (m) |
| $l_m$ | measuring volume length | (μm) |

| | | |
|---|---|---|
| $l_m'$ | effective measuring volume length | (μm) |
| $\dot{m}$ | mass flow rate | (Kg/sec) |
| N | number of fringes in the measuring volume | |
| n | number of velocity samples | |
| Pk2 | channel number of the peak after the first valley of the correlation function | |
| p | lens reference plane-to-image distance | (mm) |
| PM | photomultiplier | |
| $\Delta p$ | static pressure change | ($N/m^2$) |
| q | lens reference plane-to-source distance | (mm) |
| $\bar{q}$ | average dynamic pressure | ($N/m^2$) |
| R | correlation function damping ratio | |
| Re | Reynolds number | |
| RMS | root-mean-square | |
| $r_h$ | hydraulic radius | (m) |
| $r_o$ | unfocused laser beam radius | (mm) |
| T | experiment or correlation time | (sec) |
| t | time | (sec) |
| $t_s$ | correlator sample time | (nsec) |
| $U_\infty$ | free-stream velocity | (m/sec) |
| u | average velocity component perpendicular to the measuring volume fringes | (m/sec) |
| $u_i$ | instantaneous velocity component perpendicular to the measuring volume fringes | (m/sec) |
| $u^*$ | average velocity relative to the measuring volume fringes | (m/sec) |
| $u_i^*$ | instantaneous velocity relative to the measuring volume fringes | (m/sec) |
| V | velocity | (m/sec) |
| $\bar{V}$ | velocity vector | |
| x | linear distance | (m) |
| α | angle between the optical and collecting axes | (deg) |

| | | |
|---|---|---|
| $\beta$ | angle between the parallel laser beam plane and the collecting axis | (deg) |
| $\delta$ | boundary layer thickness | (mm) |
| $\eta$ | turbulence intensity | |
| $\eta^*$ | turbulence intensity relative to the measuring volume fringes | |
| $\theta$ | included angle between the incident laser beams or light vectors | (deg) |
| $\lambda$ | laser light wavelength | (Angstroms) |
| $\mu$ | absolute viscosity | ($N\text{-}sec/m^2$) |
| $\mu_b$ | refractive index | |
| $\nu$ | kinematic viscosity | ($m^2/sec$) |
| $\Delta\nu$ | Doppler frequency shift | (Hz) |
| $\rho$ | density | ($Kg/m^3$) |
| $\tau$ | correlator delay time | (nsec) |

## Abstract

An experimental investigation of air flow in an annular inlet and diffuser was conducted using a photon-correlating Laser Doppler Anemometer. The inlet has an inside wall radius of 22.9 ~~Centimeters~~ (9.0 in.) and a cross-sectional area of 0.0426 sq ~~meters~~ (0.4583 sq ft). The diffuser walls have a divergence half-angle of seven ~~degrees~~. Flow rates in the vicinity of 0.25 kg/sec (0.55 ~~lbm~~/sec) were studied. The Reynolds number in the annular inlet was 18300. The flow in the annulus was turbulent and ~~the~~ boundary layer growth was approximately 20% less than that predicted using flat plate boundary layer assumptions. The laser anemometer measurements are compared to hot film anemometer measurements. Good comparison was obtained except in the annular inlet. The difference is probably due to the differing boundary layer growth rates between the laser and hot film anemometer tests since they were conducted with different mass flow rates. The photon-correlating Laser Doppler Anemometer is evaluated in this application. The flexibility of a laser anemometer system in measuring ~~three~~-dimensional, internal flows is determined by two factors: the system's frequency shifting capability and the geometry of its optics. Reflected background light is inherent in measuring internal flows. Without a means of reducing the signal caused by this light, long measurement times are necessary for each data point.

# A STUDY OF ANNULAR DIFFUSER FLOW
# USING
# A PHOTON-CORRELATING LASER DOPPLER ANEMOMETER

## I. Introduction

Turbine engine designers are constantly striving to achieve more efficient engines. To realize higher performance, improvements must be made in the engine components themselves. One of these components is the pre-diffuser between the compressor and combustor. It accomplishes the important task of diffusing high velocity discharge air from the compressor to low velocities suitable for the combustor. Additionally, the diffusion must occur in as short a length as possible.

A great deal of information is available on the performance of two-dimensional diffusers. While this has some application to three-dimensional geometries, little experimental data on annular diffusers can be found. This research project is intended to increase the base of experimental knowledge of annular diffusers, particularly with regard to velocity profiles and turbulence intensity.

### Background

The initial studies in this project were done by Kelley (reference 1) in 1981. An annular flow handling apparatus was designed and pitot and hot wire anemometer probes used to investigate the diffuser flow. The initial data revealed irregular flow

in the test sections. The research was continued in 1982 by Moore (reference 2), who modified the flow handling apparatus and incorporated a Laser Doppler Velocimeter (LDV) as the primary instrumentation system. The modified flow handling apparatus became part of the Annular Diffuser Research Facility (ADRF). Preliminary data was collected; however, it only consisted of velocity measurements because of the limited data acquisition capability of the LDV system. Turbulence intensity data could not be obtained.

## Objectives

The following are the objectives of the third phase of this study:

(1) Obtain velocity and turbulence intensity profiles in the annular inlet and diffuser of the ADRF flow handling apparatus using a photon-correlating Laser Doppler Anemometer.

(2) Evaluate the capabilities of the photon-correlating Laser Doppler Anemometer to measure internal fluid flows in similar applications.

## Overview

The remainder of the report discusses this phase of the research effort. The topics include:

(1) Internal fluid dynamics, boundary layer theory and the principles of the photon-correlating Laser Doppler Anemometer.

(2) A description of the experimental apparatus and instrumentation.

(3) The procedures used to collect the data and reduce it.

(4) The results of the study.

(5) The conclusions drawn and recommendations for further research.

## II. Theory

Boundary layer theory and internal fluid dynamics relevant to the annular diffuser will be discussed. Since the Laser Doppler Anemometer (LDA) was a significant element in this research effort, a discussion of its principles of operation is also included.

### Internal Fluid Dynamics and Boundary Layer Growth

The flow in a pipe may be laminar or turbulent depending on the Reynolds number and wall roughness. The Reynolds number for a pipe is defined by Eq (1)

$$Re_{pipe} = \frac{4r_h \rho V}{\mu} \tag{1}$$

where $\mu$ is the absolute viscosity of the fluid, $\rho$ is the fluid density, V is the velocity and $r_h$ is the hydraulic radius (3:63). The hydraulic radius is defined by Eq (2)

$$r_h = \frac{A_c L}{A_w} \tag{2}$$

where $A_c$ is the cross-sectional area of the pipe, L is the pipe length, and $A_w$ is the total wetted area (3:64). The critical Reynolds number for the transition from laminar to turbulent flow for a pipe with a sharp-edged entrance is approximately 2300; however, the critical Reynolds number may exceed 10,000 for a system which is exceptionally free from disturbances (4:39). It is also a fact that at Reynolds numbers below 2000, flow in a

pipe will remain laminar even in the presence of strong disturbances (4:451).

Boundary layer growth in a pipe begins at the entrance. This is also true of an annulus. While this boundary layer may be laminar even though the flow outside of it is turbulent, roughness on the walls and turbulence in the flow outside of the boundary layer would hasten the transition from laminar to turbulent. To approximate the growth of a boundary layer on the wall of an annulus, one may use the results of boundary layer growth on a flat plate in a uniform flow. The thickness of a laminar boundary layer on a flat plate is given by Eq (3)

$$\delta = 5 \left(\frac{\nu x}{U_\infty}\right)^{0.5} \tag{3}$$

where x is the distance from the leading edge of the plate, $U_\infty$ is the free stream velocity and $\nu$ is the kinematic viscosity (4:140). On the other hand, the thickness of a turbulent boundary layer on a flat plate is determined by Eq (4) (4:638).

$$\delta = 0.37x \left(\frac{U_\infty x}{\nu}\right)^{-0.2} \tag{4}$$

While the flat plate approximation is very useful for estimating the boundary layer growth in an annulus, the three-dimensional nature of the flow channel will also affect boundary layer growth. The boundary layer on the inner wall will be thinner than on the outer wall because the shear work from the inner wall to the flow is diffused over an increasing area as the distance from the wall increases. On the outer wall, the shear work is diffused over a

decreasing area (2:5). The smaller the ratio of inner wall to outer wall radius, the smaller the ratio of inner wall boundary layer thickness to outer wall thickness.

As the boundary layer in a pipe, or annulus, grows, it will eventually cover the entire flow channel. Even after this occurs, the velocity profile will continue to develop until it reaches a point downstream where there is no further change. The flow is then called "fully-developed" and the distance from the entrance of the pipe to this point is the inlet length. Experiments have been conducted to determine the inlet length of a circular pipe. For laminar flow, the inlet length is approximately

$$l_i = (0.03d)\, Re_{pipe} \qquad (5)$$

where d is the pipe diameter (4:596). For Reynolds numbers from 1500 to 2000, it ranges from 45 to 60 pipe diameters. The inlet length for turbulent flows is typically shorter than for laminar flows. Kirsten measured its length to be about 50 to 100 diameters while Nikuradse measured an inlet length of 25 to 40 diameters (4:596).

## Laser Velocimetry

Over the last two decades, several types of laser velocimeters and various methods of signal processing have been developed. One combination, and the system used for this research, is a Laser Doppler Anemometer (LDA) using a photon-correlating signal processor. It is this particular system which will be discussed here.

The Laser Doppler Anemometer (LDA) is based on the principle of the Doppler shift of light scattered by a moving particle. If the velocity of a moving particle is represented by $\bar{V}$, the incident light beam by $\bar{k}_o$, and the scattered light beam by $\bar{k}_s$ where $|\bar{k}_s| = |\bar{k}_o| = 2\pi/\lambda$($\lambda$ is the wavelength of the incident light), then the Doppler shift of the scattered light is given by Eq (6) (5:249).

$$\Delta\nu = (\bar{k}_s - \bar{k}_o) \cdot \bar{V} \tag{6}$$

Thus, measuring the frequency of the scattered light indirectly determines the velocity of the particle which caused the scattering. However, it is impractical, in most situations, to measure the Doppler shifts inherent in low speed flows. This problem can be avoided by using two incident light beams, $\bar{k}_{01}$ and $\bar{k}_{02}$, of the same wavelength (5:250). Now, the Doppler shifts of light, from each beam, scattered by the moving particle are

$$\Delta\nu_1 = (\bar{k}_s - \bar{k}_{01}) \cdot \bar{V} \tag{7}$$

$$\text{and } \Delta\nu_2 = (\bar{k}_s - \bar{k}_{02}) \cdot \bar{V} \tag{8}$$

When the scattered light is detected, the Doppler shift will be

$$\Delta\nu_1 - \Delta\nu_2 = (\bar{k}_{02} - \bar{k}_{01}) \cdot \bar{V} = \bar{K}_o \cdot \bar{V} \tag{9}$$

where the geometry is shown in Figure 1 (5:249). This is known as the Doppler Difference Effect. Eq (9) can be written

$$\Delta\nu_1 - \Delta\nu_2 = \frac{4\pi u}{\lambda} \sin\left(\frac{\theta}{2}\right) \tag{10}$$

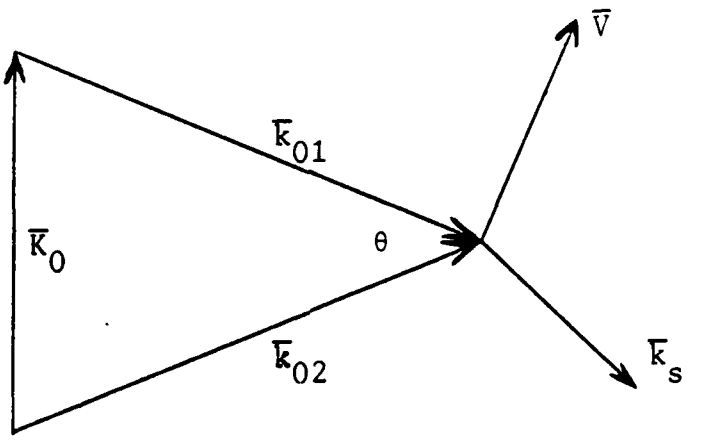


FIG. 1. DOPPLER DIFFERENCE EFFECT

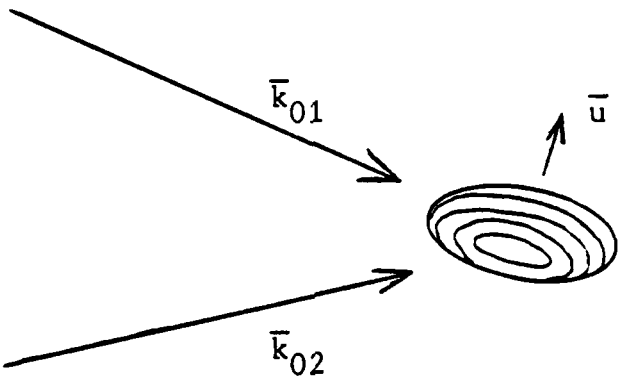


FIG. 2. MEASURING VOLUME FRINGES

where u is the component of $\overline{V}$ in the direction of $\overline{K}_o$. A significant aspect of Eq (10) and the Doppler Difference Effect is that the Doppler-shifted frequency is independent of the scattering direction. So regardless of where the scattered light is detected, the result is the same.

While the theory of the Doppler Difference Effect from the classical physics standpoint is important in understanding the LDA, the theory can also be explained using a model commonly referred to as the "fringe model". Even though it is not technically appropriate in all respects, it does yield identical velocity and turbulence intensity results.

In the Doppler difference laser anemometer, the incident laser beams cross at some point in space. The intersection of the two, finite-size beams forms an ellipsoidal volume termed the measuring volume, the region in which the fluid flow is measured. With the fringe model, the intersection of the monochromatic, coherent laser beams forms a classical interference pattern of bright and dark, planar fringes in the measuring volume. These fringe planes are perpendicular to the plane formed by the two incident beams as depicted in Figure 2. The distance between like fringes can be calculated using Eq (11) (6:6-1).

$$d_f = \frac{\lambda}{2 \sin (\frac{\theta}{2})} \tag{11}$$

As a particle, moving with the fluid, passes through the measuring volume, it scatters a "burst" of light every time it moves through a bright fringe so the frequency of the light bursts is related to

the particle's velocity by Eq (12).

$$F = \frac{u}{d_f} \tag{12}$$

The frequency of light bursts from the interference pattern is identical to the Doppler-shifted frequency ($\Delta\nu_1 - \Delta\nu_2$) of photons scattered by the particle as it moves through the "classical" measuring volume (7:97). Hence, each light "burst" scattered by a particle in the fringe model is similar to a photon scattered in the classical sense. The fringe model is also useful in understanding the principles of the remaining LDA components.

Photon correlation was used in this study to analyze the scattered light from the measuring volume. The particles, moving with the fluid, will have an ordered motion which causes the scattered light to have an order about it. The scattered light intensity varies with time as the particles move through the fringes. By determining the time correlation of the intensity, the velocity and turbulence of the flow can be calculated.

The time correlation of the light is represented by the intensity autocorrelation function defined by Eq (13)

$$G^{(2)}(\tau) = \lim_{T\to\infty} \frac{1}{T} \int_0^T I(t)I(t+\tau)\, dt \tag{13}$$

where I is the light intensity, t is time, T is the time interval over which the intensity is monitored (experiment time), and $\tau$ is the correlator delay time (8:16). The autocorrelation function is determined as a function of $\tau$ after the intensity is determined

in the time domain. Light intensities of a random nature will result in a constant autocorrelation function as T approaches infinity. However, intensities of an ordered, periodic nature will result in a periodic autocorrelation function due to the multiplication of the intensity function and time-delayed intensity function. As a result, this method of signal processing can separate the signal of interest from large amounts of background noise. Additionally, the nature of the method makes photon correlation sensitive at low scattering particle densities (9:439).

## III. Apparatus and Instrumentation

This research included the integration of a photon-correlating LDA system to the Annular Diffuser Research Facility (ADRF) flow handling apparatus designed and fabricated by Kelley (reference 1) and Moore (reference 2). A Hewlett-Packard data acquisition system was used to control the LDA system and process the data. A hot-film anemometer was also used with the ADRF flow handling apparatus. The following is a discussion of this equipment.

### ADRF Flow Handling Apparatus

The ADRF Flow Handling Apparatus (Figure 3) consists of a stilling chamber, a particle seeder, an annular interface, an inlet guide vane section, an annular inlet test section, an annular diffuser test section, and a dump section. Air is supplied to the stilling chamber by two Worthington Corporation compressors through a 7.6 centimeter (3 in) diameter pipe. These compressors are capable of steadily supplying 0.36 kg/sec (0.80 lbm/sec) of air to the flow handling apparatus. As the air enters the stilling chamber, it passes through two paper filters held in place by an aluminum holder. This filter is a recent addition to the flow handling apparatus due to the contamination of the air supply by particulate matter. The contaminate mostly consists of rust particles from the inner surfaces of the pipes. The filter allows better control over the size and types of particles in the air

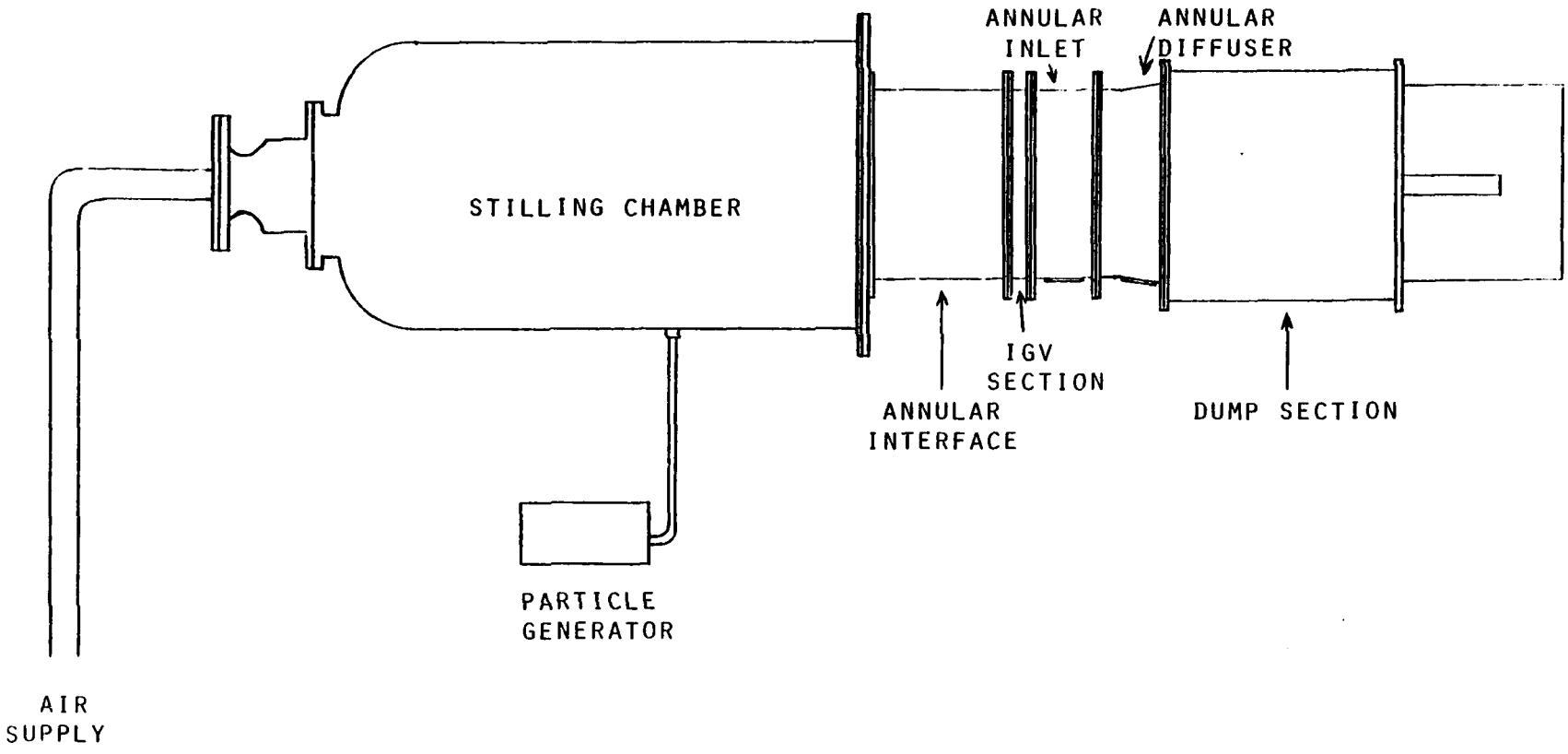


FIG. 3. ADRF FLOW HANDLING APPARATUS

flow since this is the basis for LDA measurements. The filter also prevents abrasion of the test section windows by the contaminates suspended in the flow.

The filtered air next enters a perforated cylinder which allows the air to exit radially through eighty-one, three millimeter (0.125 in) diameter holes while also reducing the pressure. The air is turned back to the axial direction and passed through four smoothing screens. After the screens, seed particles are introduced into the flow through two, six millimeter (0.25 in) diameter tubes supplied by a 9.5 millimeter (0.375 in) diameter tube which protrudes through the stilling chamber wall. A particle generator is connected to the supply tube which is contained inside a streamlined shroud to minimize flow disturbances. The particles are injected in the direction of the flow.

A TSI Model 9306 Six Jet Atomizer was used to provide a glycerin (propylene glycol) aerosol for flow seeding. The volume output of the atomizer can be varied by using from one to six of the available jets and by adjusting the input pressure of the unit. The particle concentration of the glycerin aerosol is constant at $2(10^8)$ particles per liter. The sizes of the particles vary from 0.5 to 4.0 μm (.00002 to .00016 in).

The seeded air is accelerated in an annular nozzle contained within the stilling chamber. The nozzle leads to a constant area annular interface (see Figure 3). The inner and outer radii of the annulus are nominally 22.9 centimeters (9.0 in) and 25.4 centimeters (10.0 in) respectively. At the end of the annular inter-

face is a row of sixty-six equally spaced inlet guide vanes (IGV) mounted radially between the inner and outer walls of the annulus. The IGVs are NACA 0012 airfoils with a chord of 19.1 millimeters (0.75 in) giving them an aspect ratio of 1.33.

The annular inlet test section which follows the inlet guide vanes allows flow studies in a constant area annulus (see Figure 4). Optical access for flow measurements is gained through a glass window. It measures 102 millimeters (4.0 in) in the axial direction and 19.1 millimeters (0.75 in) in the circumferential direction. The inner wall of the annulus is a wooden centerbody which is painted flat black. On the portion of the centerbody opposite the outer access window, another optical glass window is installed. It measures 8.0 millimeters (0.32 in) in the circumferential direction and 105 millimeters (4.1 in) in the axial direction. This window, as well as a similar one in the annular diffuser test section, allows the laser beams to pass through the inner wall of the annulus to the inside of the centerbody. This greatly reduces the amount of laser light reflected from the wall. LDA measurements can then be made at points closer to the wall than would be possible against the centerbody's black surface. More about the effects of the centerbody windows will be discussed in a later section.

The annular diffuser test section follows the annular inlet (see Figure 4). The flow from the inlet is diffused in this 10.2 centimeter (4.0 in) long section by walls which are set at a nominal diffusion half-angle of seven degrees. Like the inlet test

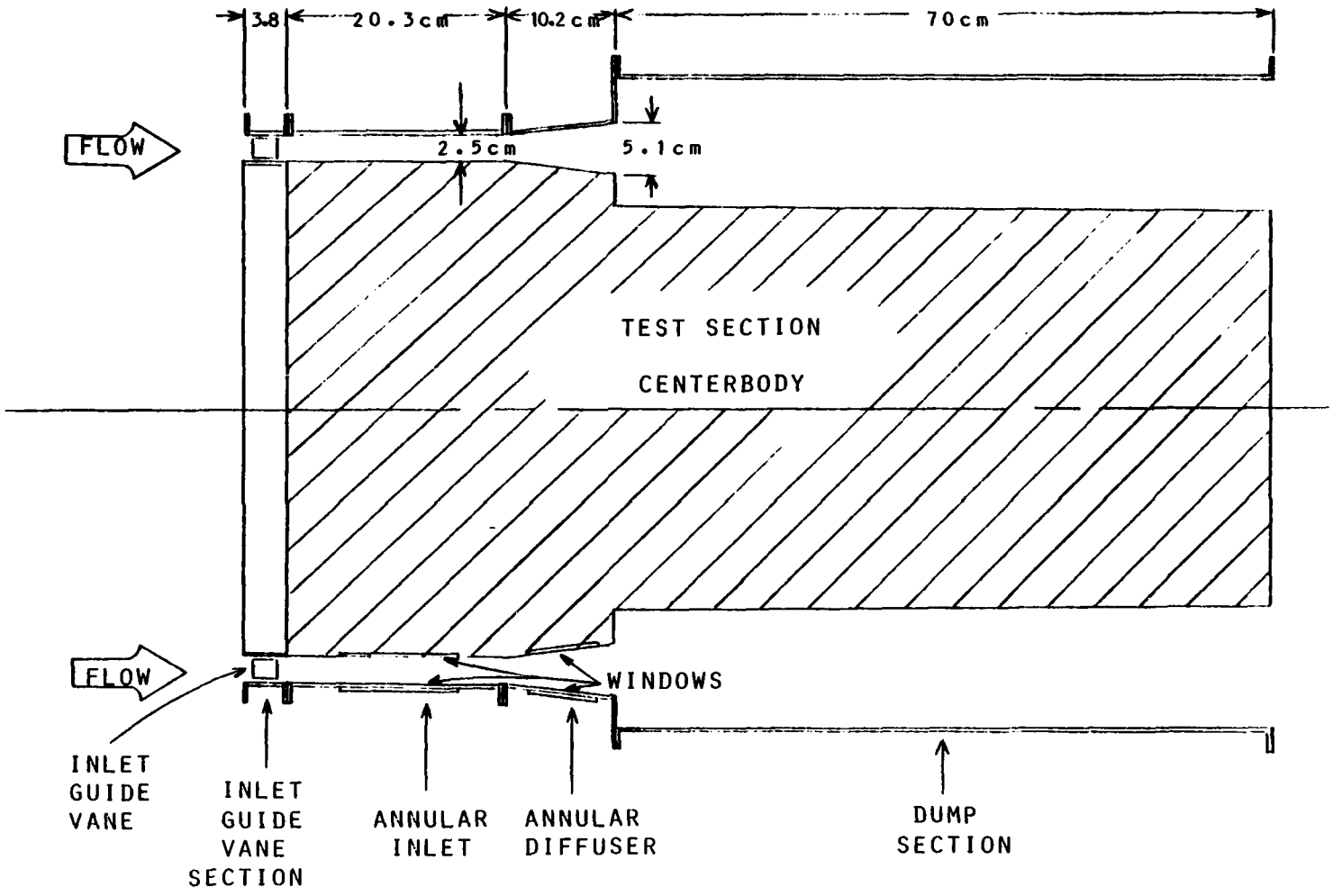


FIG. 4. ANNULAR TEST SECTIONS

section, optical access to the diffuser is gained through a glass window. This window measures 76 millimeters (3.0 in) axially by 19.1 millimeters (0.75 in) circumferentially. Another window which measures 8.0 millimeters (0.32 in) circumferentially and 76 millimeters (3.0 in) axially is installed in the test section centerbody to accomplish the same purpose as the centerbody window in the inlet test section.

The flow enters an annular dump section after exiting the diffuser. This section is designed to minimize laboratory effects on the flow in the test sections. More detailed information on any section of the ADRF Flow Handling Apparatus may be found in references 1 and 2.

## Instrumentation

Two systems, a Laser Doppler Anemometer and a hot-film anemometer, were used to make flow measurements in the test sections. The LDA system is supported by a mini-computer (primarily used for data acquisition and reduction), an oscilliscope, and a universal counter. The hot-film anemometer system is supported by a micro-computer, an analog-to-digital converter and a root-mean-square (RMS) voltmeter. Both anemometer systems are supported by a square-edged orifice plate and mercury manometer flow measuring system. A static pressure probe was used to make pressure measurements in the inlet and diffuser.

Laser Doppler Anemometer. The LDA system consists of four major components:

1) A helium-neon laser.

2) Transmitting optics.

3) Collecting optics.

4) A photon-correlating signal processor.

Laser. The first component is a Spectra Physics Model 124A fifteen milliwatt, helium-neon laser which emits a single, monochromatic beam of 6328 Angstroms wavelength. The beam has a $1/e^2$ radius of 0.55 mm (0.022 in) and a divergence angle of 1.0 milliradians. The laser is powered by a Spectra Physics Model 255 power supply which operates on 115 volt, single-phase current.

Transmitting Optics. The first element of the transmitting optics is a Malvern Instruments, Ltd. Type RF307 beamsplitter which is attached directly to the laser exit. Through a combination of partially and totally reflective mirrors, the beamsplitter divides the single beam into two, equal-intensity beams. It can be adjusted to alter the divergence or convergence angle between the two beams and their separation.

The two laser beams are directed into a Malvern Type K9023 phase modulator. The unit is designed to accept parallel beams with a separation of twenty millimeters (0.79 in). The beams pass through a pair of crystals which, when excited, modulate the phase of the beams through the Pöckels electro-optic effect, changing the frequency of one beam relative to the other (10:L36). The result is a change in the Doppler-shifted frequency of light scattered by particles moving through the measuring volume. In terms

of the fringe model, phase modulation imparts a uniform translation to the fringes in a direction perpendicular to the fringe planes. The phase modulator crystals are excited by a separate drive unit which uses a sawtooth waveform for the driving function. The drive unit can be set to shift the Doppler frequency by fixed amounts of 20, 50, 100, 200, 500, or 1,000 KHz, or continuously between 50 KHz and 1 MHz. The "fringe velocity" imparted by the phase modulator can be determined by using Eq (12) and replacing F with $\Delta F$, the phase modulator frequency shift. The result is Eq (14).

$$\text{Fringe Velocity} = \Delta F \times d_f \qquad (14)$$

The sense of the fringe motion can be changed by the DRIVE/INVERT switch on the drive unit, thus increasing or decreasing the Doppler-shifted frequency by the set amount. The output of the drive unit was monitored with a Hewlett-Packard (HP) 5325B Universal Counter.

The use of a phase modulator in a LDA system increases its flexibility. Frequency shifting is used to aid in determining the direction of flow, making measurements in highly turbulent or high speed flows, and in increasing the velocity resolution of the system. Velocity resolution will be discussed later.

The laser/beamsplitter and phase modulator are mounted on a 12.7 centimeter (5.0 in) wide steel channel which allows these units to be used as a single assembly. Once they are aligned with respect to each other on the channel, the entire assembly

can be moved to align the laser beams with the remaining optics.

The two laser beams which exit the phase modulator are directed by two, front-silvered plane mirrors through a periscope to a lens which focuses and crosses the beams to form the measuring volume (see Figure 5). The fringe spacing can be determined using Eq (11) and the focusing geometry. When parallel beams are transmitted through the focusing lens in the configuration shown in Figure 6, Eq (15) can be used to calculate the fringe spacing.

$$d_f = \frac{f\lambda}{D\mu_0} \tag{15}$$

In the above equation, f is the focal length of the focusing lens, D is the parallel beam separation, and $\mu_0$ is the refractive index of the medium where the measuring volume is located ($\mu_0$ = 1.0 for air) (6:6-2). In all of the tests conducted with the LDA system, a 250 mm focal length focusing lens and 20 mm beam separation were used. The resulting fringe spacing is 7.91 μm (0.00031 in).

Collecting Optics. The velocity and turbulence intensity of the flow are measured by analyzing the frequency content of the light scattered from the measuring volume. This is done by converting the light, through the photomultiplier effect, into an electrical signal to be analyzed by a signal processor. In using the fringe model, each light "burst" (instead of a photon in the classical sense) absorbed by the photosensitive material causes the emission of an electron or electrons which comprise the electrical signal.

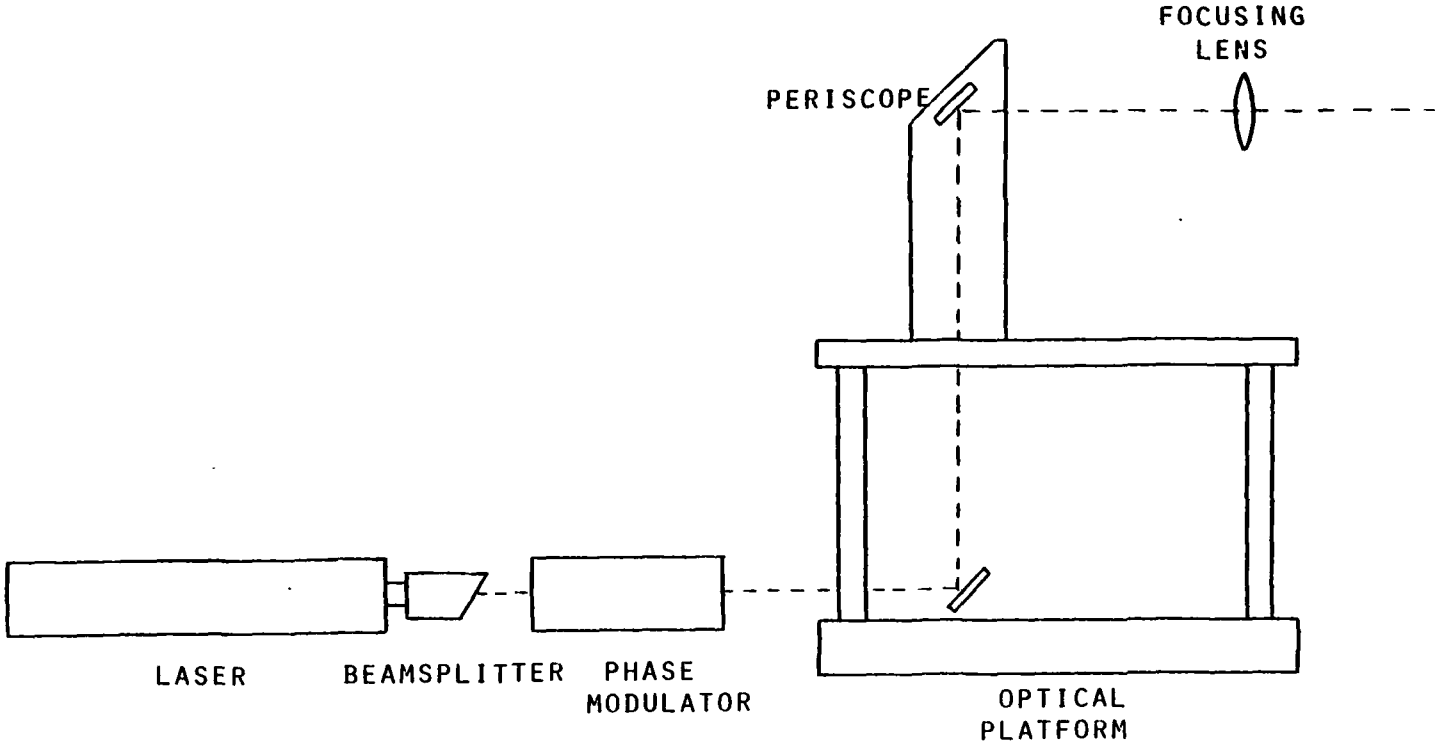


FIG. 5. TRANSMITTING OPTICS CONFIGURATION

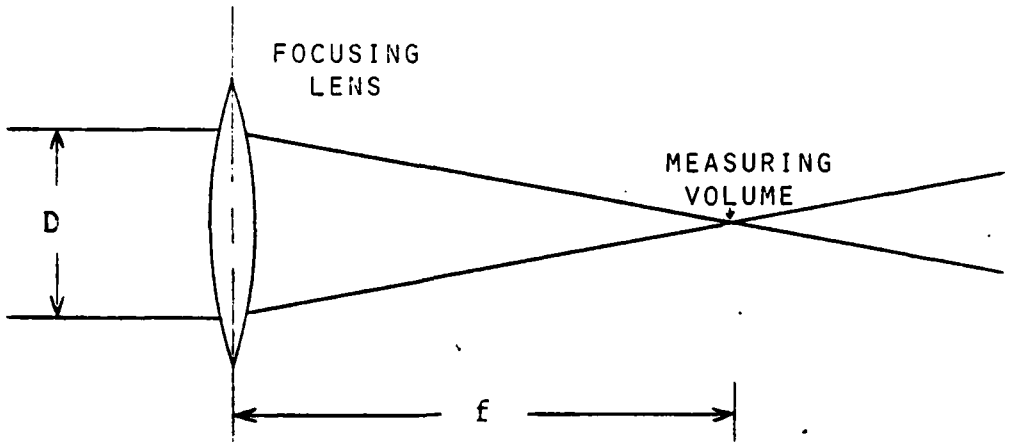


FIG. 6. FOCUSING GEOMETRY

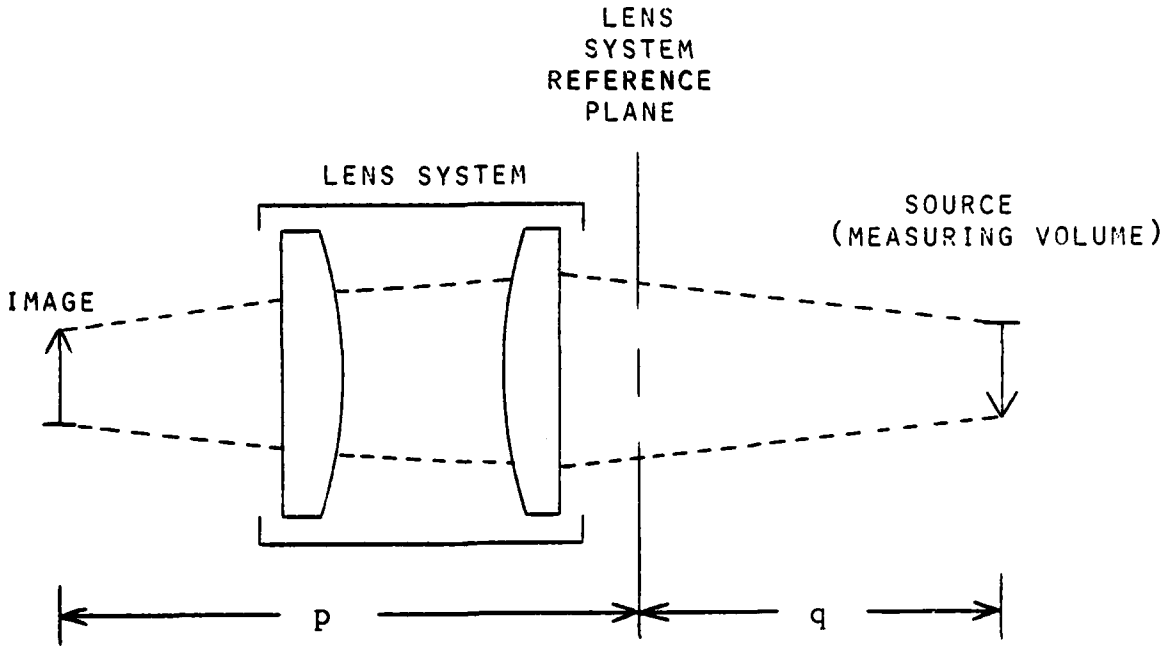


FIG. 7. LENS EQUATION DIMENSIONS

The collecting optics consist of a Tamron 105 mm telephoto lens and a Malvern Type RF313 photomultiplier (PM) assembly using an EMI 9863 KB/100 type photomultiplier tube. The laser light collected by the telephoto lens is focused on a 100 μm (0.00394 in) aperture just before the light enters the photon detection portion of the PM assembly. A 2.5, 6.5, or 9.0 cm spacer may be placed between the PM assembly and telephoto lens to allow light gathering at various distances from the measuring volume. The lens equation, Eq (16), governs the distance from the measuring volume at which the collecting optics must be set to focus the scattered light on the aperture.

$$\frac{1}{f'} = \frac{1}{p} + \frac{1}{q} \tag{16}$$

In the lens equation, f' is the focal length of the collecting lens, p is the distance from the lens system reference plane to the image on the aperture, and q is the distance from the reference plane to the measuring volume (see Figure 7).

The PM assembly was set to collect the scattered light, in backscatter, at an angle of 16.9 degrees off the optical axis defined by the bisector of the crossed laser beams. While the transmitting optics determine the actual measuring volume size (to the $1/e^2$ contour), the collecting optics geometry and aperture size determine the effective measuring volume size since the PM tube may only receive light from a portion of the actual measuring volume. Appendix A contains the actual and effective measuring volume sizes as well as the method used to determine them.

The periscope, focusing lens, and PM assembly are mounted on an optical platform which can be raised or lowered (see Figure 8). This platform can also be translated along an axis perpendicular to the test section centerbody axis. The optical platform was originally designed and used by Walterick (reference 11). With proper optical alignment, the two axis system allows the measuring volume to be positioned in the test section and traverse the annulus in the radial direction. A vernier scale is attached to the translating base to determine the measuring volume's radial position to within 0.25 mm (0.01 in). The laser and optics are mounted on a laboratory bench which rests on rollers guided by two parallel rails. A chain-and-sprocket drive system, attached to the rails and bench, turns two 3/4 x 10 threaded rods which move the bench along the rails. A mechanical counter is connected to a gear on one of the drive rods. Through the gear ratio in the counter itself, angular displacement of the drive rods is displayed to within 0.1 revolutions. Thus, the measuring volume can be moved in the axial direction and its position determined to within 0.25 mm (0.01 in).

Signal Processor. The heart of the LDA system is the Malvern Type K7023 digital correlator which analyzes the signal from the PM assembly. The correlator monitors the signal for a predetermined sample time ($t_s$), which can be set from 50 nsec to 0.995 sec, and counts the number of pulses caused by light "bursts" (fringe model) or photon detections (classical). This results in a digitized version of the intensity function I(t) discussed in

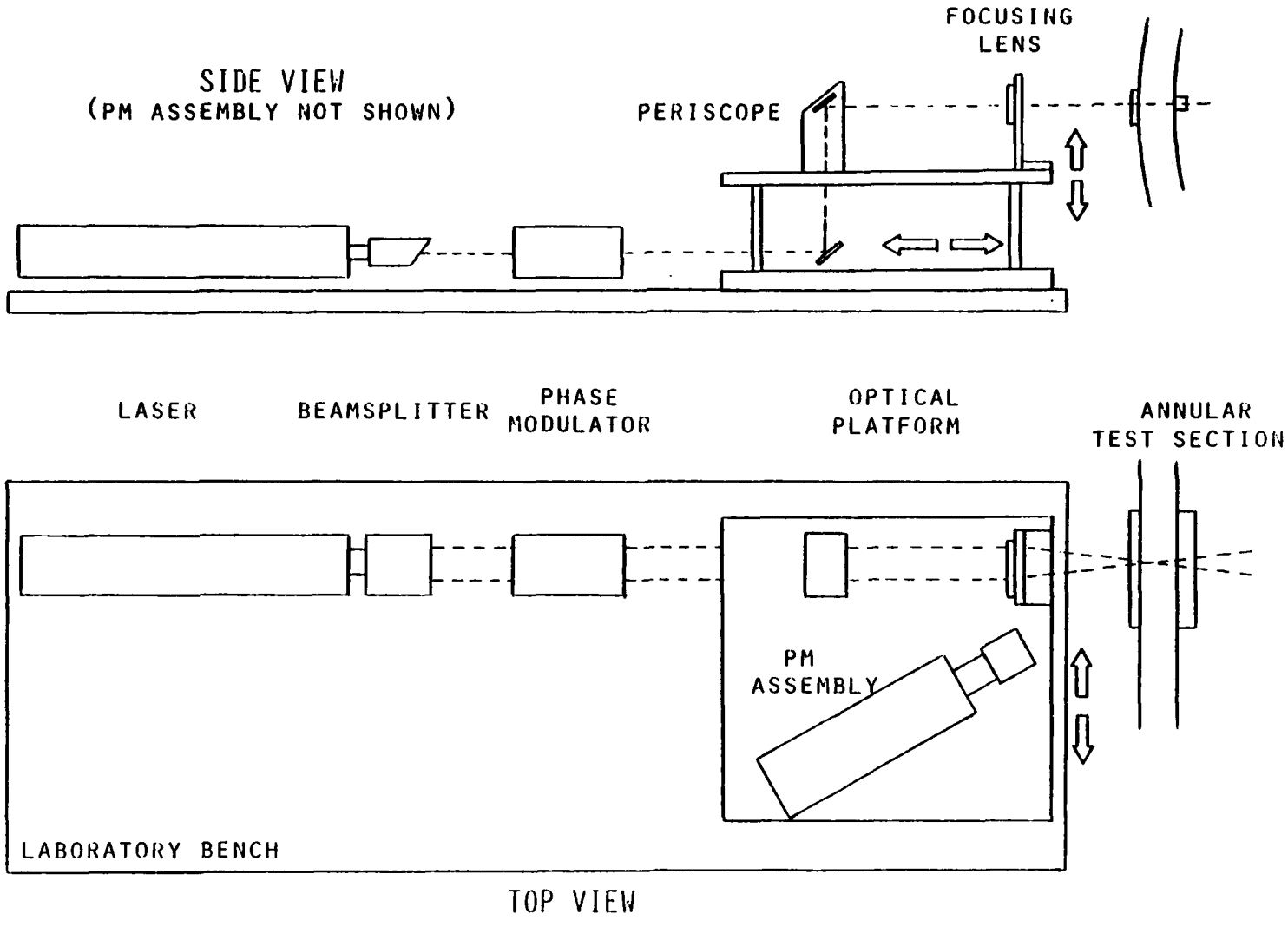


FIG. 8. LASER AND OPTICS CONFIGURATION

Laser Velocimetry Theory. Electronically, the correlator also takes the function $I(t + \tau)$, where $\tau$ varies from zero to 95 times $t_s$ in integer increments, to develop the intensity autocorrelation function. The experiment time (T) can be set for 10 to $10^9$ samples, in powers of 10, or for any time interval by simply starting and stopping the correlator when desired. The autocorrelation function, $G^{(2)}(\tau)$, is in a digital form represented by 96 channels (the 96 values of $\tau$ mentioned earlier). The correlator will display the entire function on an X-Y display or the numeric value of each channel on a digital display.

Oscilloscope. A Tektronix 465 M oscilloscope was used as an X-Y display to graphically view the correlation function on a real-time basis.

Mini-computer. A HP 3052A data acquisition system was used to control the digital correlator and process the data received from it. The interfaces and software were developed by Neyland (reference 12) in 1981 for his Master's thesis. The system was originally used with the Air Force Institute of Technology Smoke Tunnel; however, the interfaces and software were modified to satisfy the needs of this research. A summary of the interfacing and software is contained below. A more detailed description may be found in reference 12.

The LDA and data acquisition systems were not collocated so cables had to be run to connect them. Two 22.9 meter (75 ft) lengths of Belden 8773 cable were used. Each cable contains 27 twisted, shielded pairs of conductors. Forty pairs were used for

signal transmission: six computer-to-correlator control lines and thirty-four correlator-to-computer data lines. The second conductor in each pair was connected to ground; however, the shields were not grounded. The unused, twisted pairs were left unconnected.

The software used to control the correlator and process the data is contained in a program titled DARLA MOD1. A program titled DARLA (Data Acquisition And Reduction of Laser Anemometry), which was written by Neyland, is the basis of DARLA MOD1. The software performs the following functions:

1) Run the correlator for a specified period of time to develop the intensity autocorrelation function.
2) Transfer the correlation function values to the HP 3052A.
3) Store the correlation function and other test information on a flexible disk.
4) Process the data to calculate velocities and turbulence intensities.
5) Plot the velocity and turbulence intensity profiles on a HP 9872S plotter.
6) Print a summary of the data in tabular form on a HP 9871A printer.

Both DARLA and DARLA MOD1 may be found at the Air Force Institute of Technology, School of Engineering, Wright-Patterson AFB, Ohio 45433.

Hot-film Anemometer. A TSI Model 1050 Constant Temperature Anemometer and TSI Model 1051-6 Monitor and Power Supply were

used with a TSI Model 1214-20 hot-film sensor to gather additional velocity and turbulence information in the annular inlet and diffuser. The probe was mounted to the dump section sidewall and inserted upstream into the inlet and diffuser test sections. It is adjustable in both the radial and axial directions. The anemometer bridge output was connected to a HP 3400A RMS voltmeter and an Alpha Product Co. eight bit, analog-to-digital converter. The RMS voltage was read from the voltmeter to get turbulence intensity information. A Radio Shack TRS-80 Model III micro-computer was used to sample the output of the analog-to-digital converter and average the samples to obtain an average DC voltage. The sampling rate of the TRS-80 is approximately 50 Hertz.

Flow Meter. A Meriam Instrument Co. square-edged orifice plate, a Meriam U-tube mercury manometer, and a Bourdon tube pressure gage were used to measure the air flow rate into the flow handling apparatus. The orifice is 2.5 centimeters (1.0 in) in diameter inside a 7.6 centimeter (3.0 in) pipe. Flange taps were used for the pressure measurements. The pressure measurement upstream of the orifice has an accuracy of ±6890 N/sq meter (1.0 psig). The measurement of the pressure drop across the orifice has an accuracy of ± 1.3 millimeters (0.05 in) of mercury. The air temperature was measured in the dump section with a mercury thermometer to an accuracy of ±0.5 degrees Fahrenheit. Since low velocities are involved, this temperature measurement is representative of the static air temperature at the orifice plate to within 0.75 degrees Fahrenheit.

Static Pressure Probe. A locally-built static pressure probe was used to measure the pressure in the annular inlet and diffuser (see Figure 9). The probe was mounted to the dump section sidewall in the same manner as the hot-film anemometer probe and inserted upstream into the test sections. The pressure was indicated by a Meriam Instrument Co. water micro-manometer. The ambient air pressure was measured with a Fortin-type, mercury barometer.

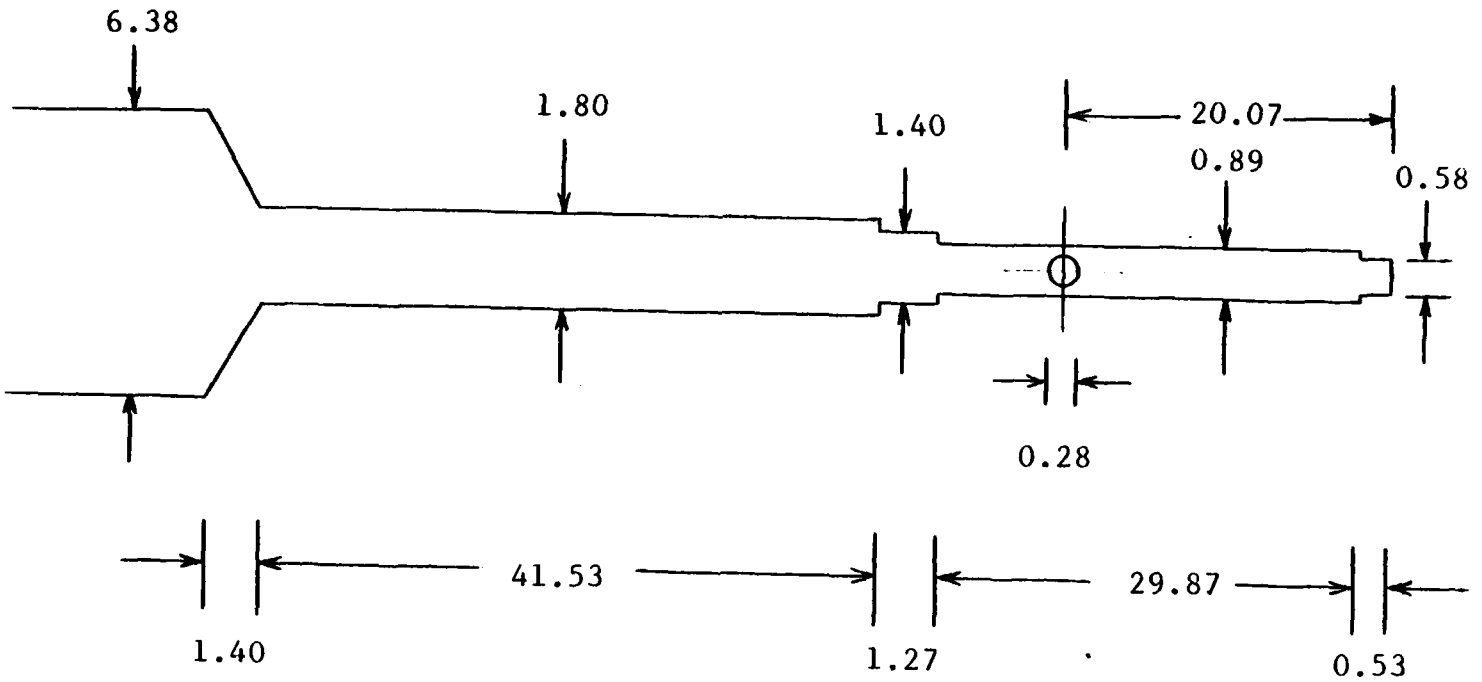


ALL DIMENSIONS ARE IN MILLIMETERS.

FIG.9. STATIC PRESSURE PROBE

# IV. Experimental Procedure

The procedure used to collect and reduce the data will be discussed in this section. It can be divided into four segments: laser and optical alignment, LDA measurements and data reduction, hot film anemometer measurements and data reduction, and static pressure measurements.

## LDA Optical Alignment

A critical step in making flow measurements with an LDA system is the alignment of the laser and optics. The alignment of the LDA system used in this research meets the following criteria:

1) As the optical platform translates, the measuring volume moves only in the radial direction of the flow handling apparatus.
2) As the laboratory bench translates, the measuring volume moves only in the axial direction.
3) The measuring volume always remains fixed in space with respect to the PM assembly so the two will remain aligned as the optical platform is translated.

The alignment procedure is decribed in Appendix B.

## LDA Flow Measurements

LDA measurements were collected with the digital correlator in the single-clipped autocorrelation mode (without clipping). Each test consists of a traverse of the flow channel at

one axial position. For each test, all room lighting was extinguished because of its detrimental effect on data collection. The reason for this will be evident later in this section. The air flow through the flow handling apparatus was allowed to reach a steady state before the tests began since there is no active control of the flow rate.

The goal of each LDA measurement is a smooth correlation function with three peaks and valleys, similar to Figure 10, in the shortest possible time. After positioning the measuring volume at the desired point in the flow, the aperture on the collecting lens is set. A smaller aperture requires a longer correlator run time (correlation time) to develop the same correlation function. The frequency shift ($\Delta F$) and sample time ($t_s$) should be set, based on Eq (17) if the approximate velocity being measured is known.

$$u = \frac{d_f}{(Pk2\text{-}3)} + \Delta F(d_f) \qquad (17)$$

If the velocity (u) cannot be estimated, different combinations of $\Delta F$ and $t_s$ must be tried to obtain the desired correlation function. Frequency shifts in the INVERT mode reduce the damping of the correlation function and are useful in high turbulence flow regions to obtain more distinct peaks and valleys. In the DRIVE mode, frequency shifts increase damping and are normally used only in laminar and low turbulence flows ($\eta < 25\%$).

The correlator is run for a specified period of time to obtain the correlation function for the flow measurement. If a

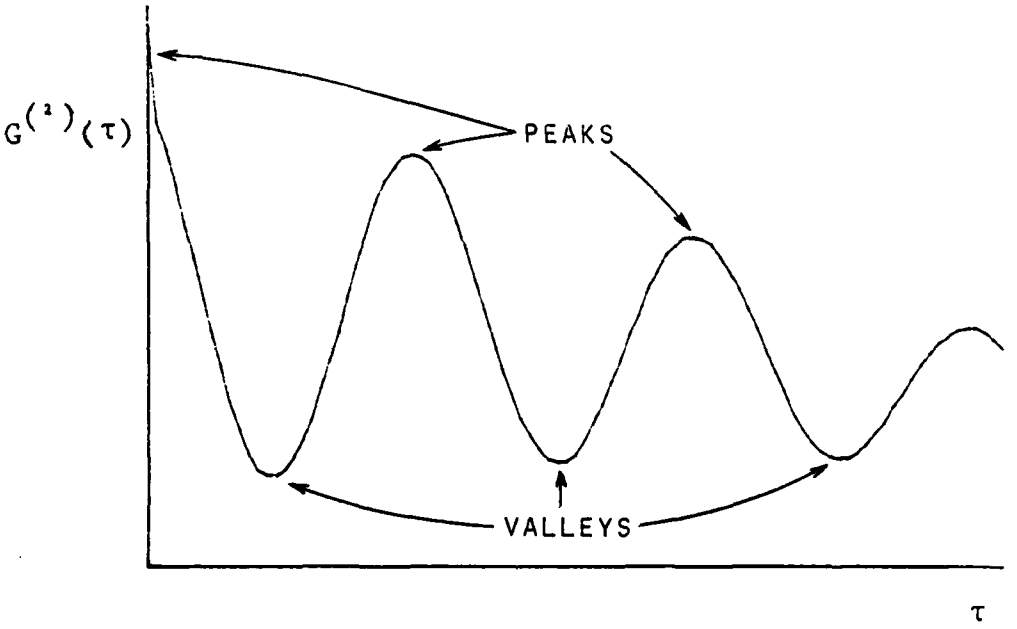


FIG. 10. CORRELATION FUNCTION: PEAKS AND VALLEYS

real-time display on the oscilloscope is desired, the correlator can be operated from the unit itself using the START and STOP buttons. Correlator data cannot be transferred to the HP 3052A while the oscilloscope display is active. If the HP 3052A is used to control the correlator through the program DARLA MOD1, the correlation time is input after which the computer will immediately start the correlator and stop it after the specified time has elapsed. The correlator channel contents are transferred to the computer and the correlation function is displayed on the computer's video display. If the function is smooth and has at least three peaks and valleys, the data is kept in the computer memory for subsequent transfer to flexible disk. If the correlation function is not smooth or has fewer than three peaks and valleys, the data is rejected by the experimenter and a new correlation function obtained.

The most significant factor determining the correlation time needed to obtain a smooth correlation function is the amount of background light which enters the PM assembly. There are two sources of this background light. The phase modulator and periscope mirrors, the first source, diffuse a large amount of laser light and create stray beams which are then transmitted through the focusing lens and projected on the outer surface of the test section access windows (see Figure 11a). This light reflects off the windows into the PM assembly. The second source is the portion of each primary laser beam which is reflected by the test section centerbody window surfaces each time the beam crosses a surface

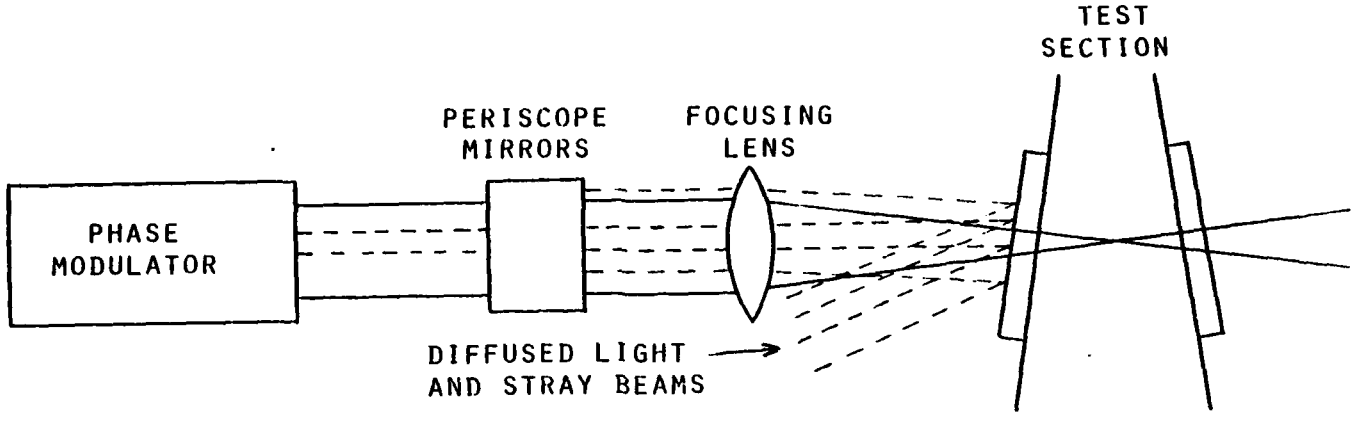


(A) PHASE MODULATOR AND PERISCOPE MIRRORS

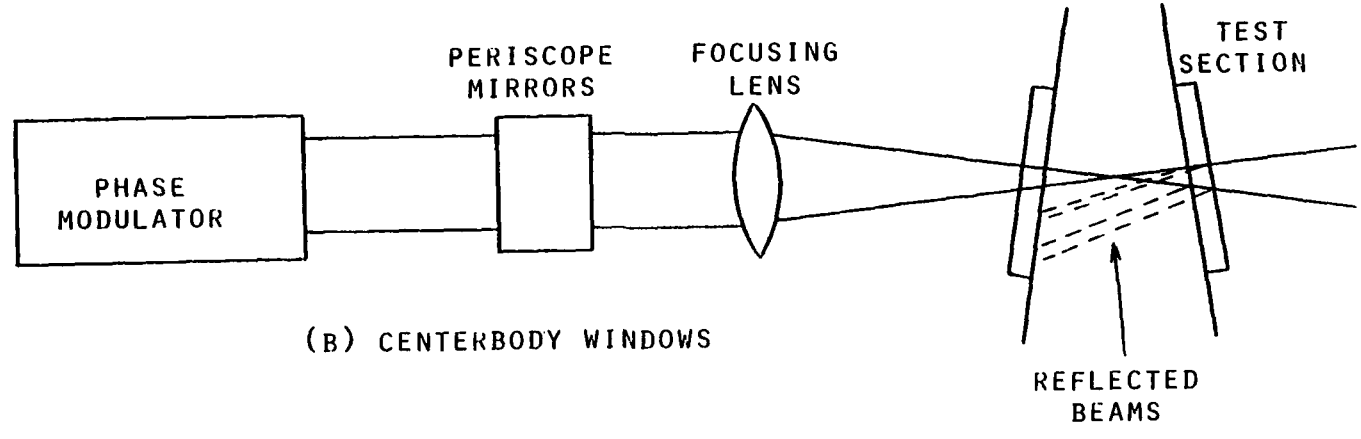


(B) CENTERBODY WINDOWS

FIG. 11. SOURCES OF BACKGROUND LIGHT

(see Figure 11b). The reflected beams cross the flow channel. If these beams which reflect into the flow channel are in the vicinity of the collecting axis, the scattered light from them will tend to mask the light from the measuring volume. This results in points in the flow channel, away from the walls, which have large amounts of background light. Because of the centerbody and collecting optics geometry, this is a particular problem in the diffuser test section.

Bright background light has several detrimental effects on LDA flow measurement. It may be so bright that it saturates the PM tube and the correlation function fails to develop at all. Using a smaller collecting lens aperture will normally solve this problem. However, the amount of light may be great enough that even if the correlation function develops, it cannot develop enough to distinguish the peaks and valleys. In some situations when the effective measuring volume is near, but not on a wall, the dominant signal may be a reflection of the actual measuring volume which gives a zero velocity measurement. This usually occurs in the diffuser test section as much as 1.0 millimeters (0.04 in) from the inner wall. Flow measurements cannot be made in these situations. On the other hand, if a correlation function develops to a point where peaks and valleys are distinguishable (as in Figure 12), a longer correlation time will improve the function.

The amount of background light reaching the PM assembly is controlled in several ways. A paper mask was placed over the

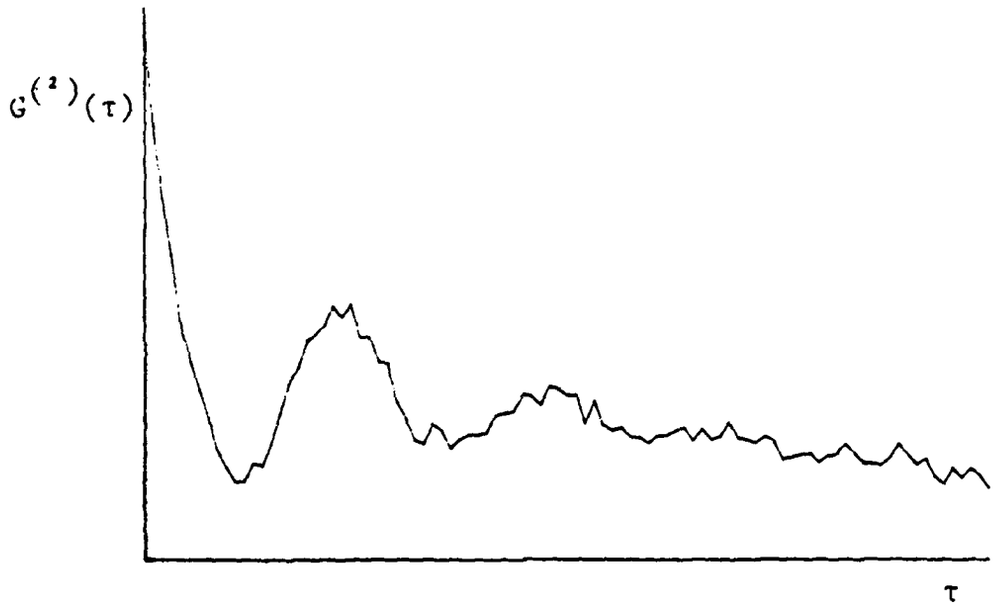


FIG. 12. UNDER-DEVELOPED CORRELATION FUNCTION

focusing lens which allowed only the two parallel laser beams to pass. When near the inner wall of the annulus, the test section centerbody windows reflect much less light than the black, painted surface. However, when the measuring volume is more than three to five millimeters from the inner wall, the centerbody is rotated to move the windows out of the beam paths. This avoids the problem caused by the reflected beams passing through the flow channel.

Tests were run at the following axial positions (see Figure 13):

34.3 mm (1.35 in) from the IGV trailing edges
48.8 mm (1.92 in) " " " " "
110.0 mm (4.33 in) " " " " "
215.4 mm (8.48 in) " " " " "
240.0 mm (9.45 in) " " " " "
262.4 mm (10.33 in) " " " " "

Data points were taken every 0.5 millimeters (0.02 in) across the flow channel except when prohibited by excessive background light. Points to within 0.5 mm of the inlet walls were obtained. In the diffuser, data points were obtained to within 2.5 mm of the inner wall and 1.0 mm of the outer wall.

For all of the tests, atomized glycerin was used to "seed" the flow. The seeder output ranged from 22.8 to 26.4 liters per minute with $2(10^8)$ particles per liter. The particles varied in size from 0.5 to 4.0 μm (.00002 to .00016 in). Correlation times in the annular inlet ranged from 30-45 sec away from the walls to 90-120 sec near the walls. In the diffuser test section, corre-

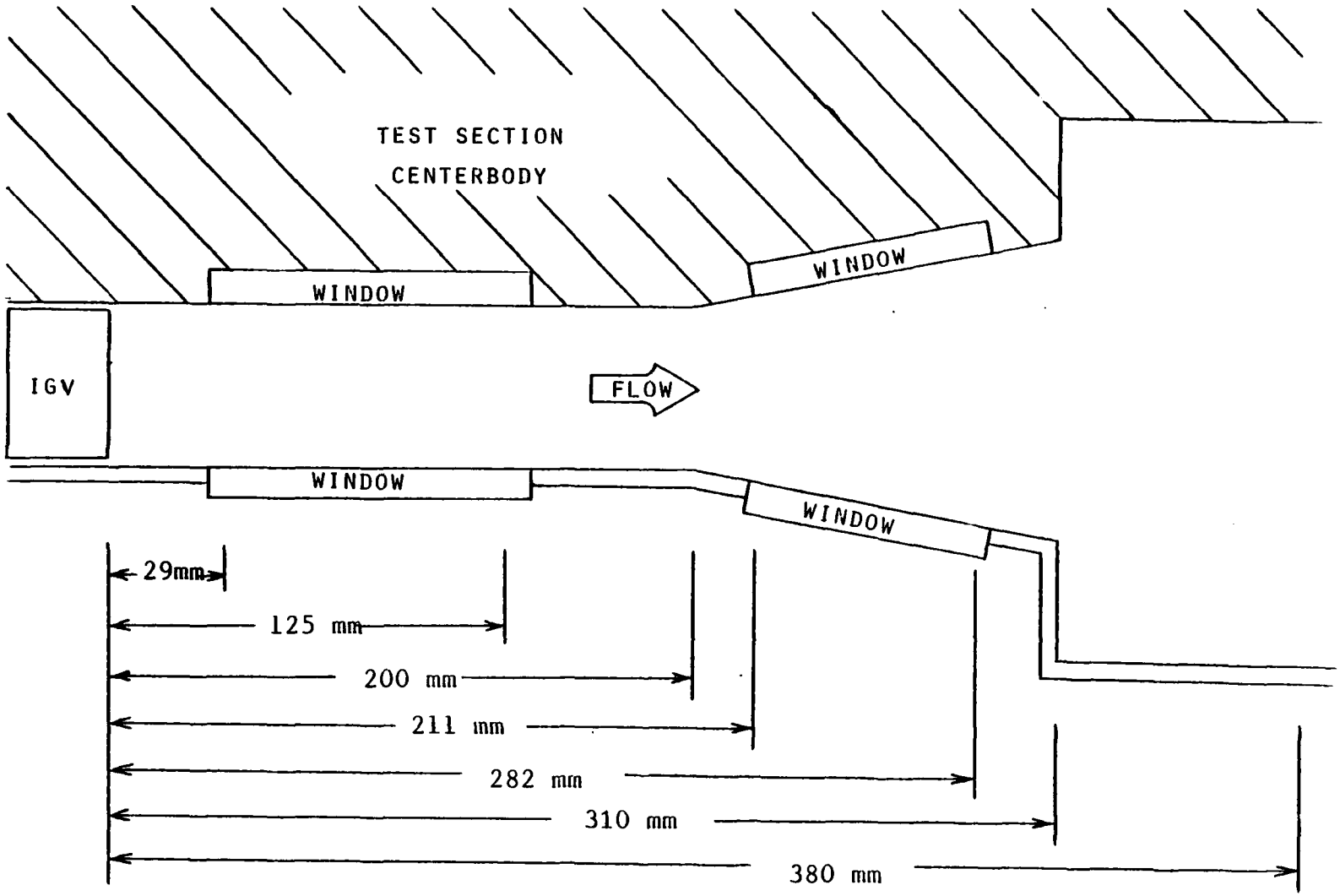


FIG. 13. DATA COLLECTION POSITIONS

lation times were 60-90 sec away from the walls to 180-420 sec near the walls. For the tests on 20 SEP 83 and thereafter, the air supply mass flow was measured at periodic intervals during the tests using the square-edged orifice plate. After reaching a steady-state, the mass flow was constant so only periodic measurements were necessary to ensure gross fluctuations in the flow rate did not occur during a test.

LDA Data Reduction

The data was reduced using the program DARLA MOD1 on the HP 3052A data acquisition system. The method is described in Appendix C. The velocity and turbulence intensity data was plotted to provide a visual representation of the profiles. A separate program was used to integrate the velocity profiles of each test to calculate the mass flow through the annulus. The integration was carried out by estimating the area under the profiles by a series of rectangles whose width is the distance between adjacent data points and height is the average of the velocities at the two points.

Hot Film Anemometer Measurements

Flow measurements were also made with the hot film anemometer. As before, the air flow was allowed to reach a steady state before the test began. These tests were not made in conjunction with the LDA tests because the glycerin particles would alter the heat transfer on the sensor and introduce an unknown amount of error into the data.

The hot film tests were made at the same axial positions as the LDA tests except for the 34.3 mm position. The laser was used to determine the position of the sensor by focusing the beams on the probe and reading the position on the optical platform's vernier scale. Data points were taken at intervals from one to two millimeters across the flow channel. At each point, the TRS-80 computer calculated the average DC voltage of the bridge output by averaging 500 samples. During this time, the RMS voltmeter was visually monitored and the average RMS voltage of the bridge output was estimated.

## Hot Film Anemometer Data Reduction

The bridge voltages and sensor calibration curve points were input into the HP 3052A to reduce the data. A program which compared the voltages and calibration curve was used to calculate the average velocity and turbulence intensity. The average velocity is derived from the DC voltage, while the turbulence intensity is derived from the RMS voltage. The hot film data was also plotted to give a visual representation of the profiles. The velocity profiles were integrated, using the method described earlier, to calculate the mass flow.

## Static Pressure Measurements

The static pressure in the annular inlet and diffuser was measured at various axial positions with a static pressure probe and water micro-manometer. The air flow was allowed to reach a steady-state before measurements were taken. The laser was used

to position the static pressure port in the axial direction by focusing the beams on the pressure port. The position was determined by the reading on the mechanical counter of the laboratory bench translating system. Measurements were taken at 19 mm (0.75 in) intervals in the axial direction in the inlet and at 13 mm (0.50 in) intervals in the diffuser.

## V. Results

A total of twelve tests were run with the LDA system. A test was conducted at each of the following axial positions: 34.3, 48.8, 110, 215.4, 240, 262.4 mm. Three additional tests were made at both the 48.8 and 110 mm positions to establish the repeatability of the system. Five tests were run with the hot film anemometer: one at each axial position used with the LDA except the 34.3 mm position. A profile of the static pressure in the axial direction of the annulus was made with pressure measurements in the inlet and diffuser. This section discusses the results of the flow investigation and evaluation of the LDA system.

### Flow Characteristics

The velocity profiles acquired with the LDA at each of the six axial positions used for testing are shown in Figures 14 through 19. The dotted lines on the plots represent the test section walls with the channel width indicated on the abscissa. The mass flows were obtained by integrating the profiles over the annulus using the method described in the previous section. The calculated mass flows were within 5% of the values measured with the orifice plate flow meter. As expected, the profiles in Figures 16 through 19 show a thinner boundary layer on the inner annulus wall than on the outer wall. This effect is more pronounced in the annular diffuser where the ratio of the inner to outer wall radii is smaller (see Figures 17 through 19). The turbulence in-

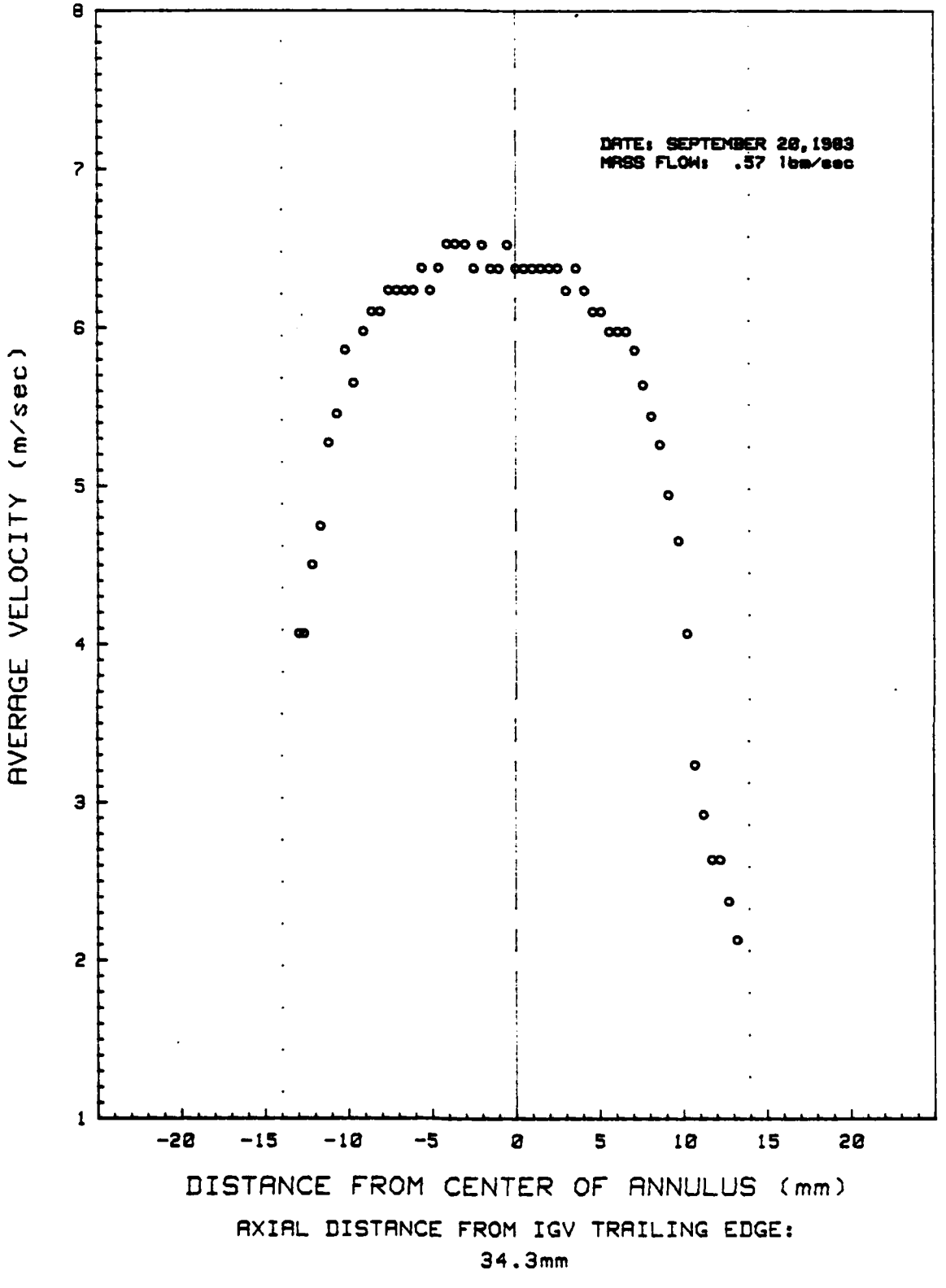


FIG. 14. AVERAGE VELOCITY PROFILE

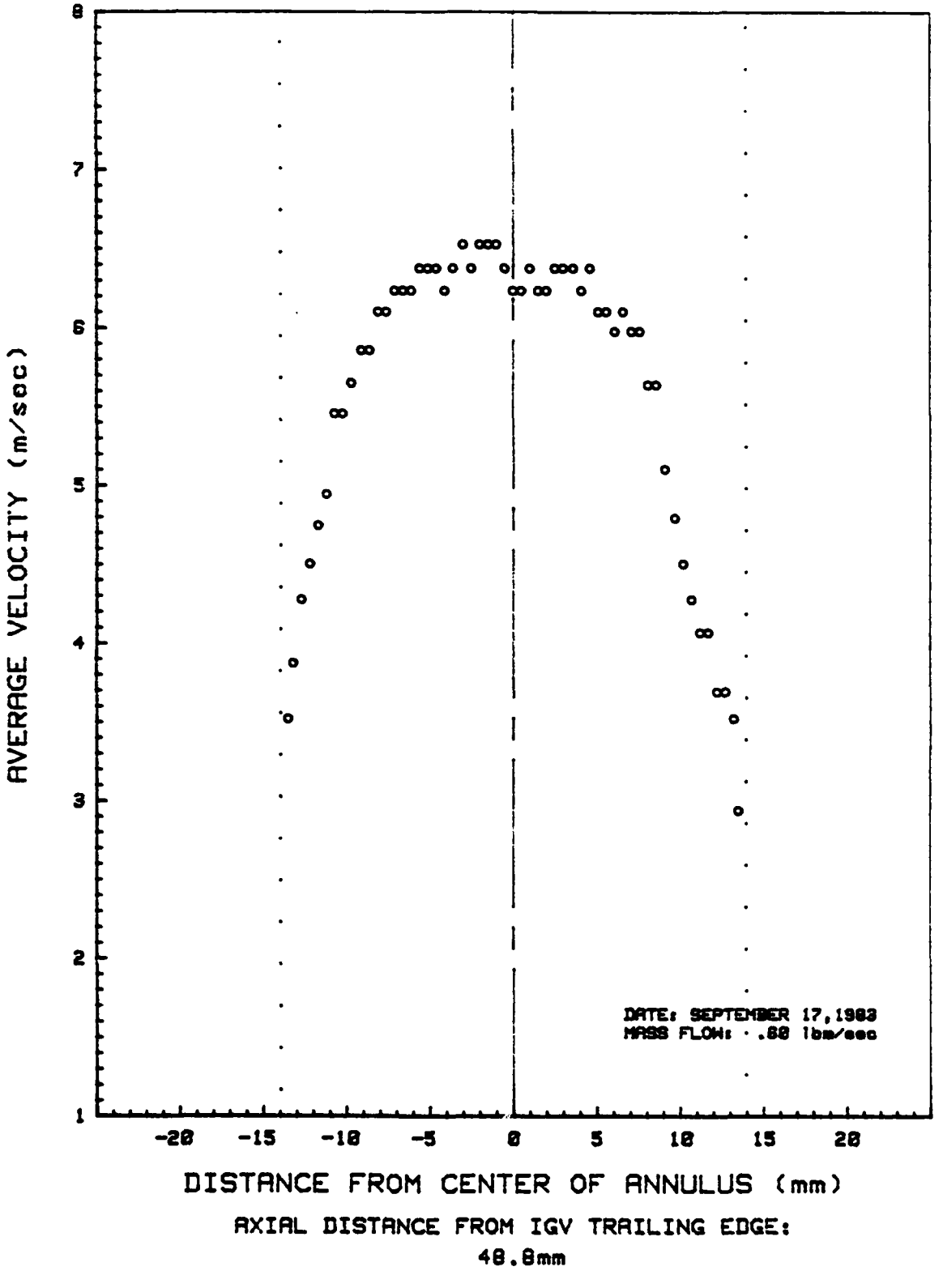


FIG. 15. AVERAGE VELOCITY PROFILE

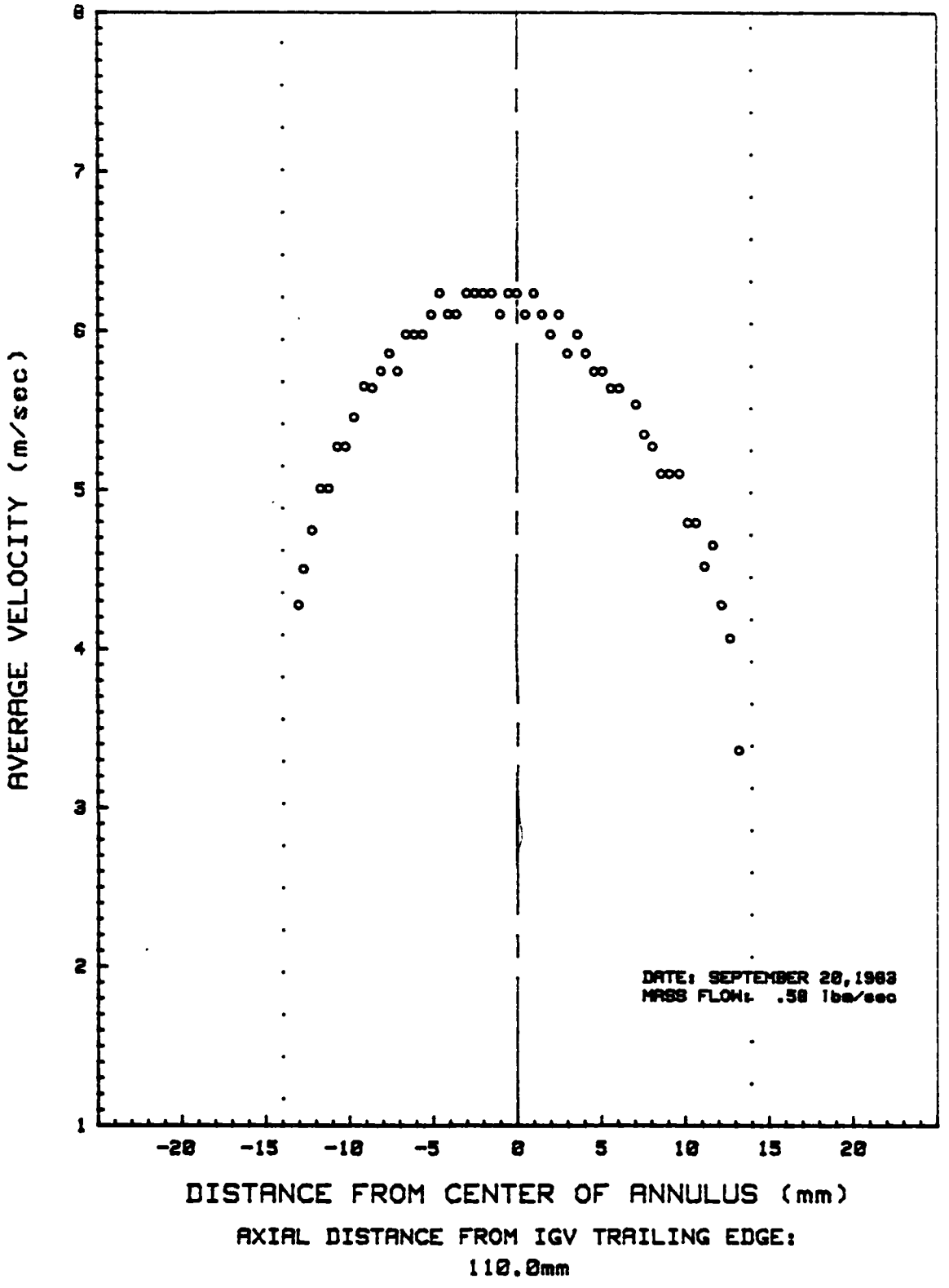


FIG. 16. AVERAGE VELOCITY PROFILE

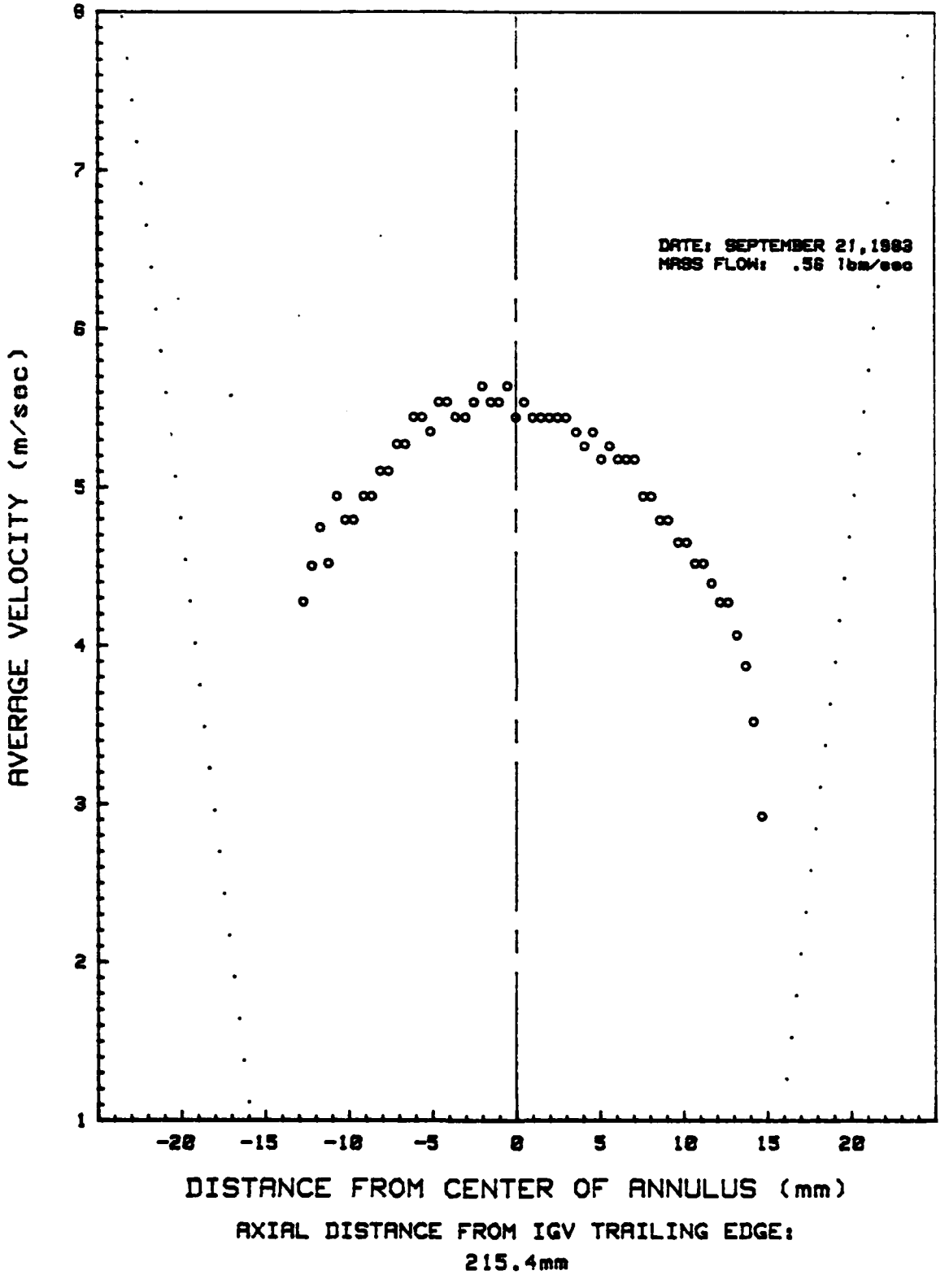


FIG. 17. AVERAGE VELOCITY PROFILE

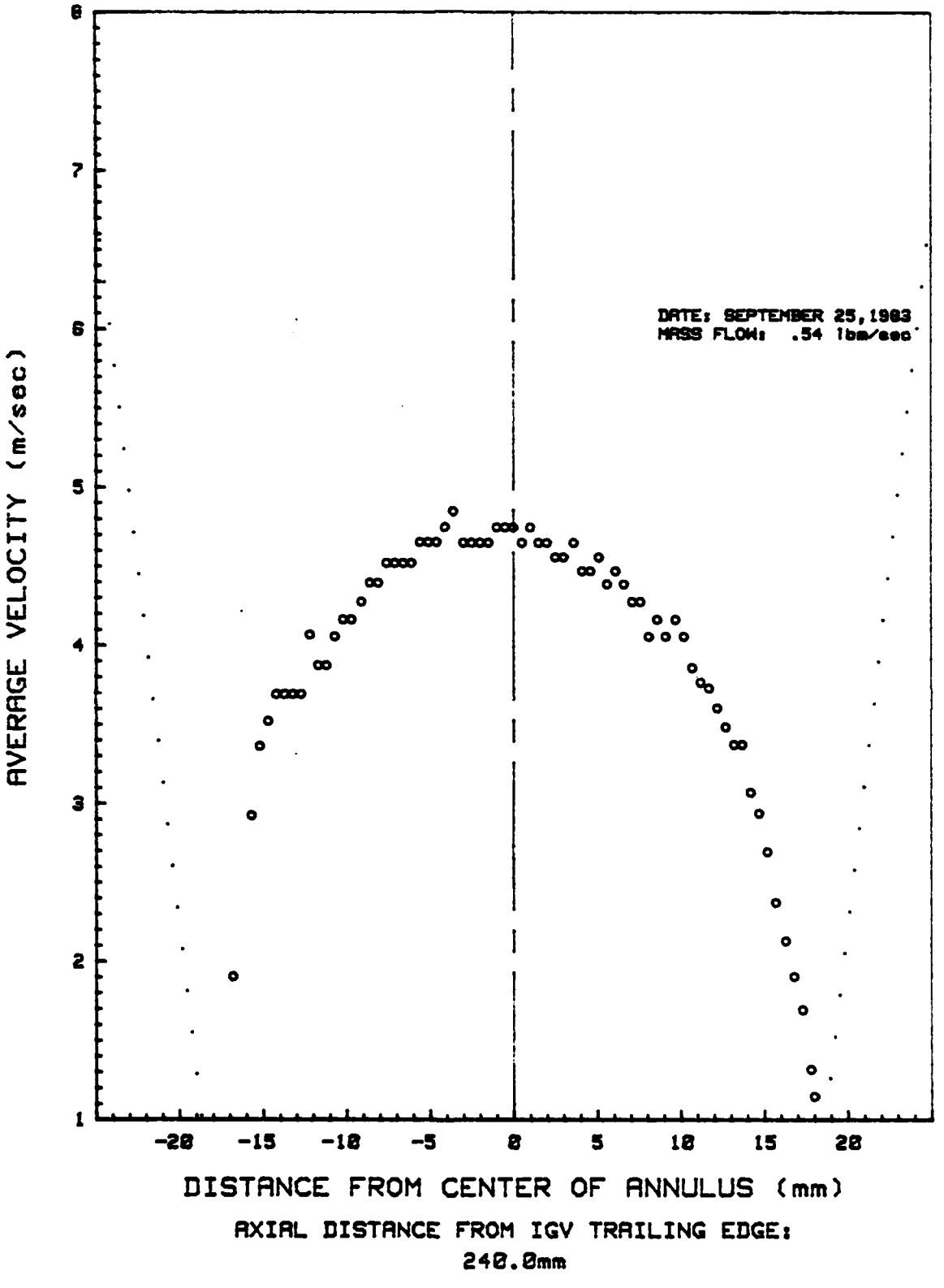


FIG. 18. AVERAGE VELOCITY PROFILE

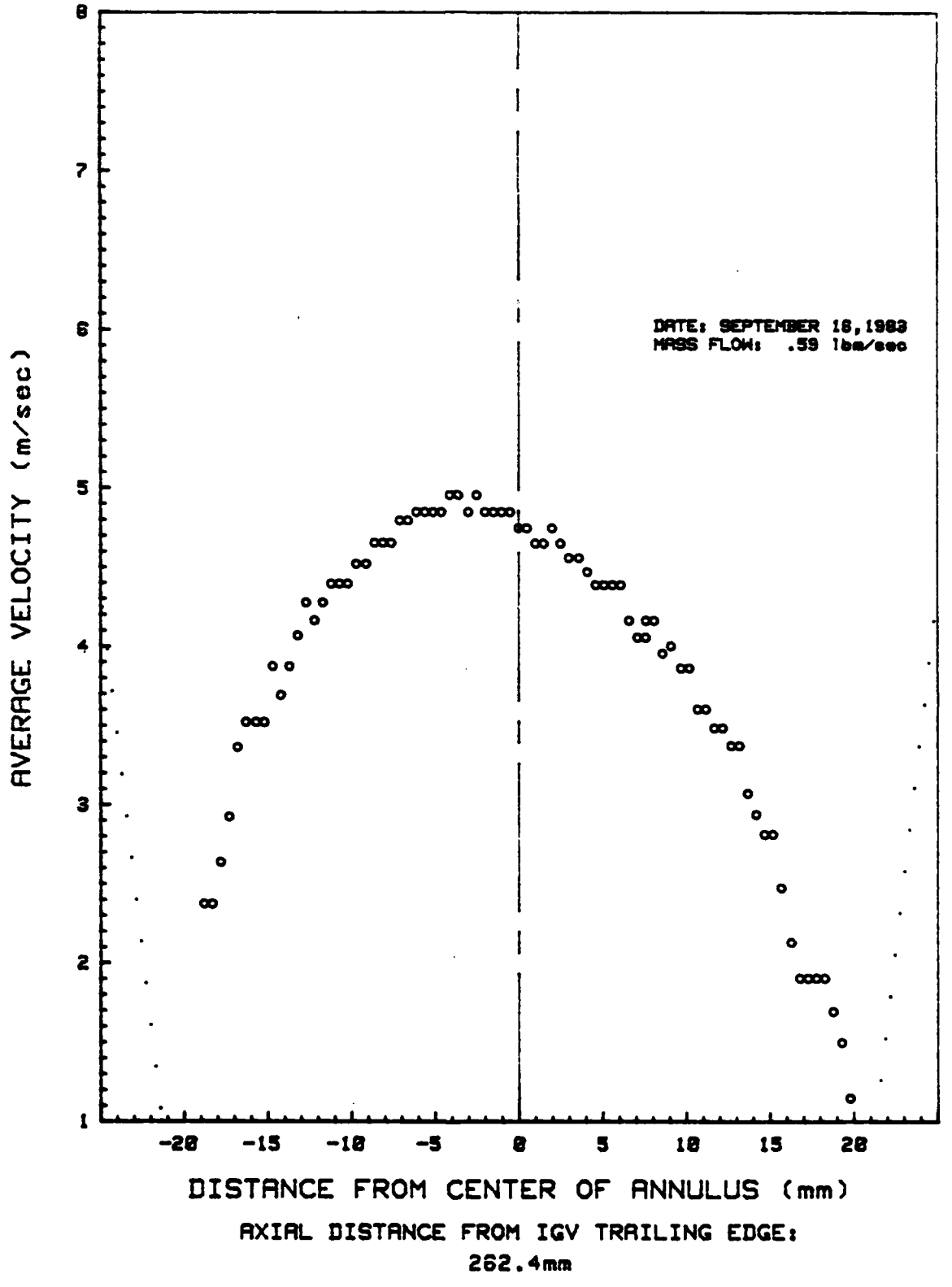


FIG. 19. AVERAGE VELOCITY PROFILE

tensity profiles corresponding to these velocity profiles are shown in Figures 20 through 25. The turbulence intensity is defined as the standard deviation of the velocity at each radial position divided by the average velocity at that position. The flow in the annulus, outside the boundary layers, is turbulent. This is consistent with the pipe Reynolds number of 18300 calculated with Eq (1). The turbulence intensity is approximately 8% in the inlet and 10% in the diffuser. The boundary layers are also turbulent. This is consistent with the theoretical predictions using a Reynolds number in the annular inlet of 3.42 ($10^5$) and the fact that the freestream flow is turbulent throughout the annular interface. A disturbance along the outer wall in the annular inlet is noticeable in the turbulence intensity profiles of Figures 20 through 22. This is caused by a step discontinuity in the outer wall between the IGV section and annular inlet test section. The step increases the width of the flow channel in this region by about two millimeters (0.08 inches). A summary of the data for these velocity and turbulence profiles is contained in Appendix D.

## Flow Development

The development of the velocity and turbulence intensity profiles in the annular inlet are shown in Figures 26 and 27 respectively. The velocity profiles are nondimensionalized using a reference velocity determined with Eq (18)

$$V_{ref} = \frac{\dot{m}}{\rho A_{inlet}} \qquad (18)$$

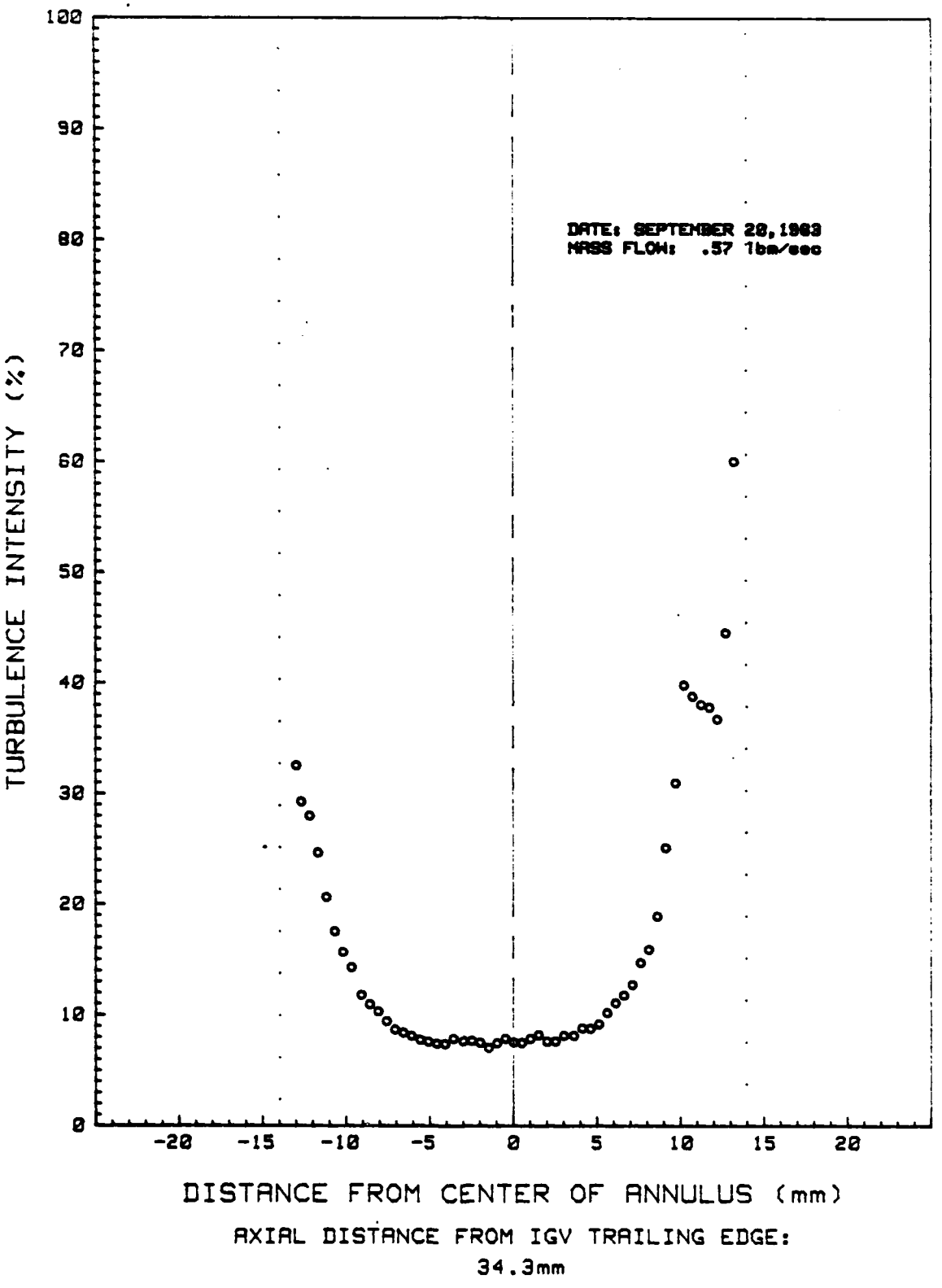


FIG. 20. TURBULENCE INTENSITY PROFILE

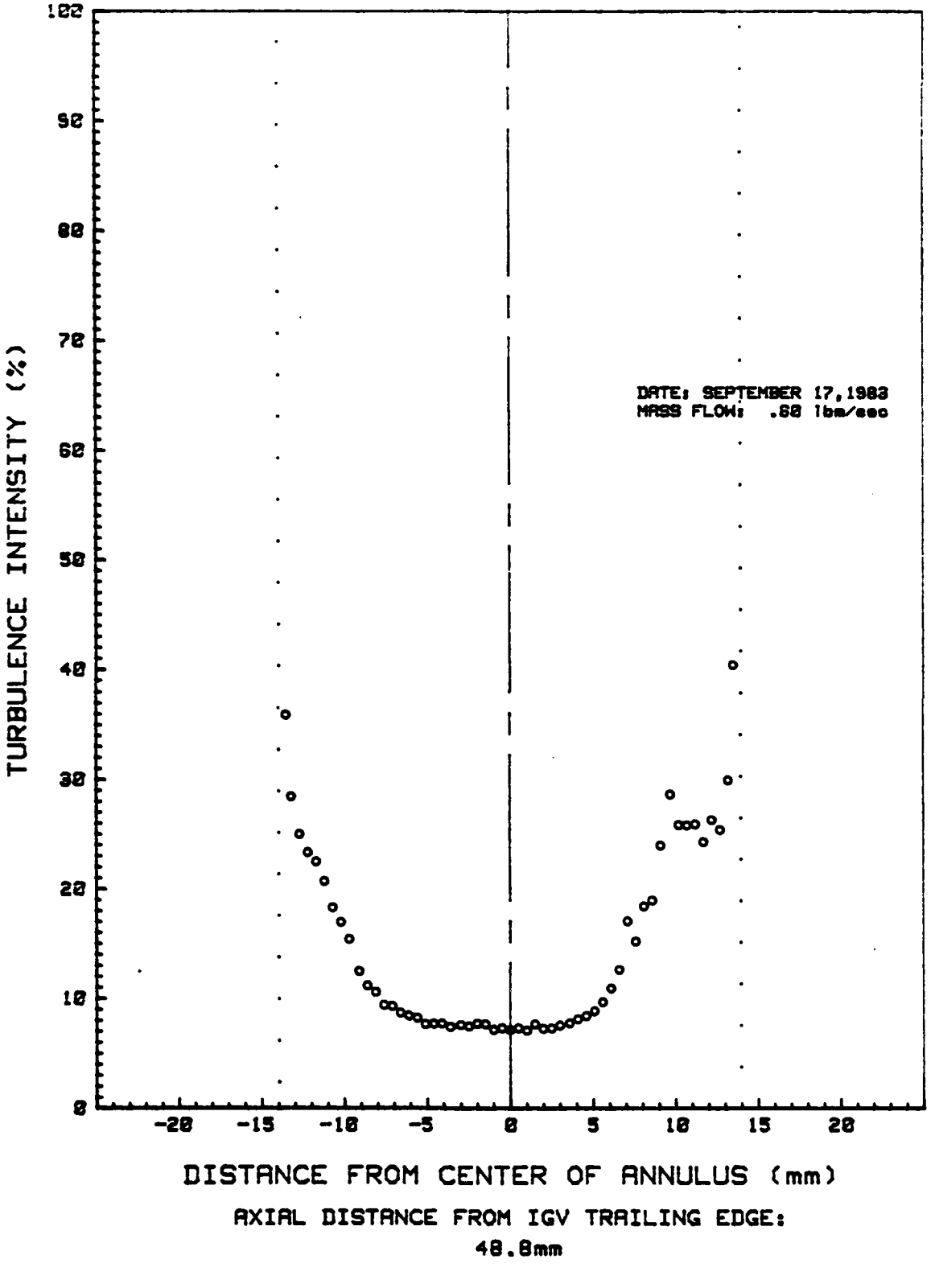


FIG. 21. TURBULENCE INTENSITY PROFILE

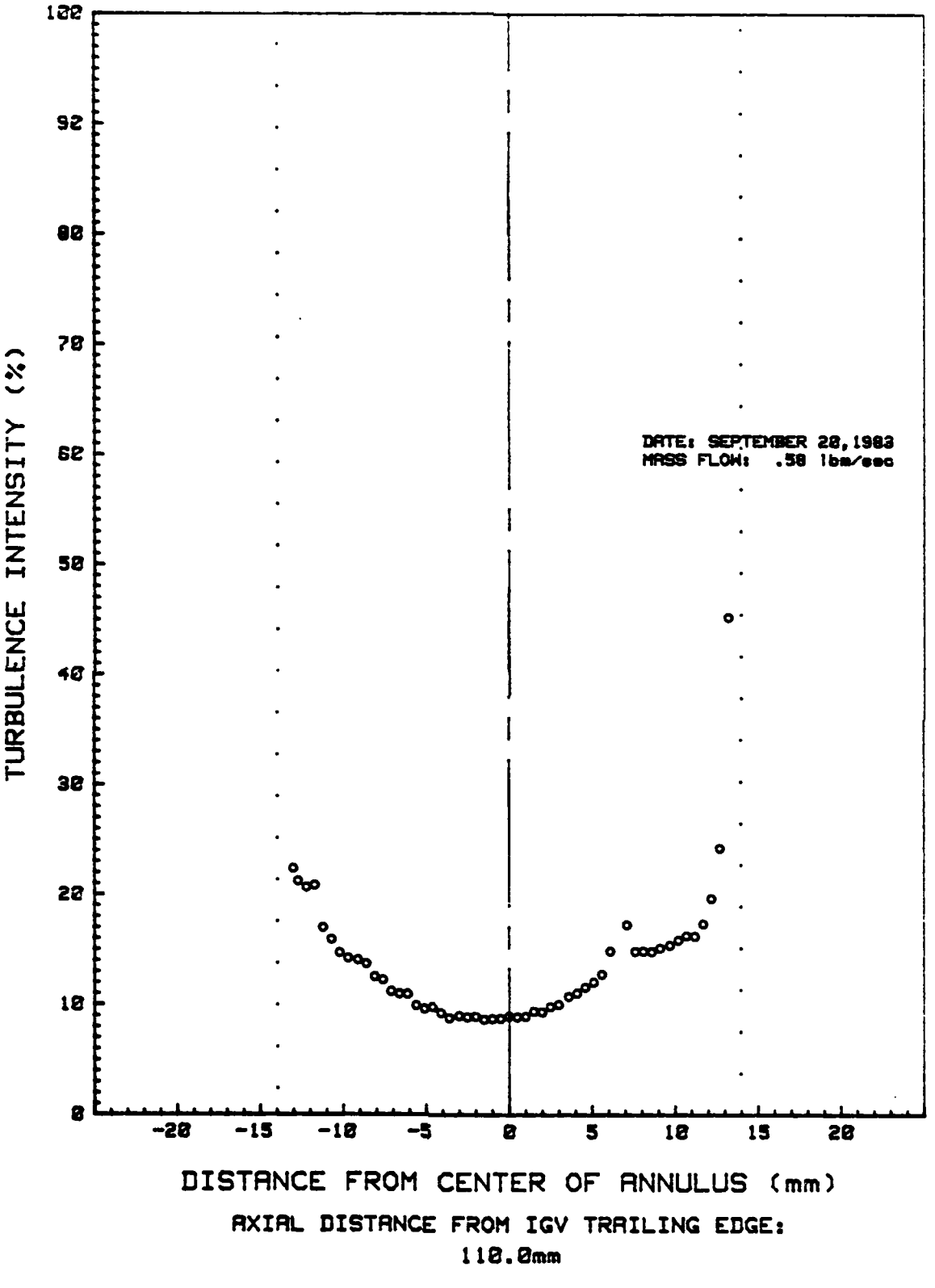


FIG. 22. TURBULENCE INTENSITY PROFILE

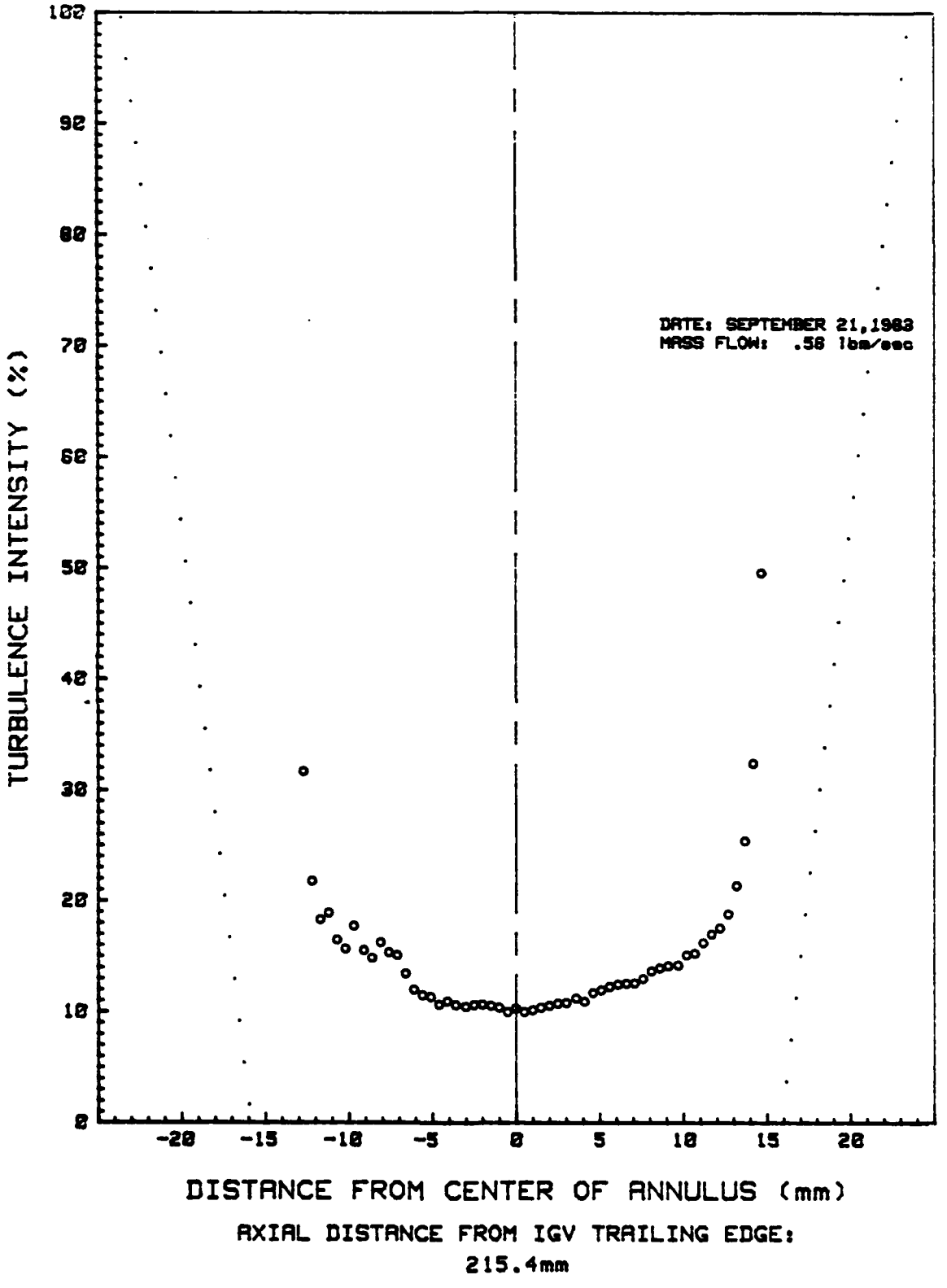


FIG. 23. TURBULENCE INTENSITY PROFILE

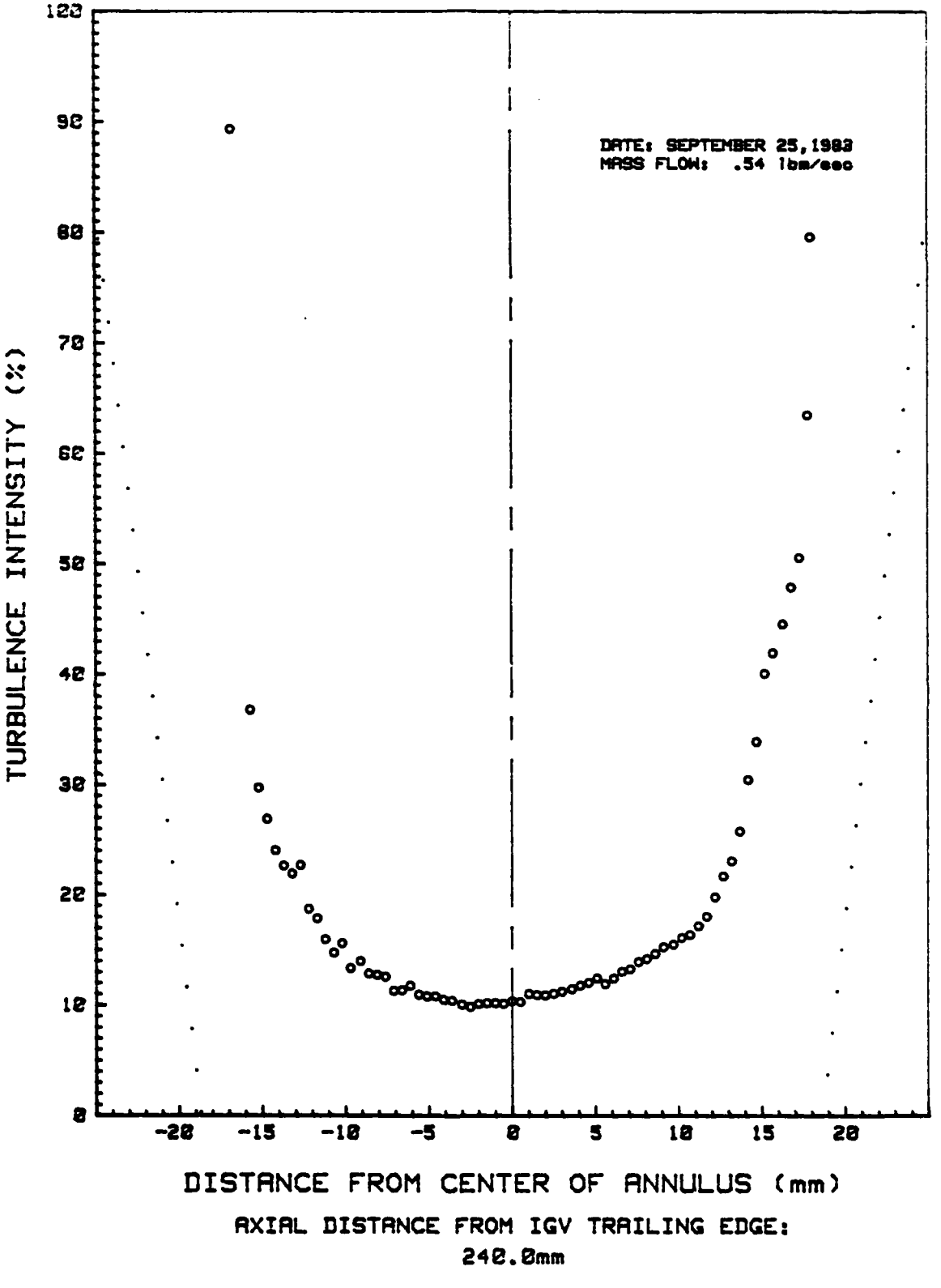


FIG. 24. TURBULENCE INTENSITY PROFILE

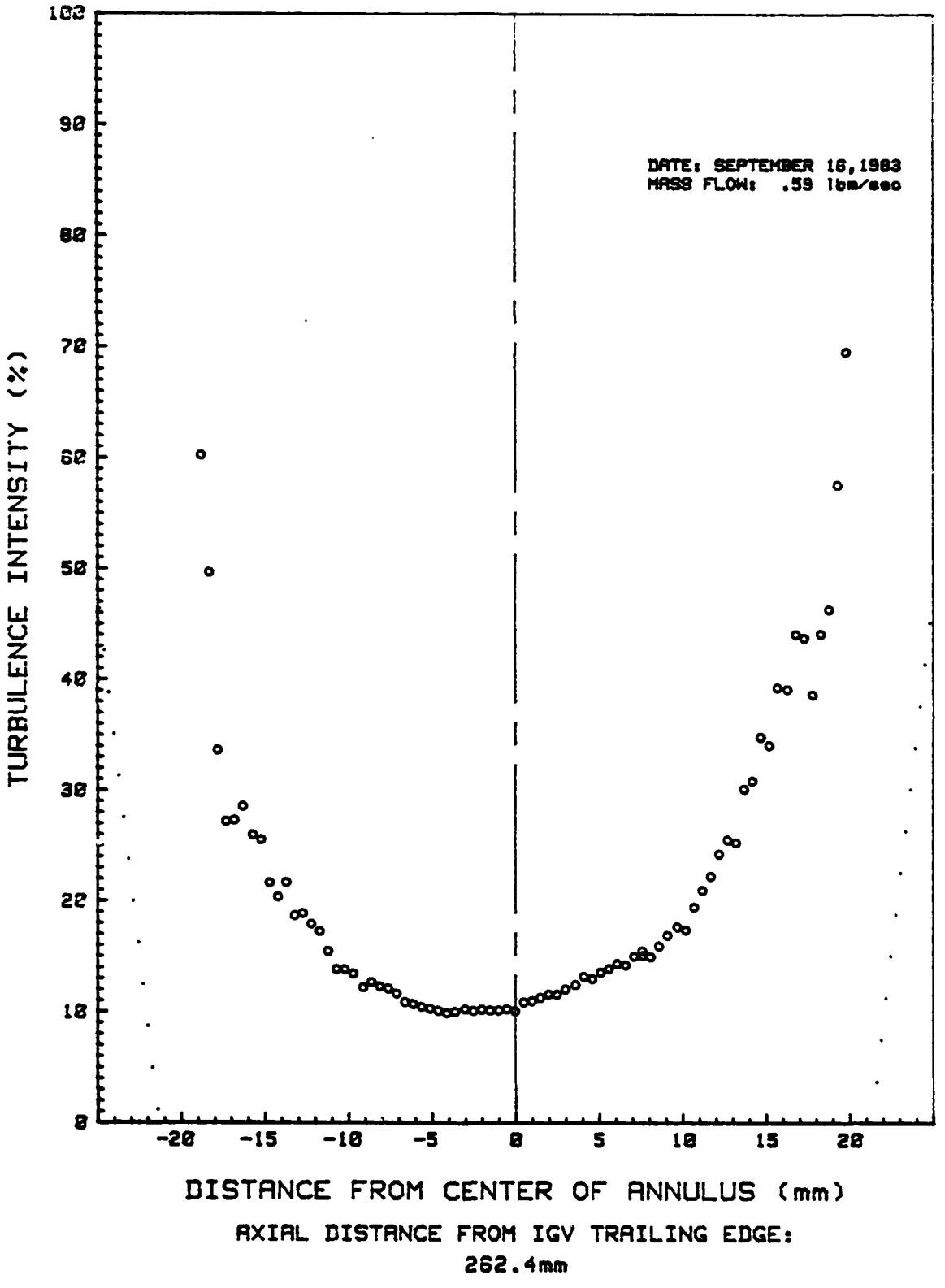


FIG. 25. TURBULENCE INTENSITY PROFILE

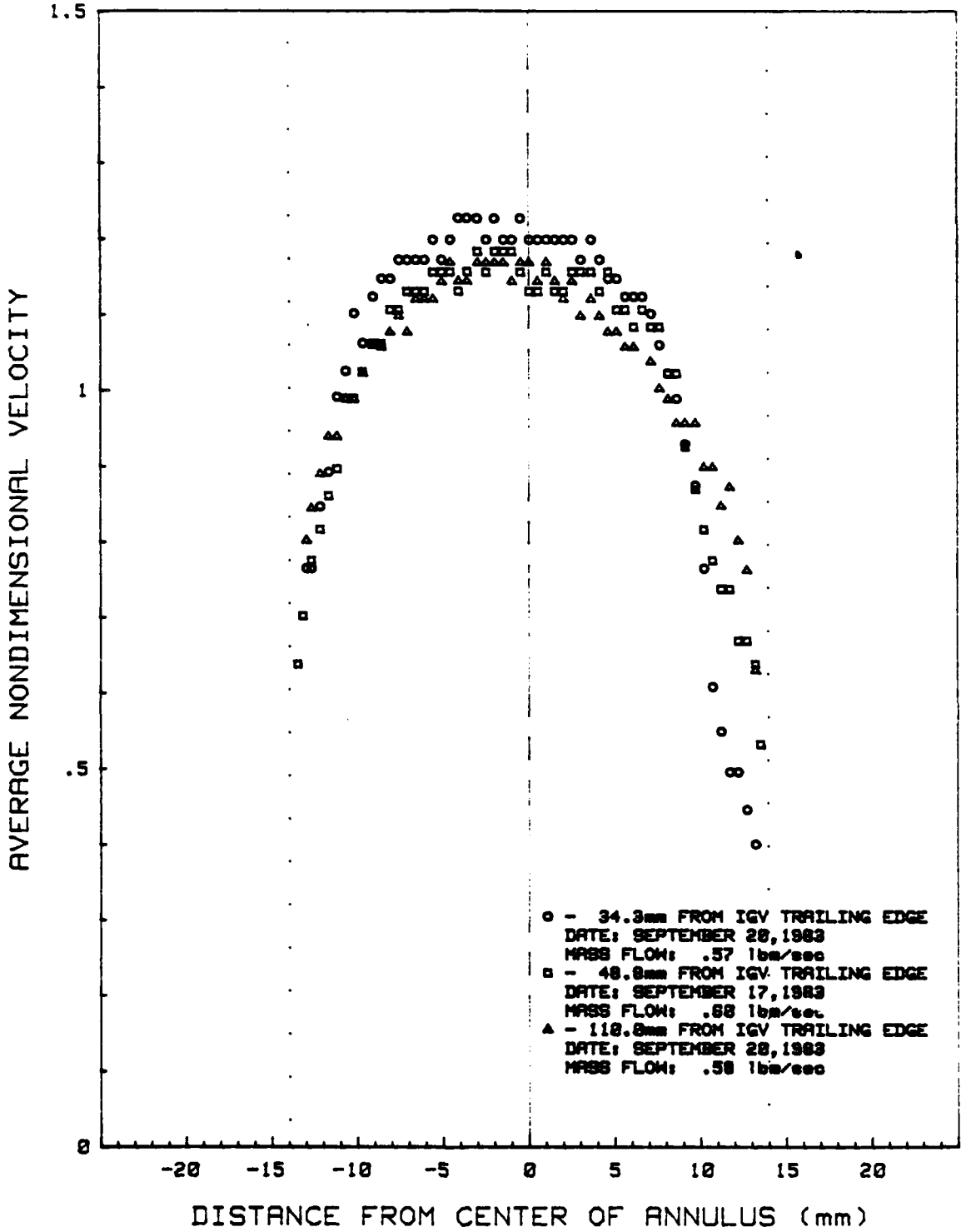


FIG. 26. ANNULAR INLET VELOCITY PROFILE DEVELOPMENT

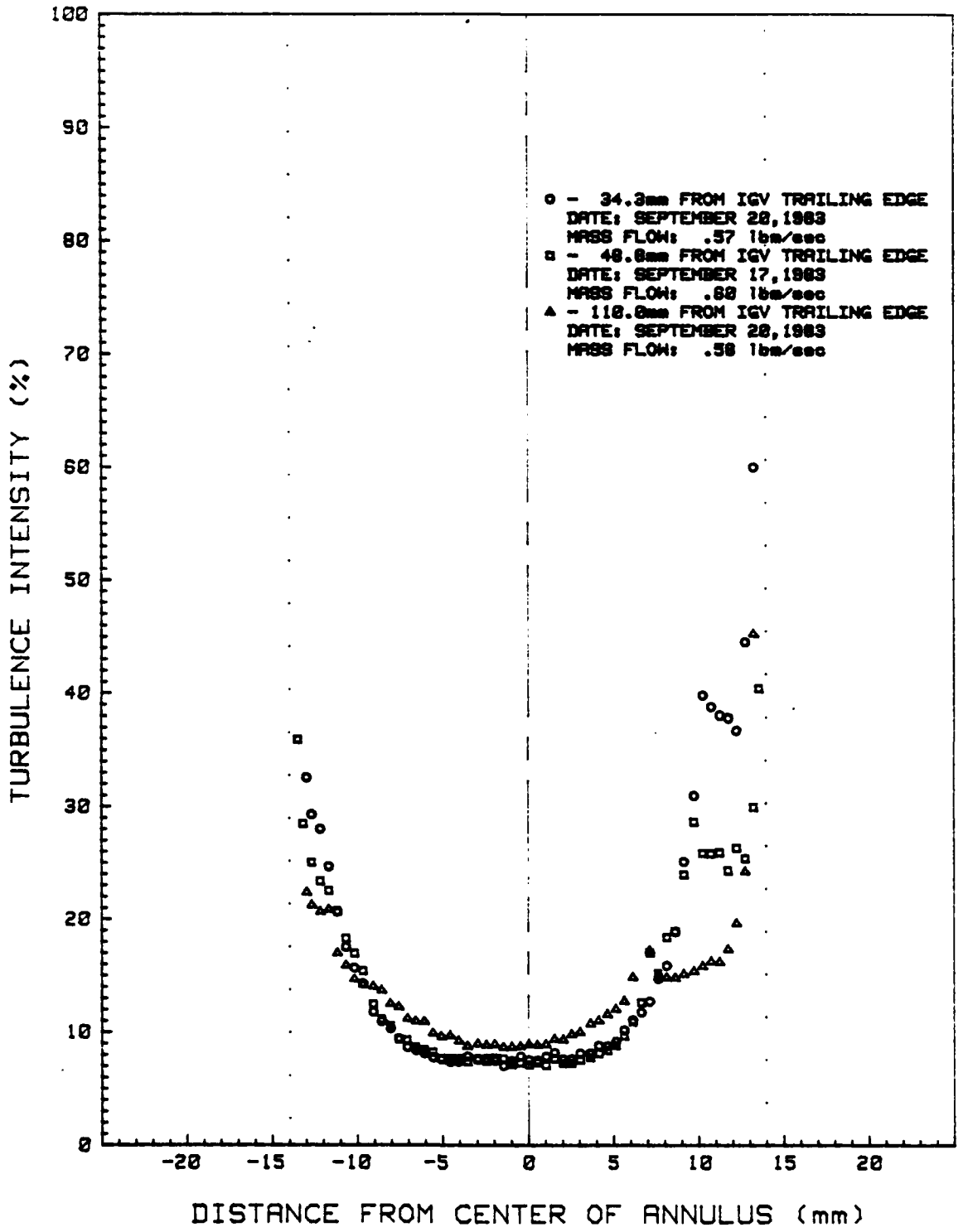


FIG. 27. ANNULAR INLET TURBULENCE INTENSITY PROFILE DEVELOPMENT

where $\dot{m}$ is the mass flow calculated from the integrated velocity profile, $\rho$ is the density of the air, and $A_{inlet}$ is the annular inlet area of 0.0426 sq meters (0.4583 sq ft) based on the measured flow channel width of 27.9 millimeters (1.10 in). From Figure 26, it appears that the inner and outer wall boundary layers have not merged until the vicinity of the 110 mm axial position. Near the centerline of the flow channel at the 110 mm axial position, the velocity profile has a more parabolic shape representative of merged boundary layers. On the other hand, the velocity profile at the 48.8 mm position shows a region of uniform flow near the center of the channel. Flat plate boundary layer predictions of a turbulent boundary layer growing from the beginning of the annular interface estimate the thickness to be 15.2 mm (0.60 in) at the 34.3 mm axial position. The calculation is based on the reference velocity and the distance from the start of the annular interface to the axial position of interest. This would indicate the boundary layers should just cover the entire flow channel. Due to differences in the flow over a flat plate and internal flow, this estimate is only an approximation. Additionally, scatter in the data points and insufficient velocity resolution (0.15 m/sec) near the center of the flow do not allow a conclusive determination of whether or not the boundary layers have merged at the 34.3 or 48.8 mm axial positions. At the 110 mm position, however, the velocity profile shows the effects of merged boundary layers (see Figure 26). As the flow velocities near the centerline have decreased from the values upstream, the velocities

in the boundary layers have increased in order to satisfy continuity. Figure 27 shows that the turbulence in the annular inlet gradually increases in the center of the flow but decreases near the walls. Also, the disturbance caused by the wall discontinuity is seen to decrease as well as move away from the outer wall.

The boundary layers cover the entire flow channel at the 110 mm position but the velocity profile continues to develop as the flow moves downstream. The inlet length may be estimated using the results of Kirsten or Nikuradse discussed in the Theory section. In the case of an annulus, the channel width would be an appropriate characteristic dimension to use in determining the inlet length, since it is analogous to the diameter of a circular pipe when considering boundary layer growth. Based on Kirsten's work, the inlet length is at least 127 cm (50 inches) from the entrance to the annular interface. The minimum inlet length based on Nikuradse's results is 63 cm (25 inches). The entrance to the annular diffuser is 60 cm (23.5 inches) from the annular interface entrance.

The velocity profile development in the annular diffuser is shown in Figure 28. It shows the degree to which the velocities decrease as the flow channel increases in area. The movement of the peak velocities toward the inner wall due to its smaller boundary layer is also evident. Figure 29 shows the development of the turbulence intensity profile. There is no marked change in turbulence intensities although they are slightly less near the walls as the flow travels through the diffuser. These profiles, like

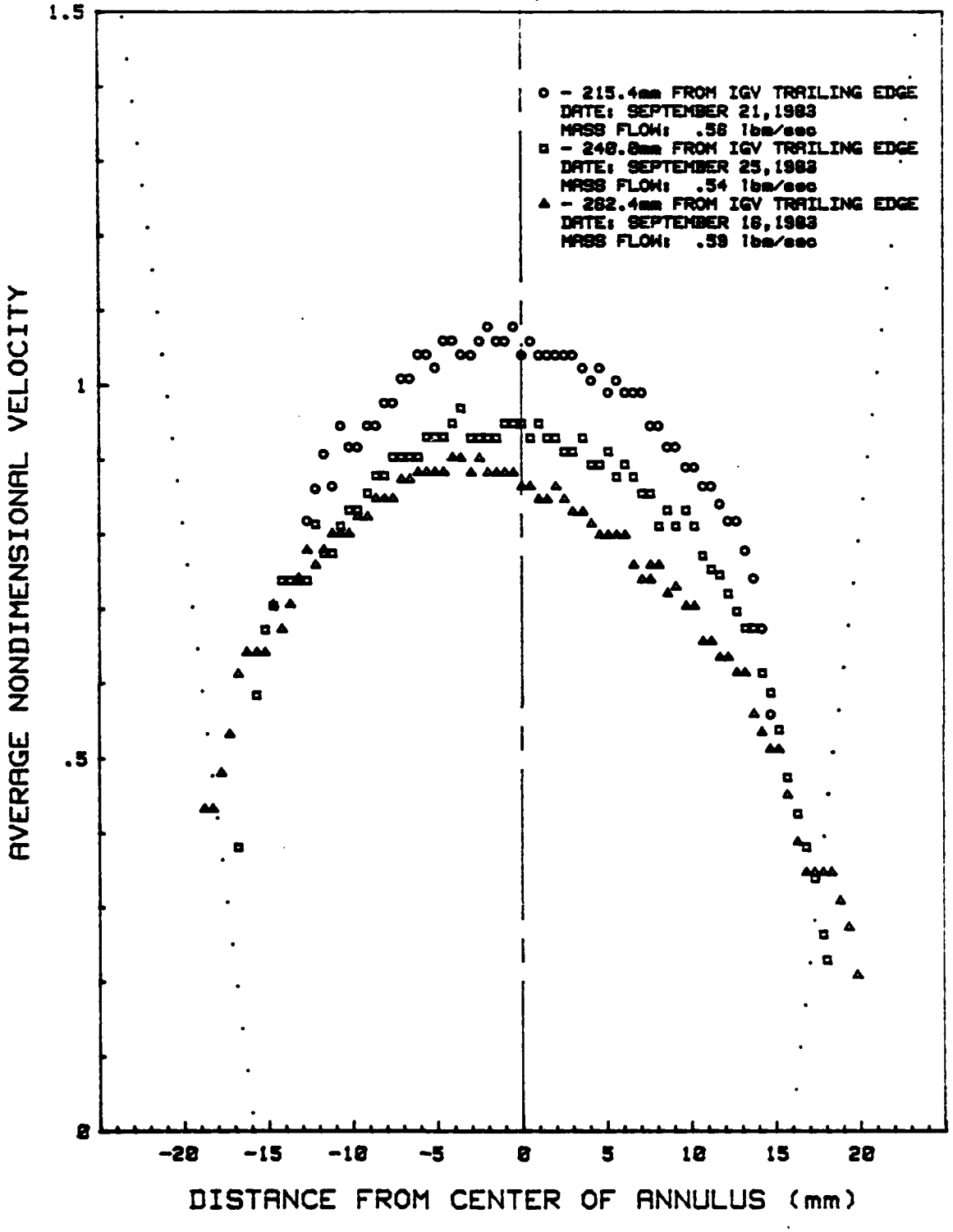


FIG. 28. ANNULAR DIFFUSER VELOCITY PROFILE DEVELOPMENT

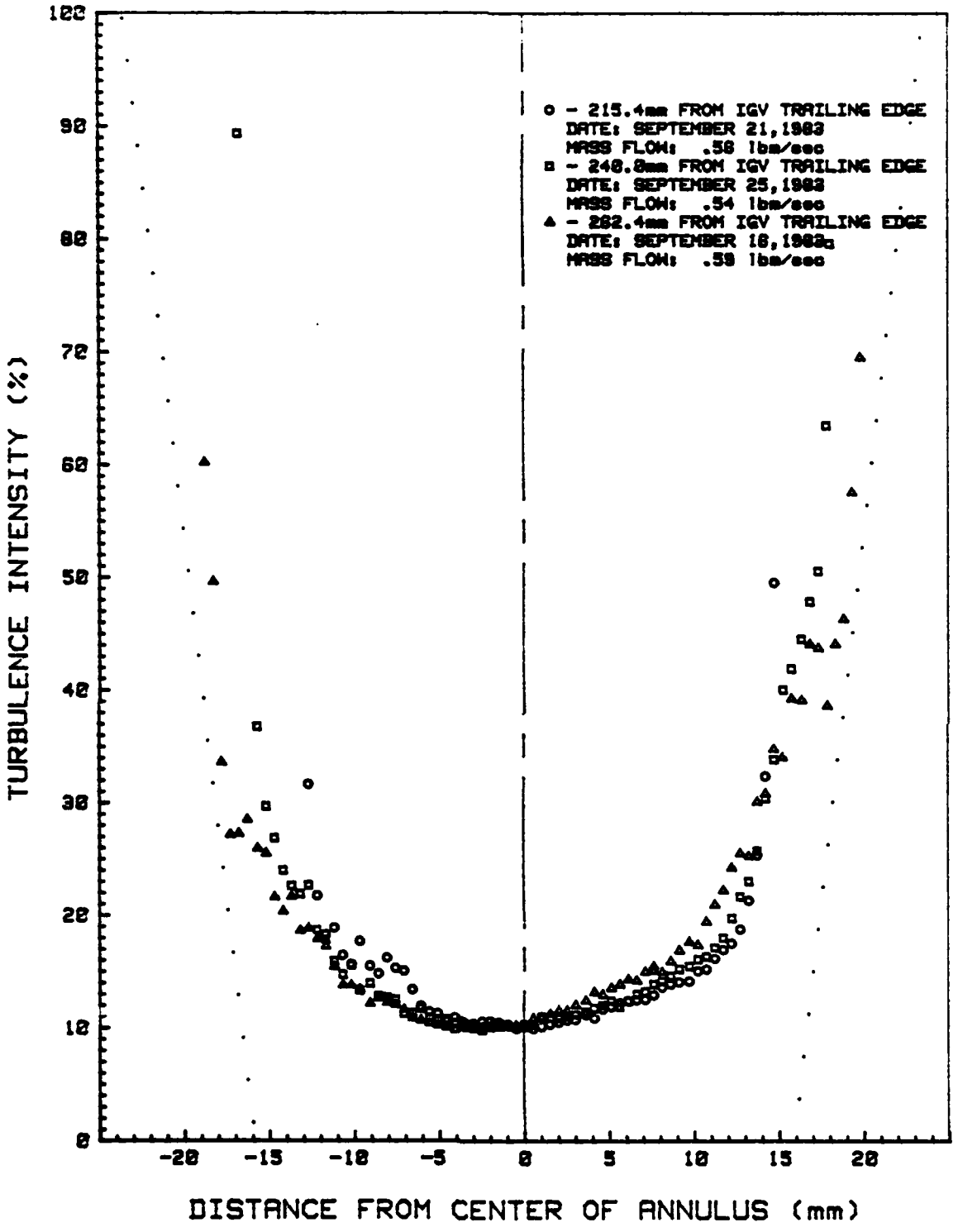


FIG. 29. ANNULAR DIFFUSER TURBULENCE INTENSITY PROFILE DEVELOPMENT

the velocity profiles, are skewed toward the inner wall because the turbulence intensity is calculated using the average velocity at each point.

LDA Repeatability

Figures 30 through 33 show the results of multiple tests at the 48.8 and 110 mm axial positions. The repeatability of the LDA measurements in the flow handling apparatus is quite good. Scatter in the data points on the velocity profiles can be due to the finite correlation time used to measure the flow. The resultant average velocity may be different than the true average obtained if the correlation time were allowed to approach infinity. Another cause for velocity point scatter, particularly near the center of the flow, is a velocity resolution which is approximately the same value as the velocity change between adjacent data points. Due to the digital nature of the correlation function, a velocity change of this amount may or may not be detected by the LDA system. For a development of the velocity resolution for this LDA system, see Appendix E.

The single biggest reason for scatter in turbulence intensity measurements is inadequate correlation times in high background light environments. Large amounts of background light and short correlation times at points in the outer half of the annulus at the 110 mm position caused the scatter in the points of Figure 33 between the 2.0 and 9.0 mm radial positions. A highly skewed and damped correlation function will also cause inaccurate, scattered

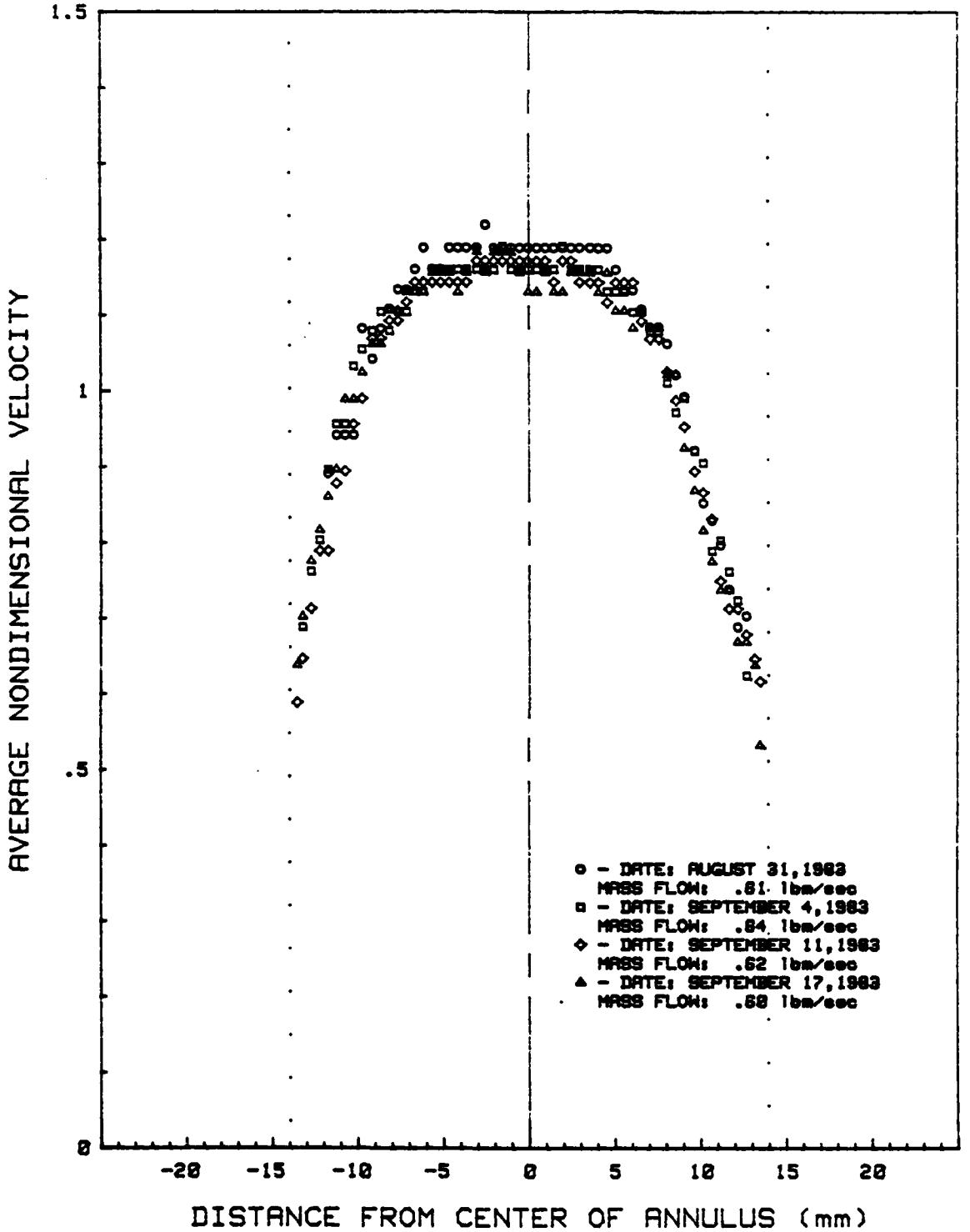


FIG. 30. LDA REPEATABILITY: VELOCITY PROFILE

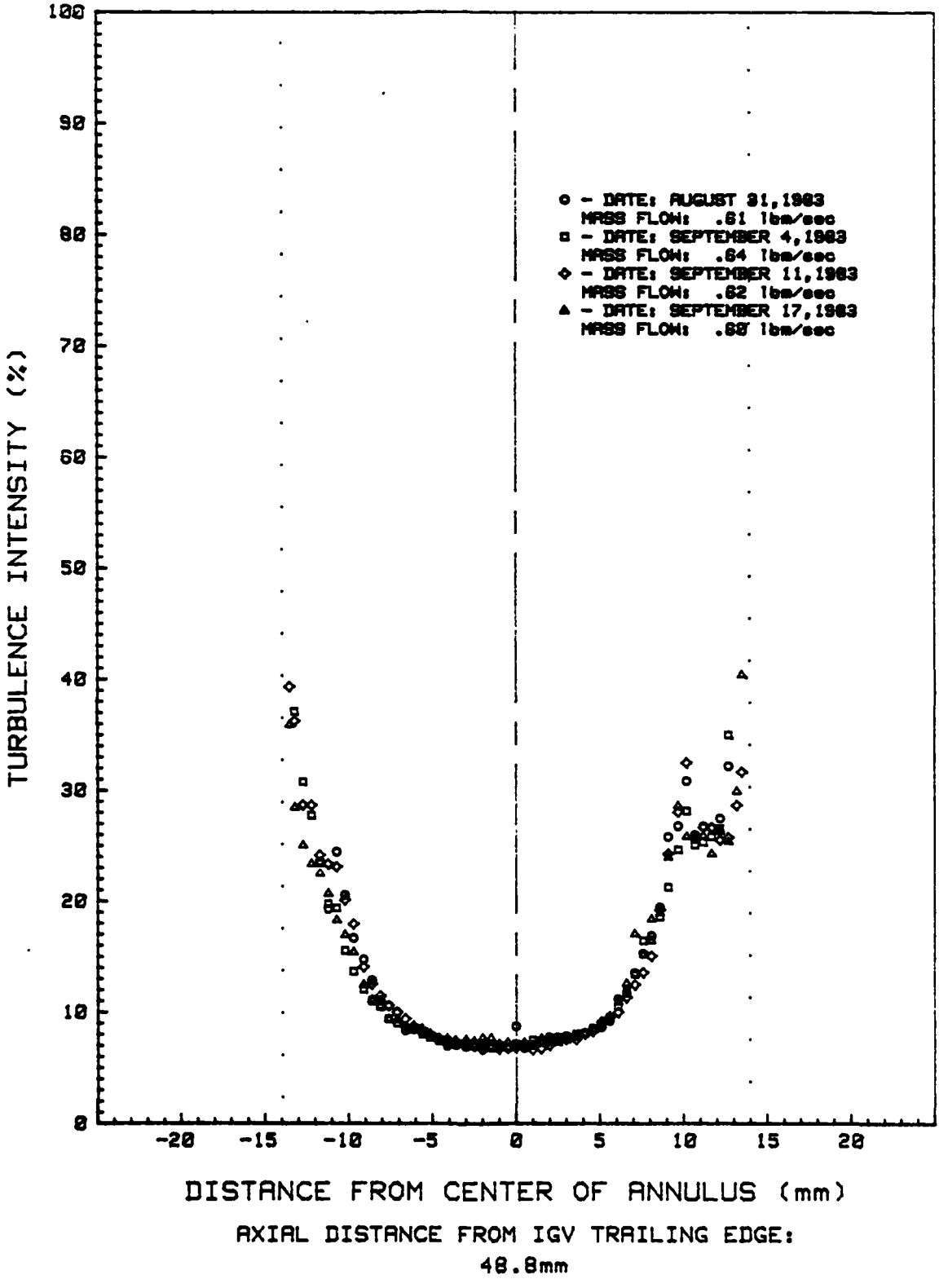


FIG. 31. LDA REPEATABILITY: TURBULENCE INTENSITY PROFILE

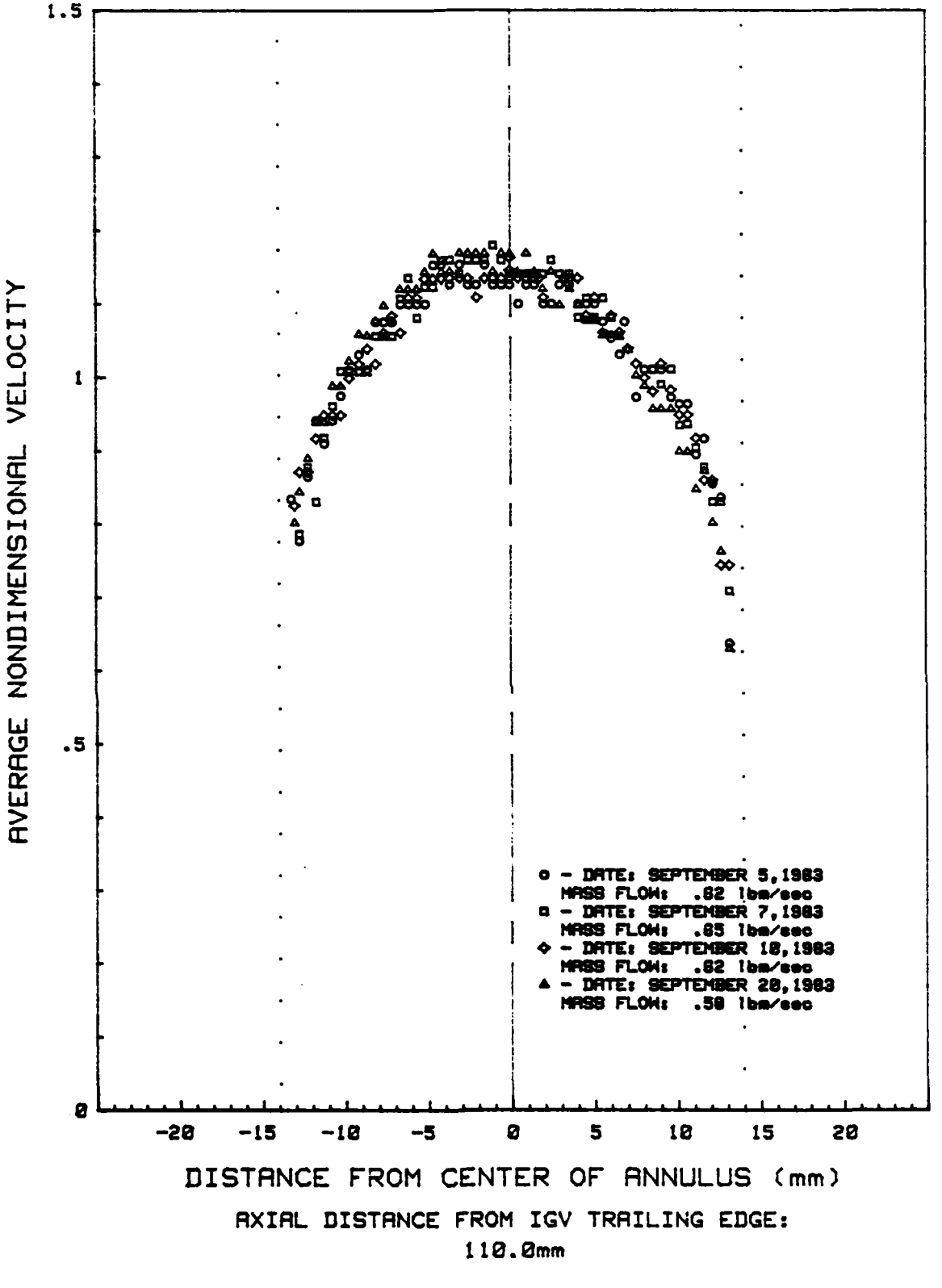


FIG. 32. LDA REPEATABILITY: VELOCITY PROFILE

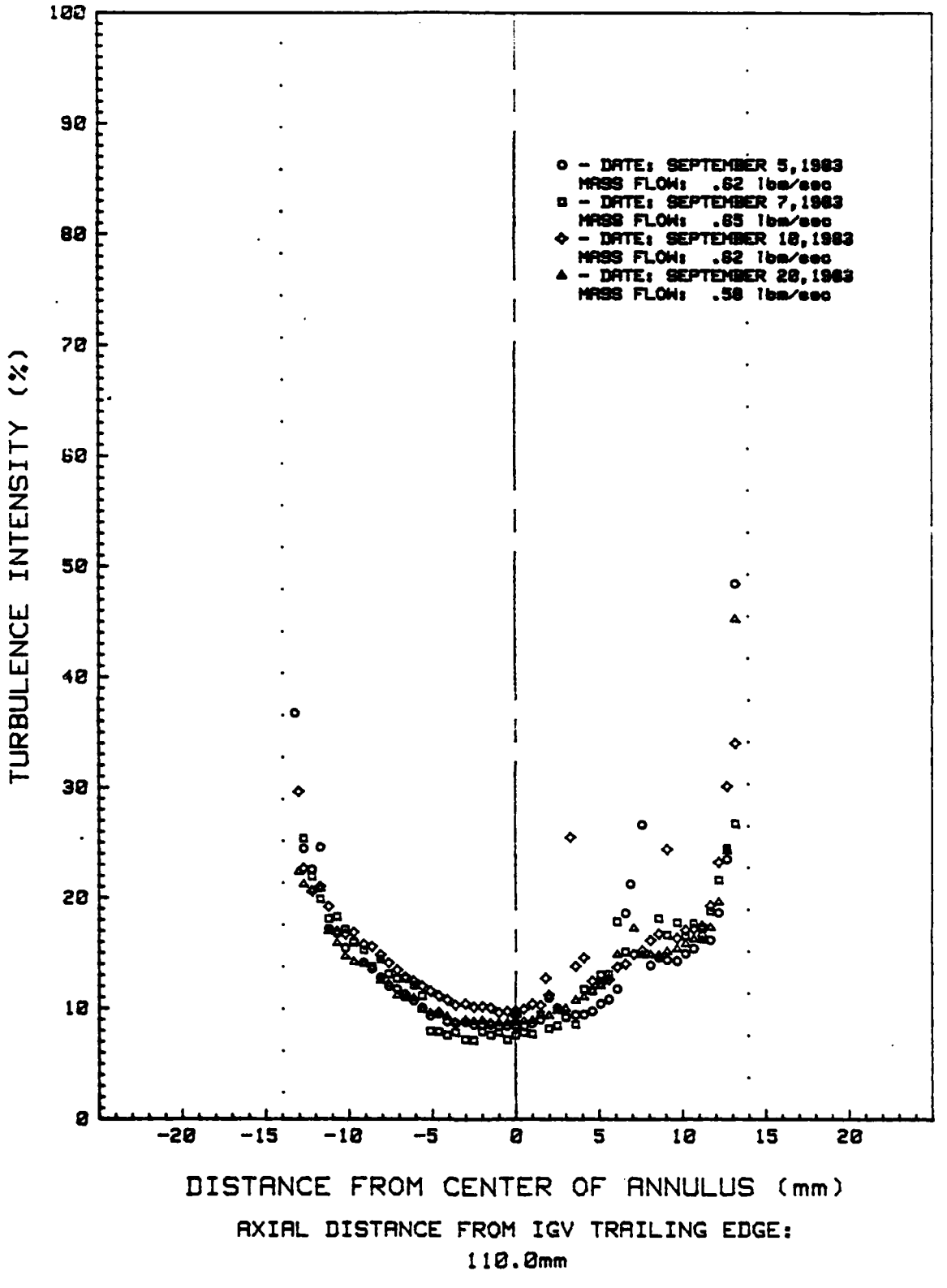


FIG. 33. LDA REPEATABILITY: TURBULENCE INTENSITY PROFILE

turbulence measurements because the data reduction method to unskew the function cannot do it as accurately as if an unskewed or slightly skewed function were generated from the start.

LDA and Hot Film Anemometer Comparison

The velocity measurements with the hot film anemometer are compared to the LDA measurements in Figures 34 through 38. The profiles agree closely except in the annular inlet test section (see Figures 34 and 35). The hot film velocities are higher near the center of the channel but close to the LDA measurements near the walls. A possible cause for this is the growth of thicker boundary layers in the hot film anemometer tests. The mass flow for the hot film tests was significantly lower than that of the LDA tests. This would result in more rapid boundary layer growth and a more rapid acceleration of the flow in the center of the channel as the flow progresses axially. After the boundary layers merge and the flow continues to develop in the inlet, the air enters the diffuser where the effect of the more rapid boundary layer growth is unnoticeable (see Figures 36 through 38).

The turbulence intensity profiles taken with the hot film anemometer are compared to the LDA data in Figures 39 through 43. The shapes of the hot film profiles are similar to the LDA profiles except in the annular inlet (see Figures 39 and 40). This difference seems to be related to the wall discontinuity. The turbulence from the discontinuity could move away from the wall more rapidly because of the quicker growth of the boundary layer in the hot film tests as compared to the LDA tests. Not including the wall

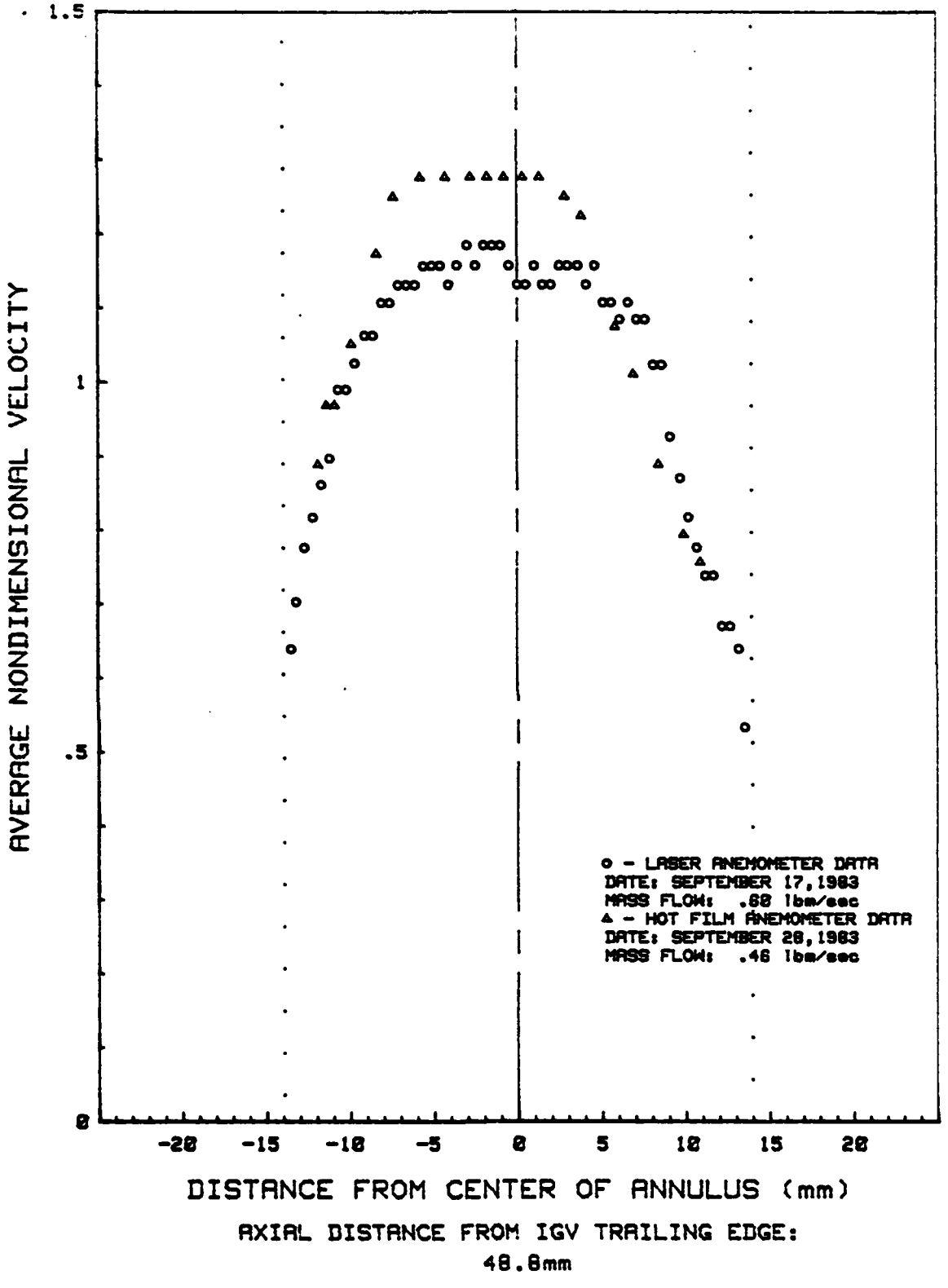


FIG. 34. LDA/HOT FILM ANEMOMETER VELOCITY PROFILE COMPARISON

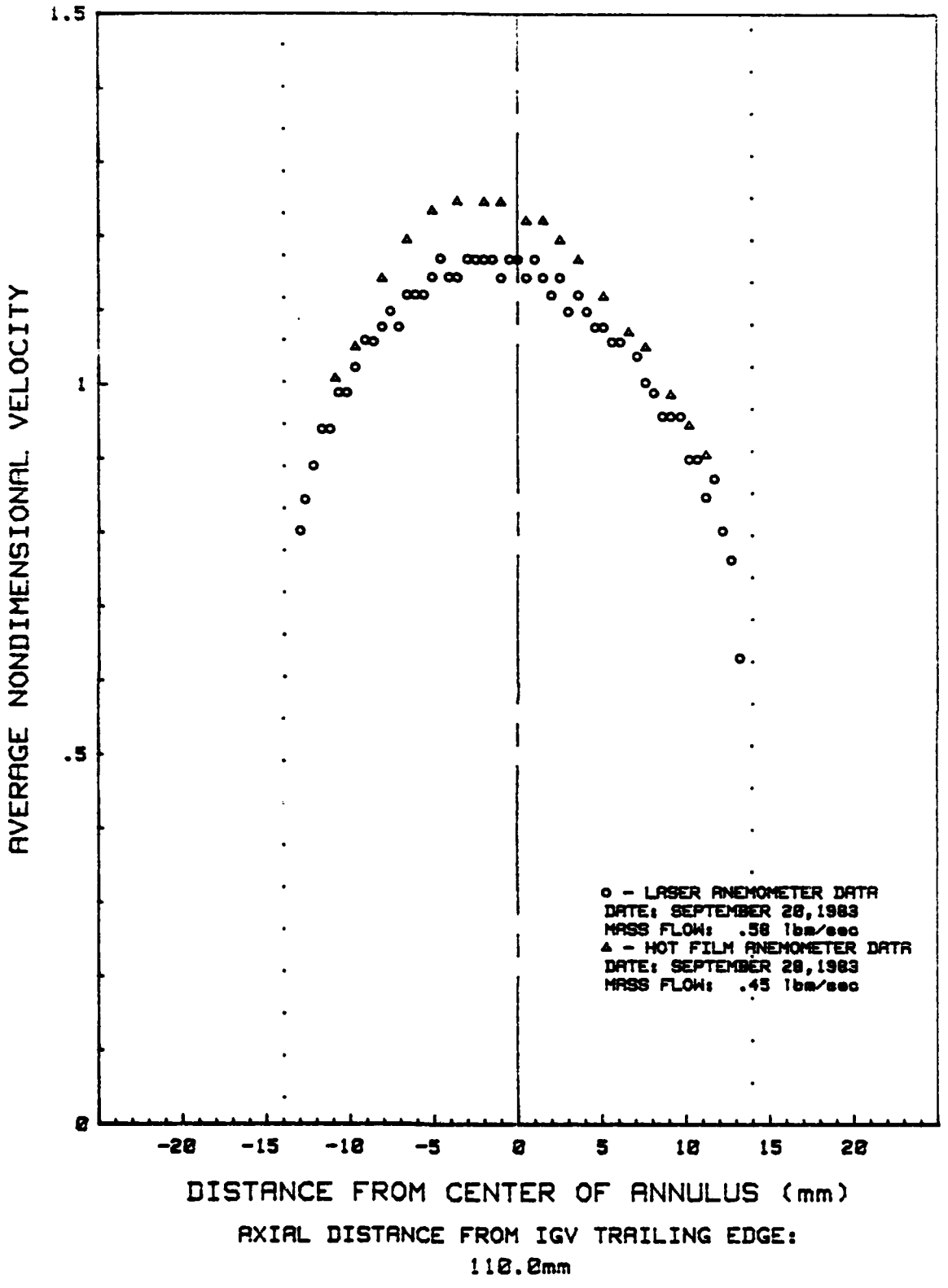


FIG. 35. LDA/HOT FILM ANEMOMETER VELOCITY PROFILE COMPARISON

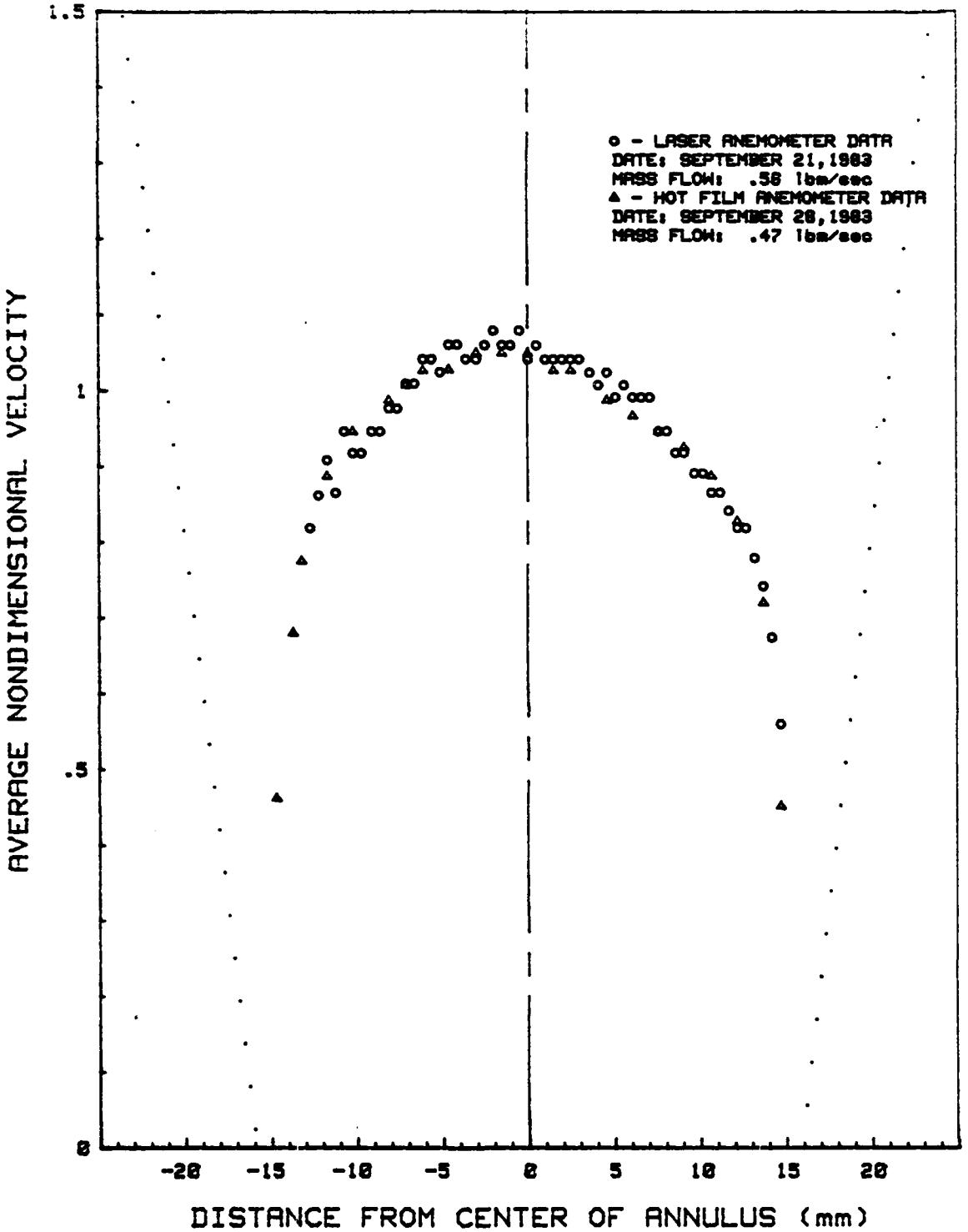


FIG. 36. LDA/HOT FILM ANEMOMETER VELOCITY PROFILE COMPARISON

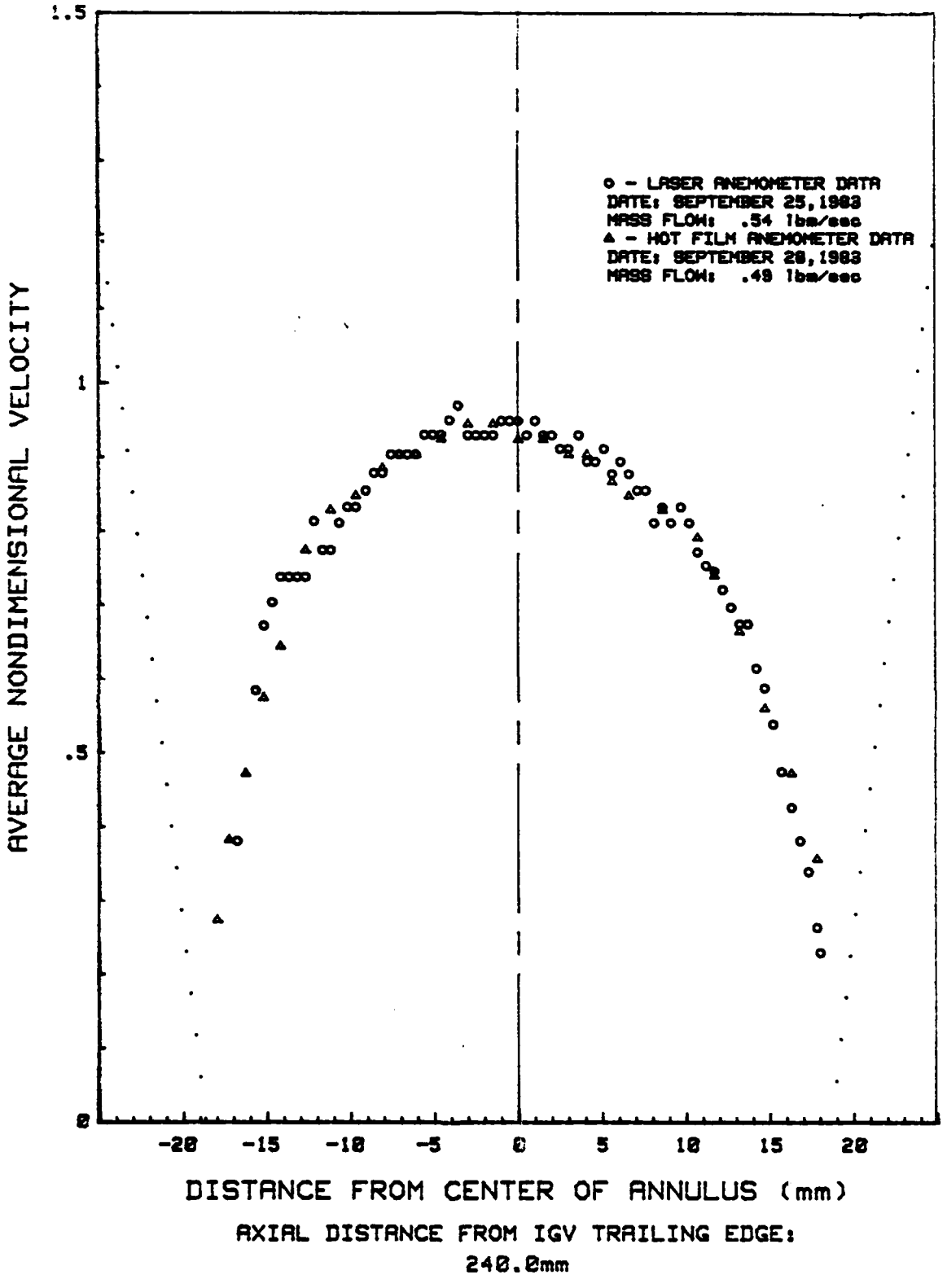


FIG. 37. LDA/HOT FILM ANEMOMETER VELOCITY PROFILE COMPARISON

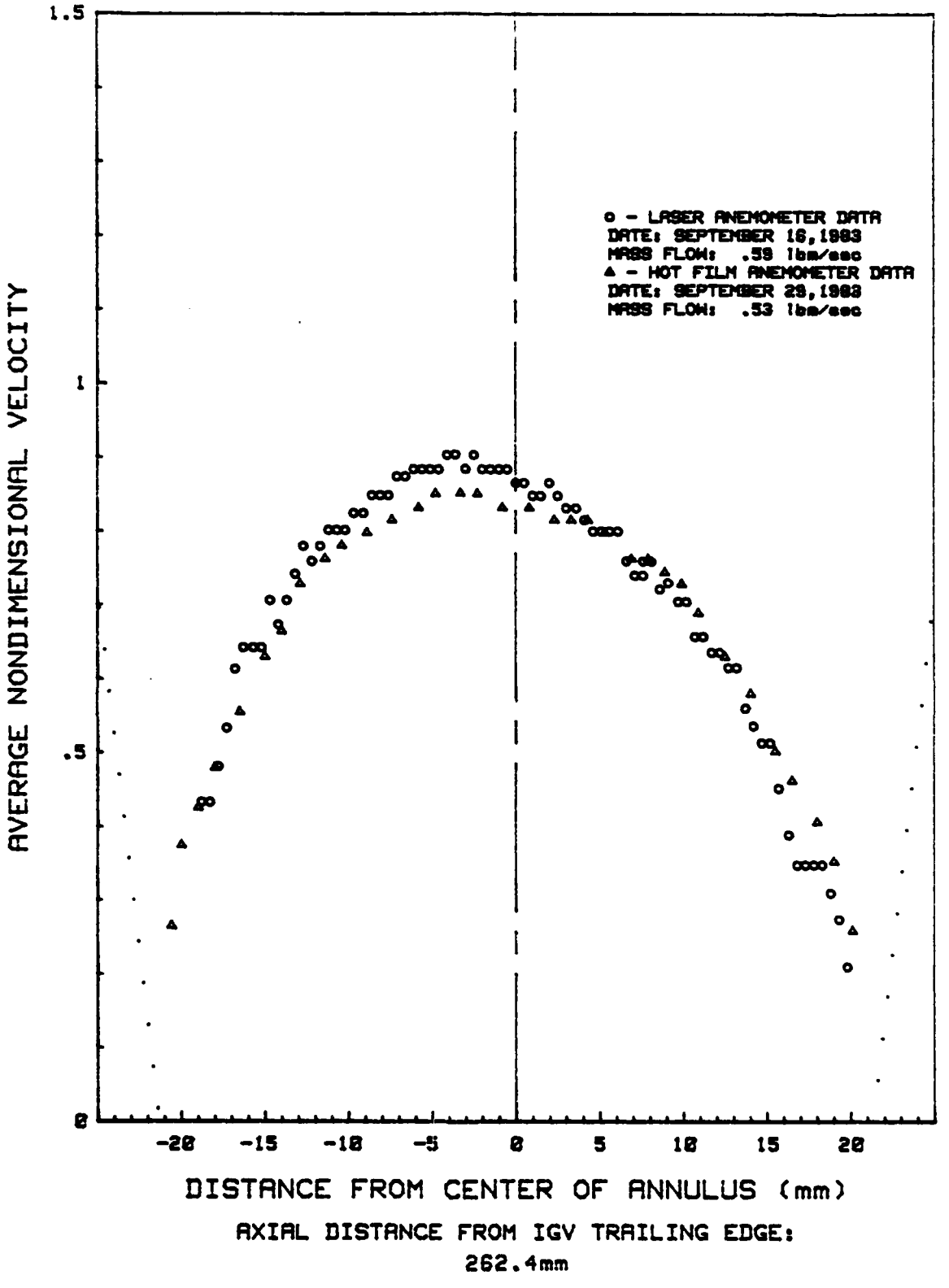


FIG. 38. LDA/HOT FILM ANEMOMETER VELOCITY PROFILE COMPARISON

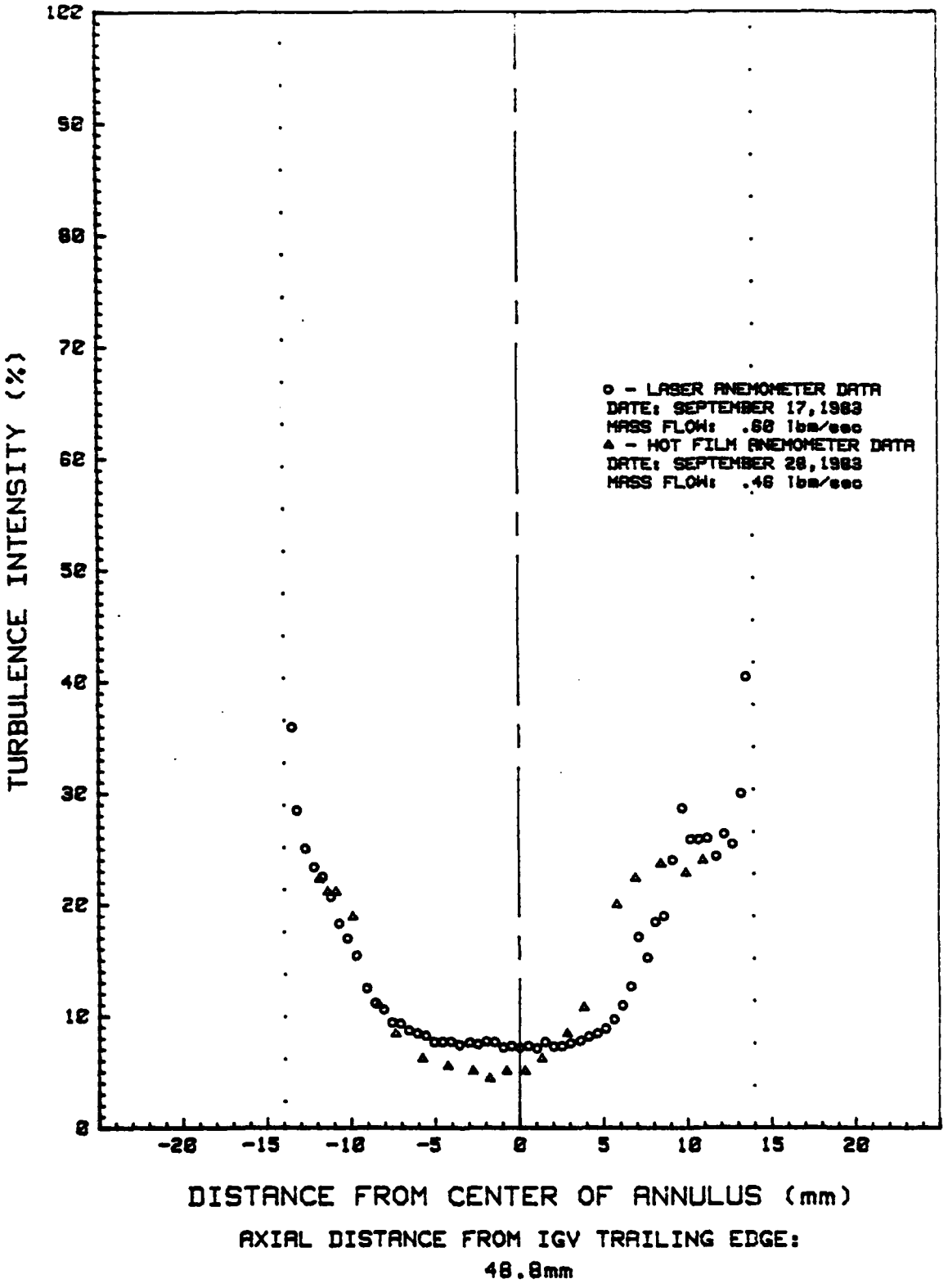


FIG. 39. LDA/HOT FILM ANEMOMETER TURBULENCE INTENSITY PROFILE COMPARISON

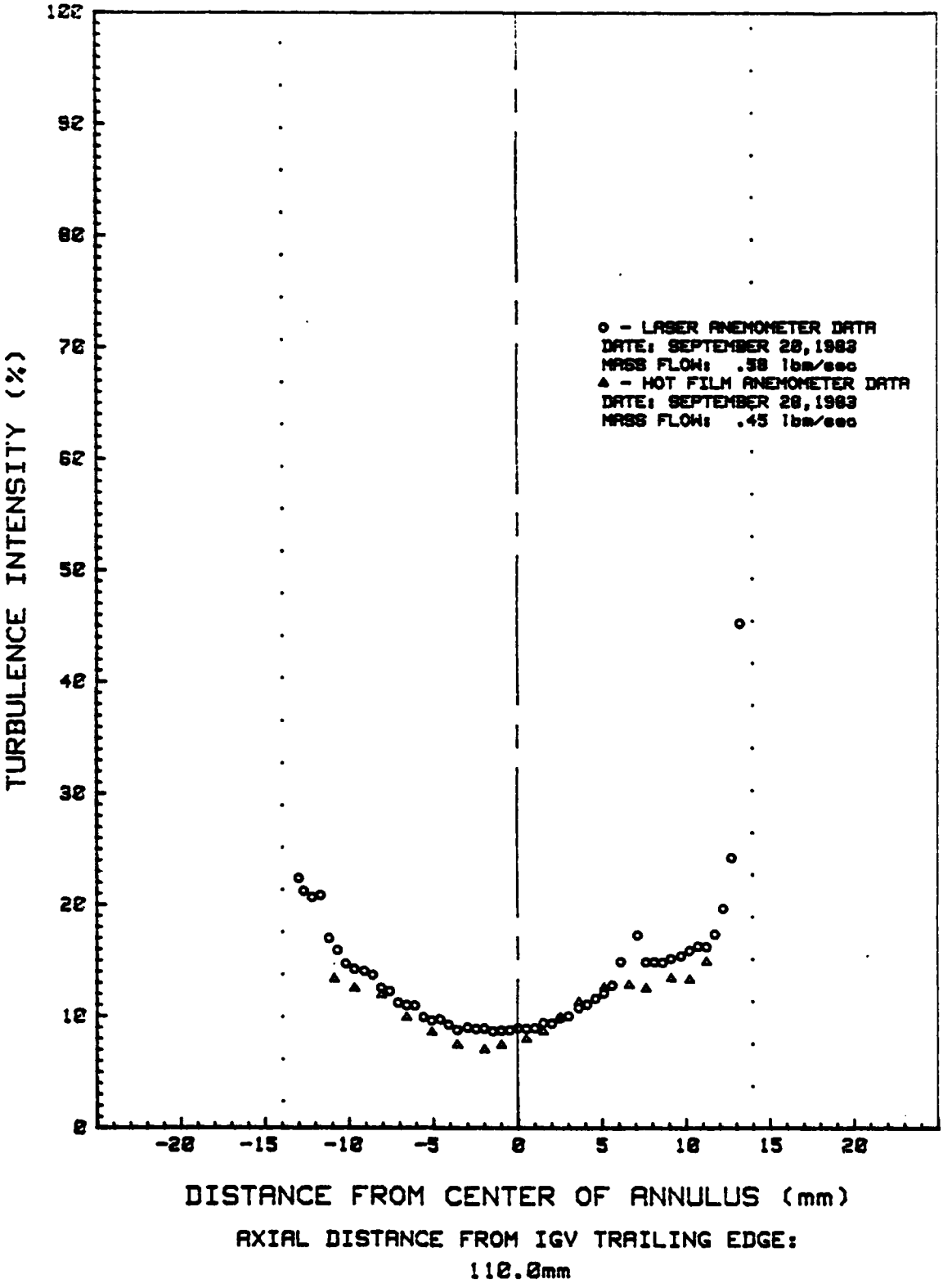


FIG. 40. LDA/HOT FILM ANEMOMETER TURBULENCE INTENSITY PROFILE COMPARISON

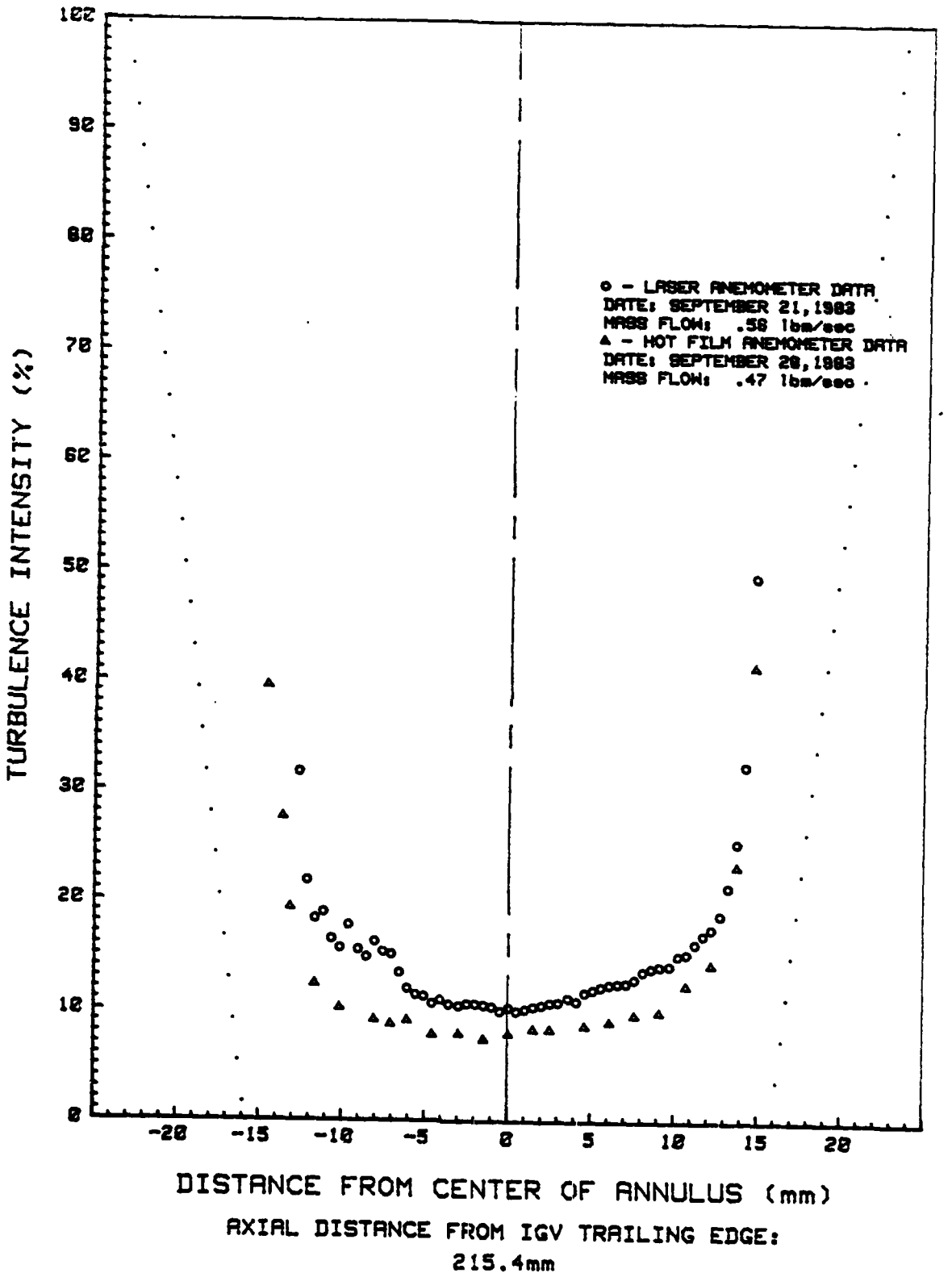


FIG. 41. LDA/HOT FILM ANEMOMETER TURBULENCE INTENSITY PROFILE COMPARISON

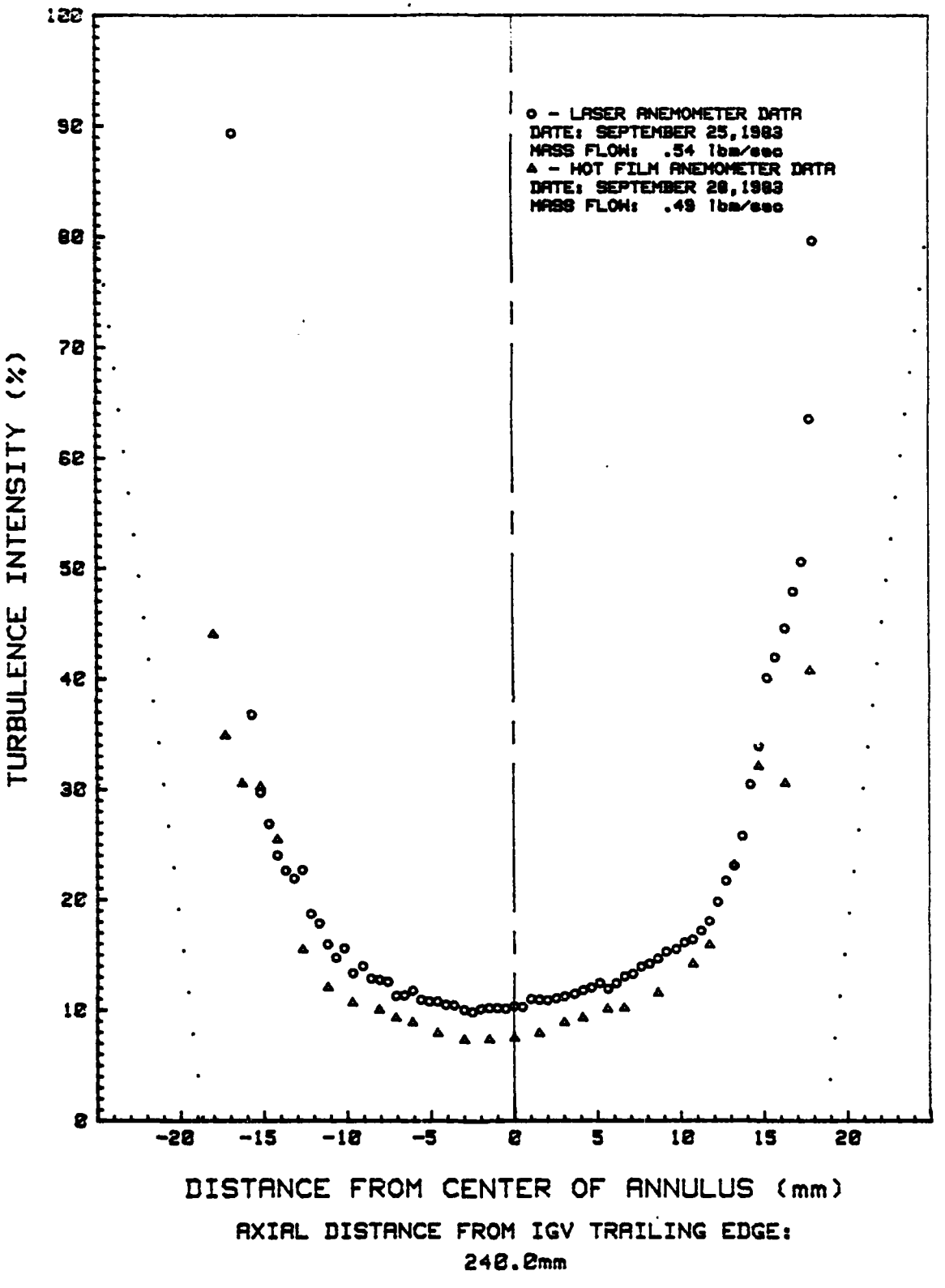


FIG. 42. LDA/HOT FILM ANEMOMETER TURBULENCE INTENSITY PROFILE COMPARISON

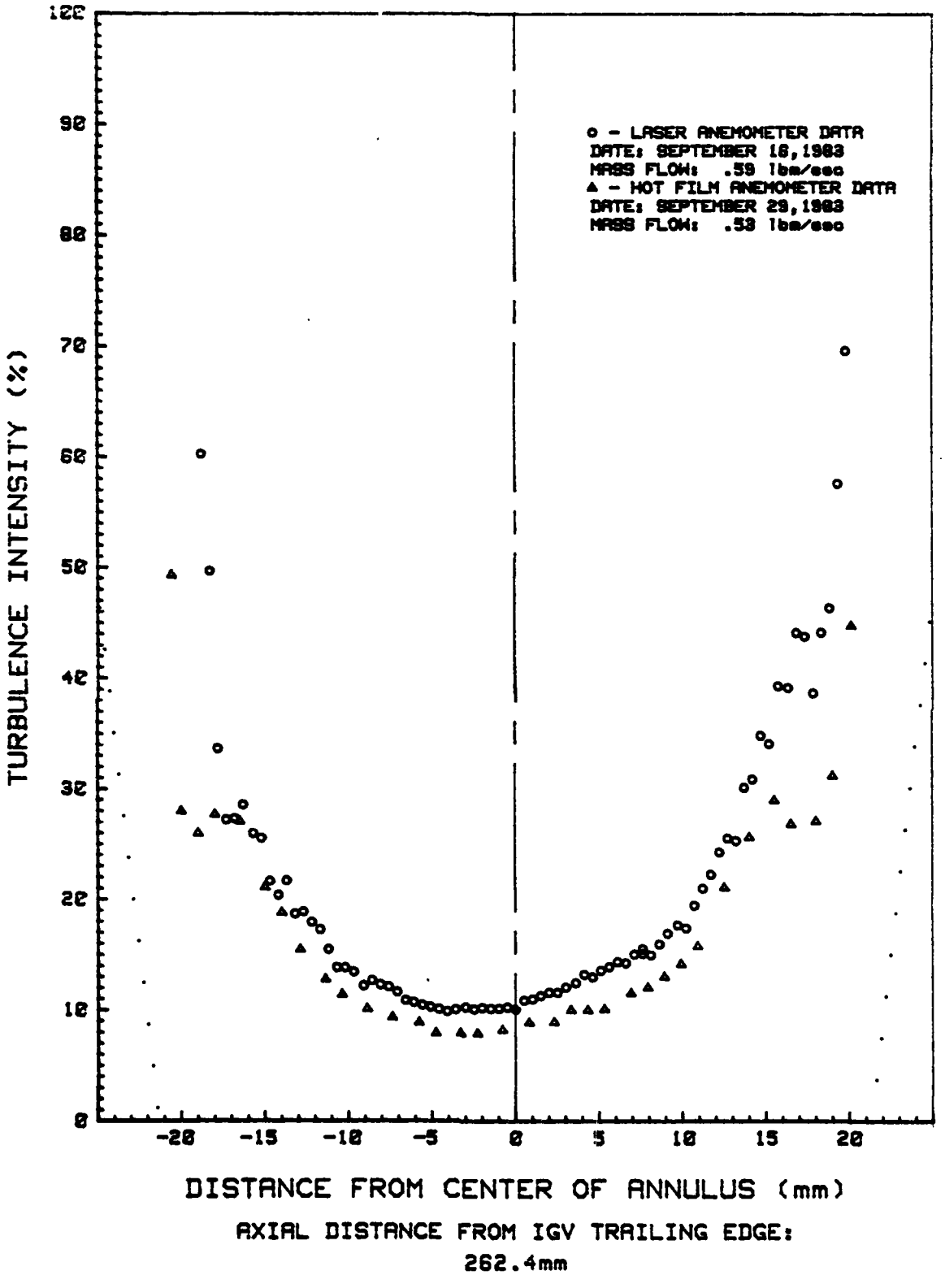


FIG. 43. LDA/HOT FILM ANEMOMETER TURBULENCE INTENSITY PROFILE COMPARISON

discontinuity disturbance, the turbulence intensities of the hot film tests are consistently lower than the LDA tests. This difference is probably due to the fact that seed particles were injected into the flow during the LDA measurements, but not during the hot film measurements. When the particle generator is operating, it injects the particles into the flow through the two 6.3 millimeter diameter orifices at jet velocities from 6.00 m/sec (19.7 ft/sec) to 6.94 m/sec (22.8 ft/sec), depending on the volume output of the unit. The local velocity of the main air flow is approximately 0.6 m/sec (2 ft/sec) at the point where the seed particles are introduced. The turbulence created by the mixing of these two streams would be carried downstream through the annular inlet and diffuser test sections.

Static Pressure Profile

The results of the static pressure measurements are contained in Table 1. The mass flow through the annulus was measured with the orifice plate flow meter and was 0.23 kg/sec (0.50 lbm/sec). The pressure recovery coefficient, $\Delta p/\bar{q}$, is defined as the static pressure rise from the pressure measured at the 29 mm axial position divided by the average dynamic pressure at the 29 mm position. (Figure 13 shows the relative positions of the data points in the test sections.) The average dynamic pressure was calculated using the air density at the 29 mm position and the continuity equation, $\dot{m} = \rho A\bar{V}$. The pressure recovery coefficient, as expected, is constant in the annular inlet. In the diffuser, it steadily in-

Table I

Static Pressure Profile

| Axial Position (mm) | Static Pressure Rise from 29mm position (N/sq m) | Pressure Recovery Coefficient |
|---|---|---|
| 29 (INLET) | 0 | 0 |
| 48 " | 0.479 | .039 |
| 67 " | 0.479 | .039 |
| 86 " | 0.479 | .039 |
| 105 " | 0.479 | .039 |
| 200 " | 0.479 | .039 |
| 211 (DIFFUSER) | 0.958 | .078 |
| 224 " | 2.394 | .196 |
| 237 " | 3.830 | .314 |
| 249 " | 5.267 | .431 |
| 262 " | 5.746 | .471 |
| 275 " | 6.224 | .510 |
| 295 " | 6.703 | .549 |
| 380 (DUMP SECTION) | 7.182 | .588 |

creases, although most of the pressure recovery occurs in the first half of the diffuser. This data indicates a well-behaved diffuser with no separated regions causing jet flow.

Photon-correlating LDA Evaluation

The above discussions have alluded to some of the advantages and disadvantages of the photon-correlating LDA system. These will now be covered in more detail.

The photon-correlating LDA provides a non-intrusive means of measuring fluid flow in small flow channels and regions close to boundary surfaces. With good optical access, the LDA can measure internal flows where it would be difficult or impossible to insert a pitot or hot film probe. Good resolution is possible in low velocity flows as is evident in the velocity and turbulence profiles discussed earlier. The low light capabilities of the photon-correlating LDA make it ideal for low scattering particle densities and low-power lasers.

Laser anemometer systems also have their drawbacks. Without a method of filtering the signal caused by high background light levels, the long correlation times of a photon-correlating LDA mean long test times to obtain the same amount of data when compared with other flow measuring systems. Long correlation times eliminate any capability to make measurements of a dynamic fluid flow. Good optical access is an absolute requirement. Additionally, the laser light reflections inherent in measuring internal flows must be controlled or avoided so they do not mask

the data completely or cause unnecessarily long correlation times. In high background light caused by these reflections, the correlation time necessary to acquire an accurate measurement cannot be predetermined. This requires a high degree of monitoring and control by the experimenter if correlation times are to be kept as short as possible. Thus, it becomes difficult to automate the flow measuring process.

The particular LDA system used in this research has limited flexibility in measuring the flow through the ADRF flow handling apparatus. The reason is a lack of phase modulator frequency shifts above one megahertz (positive or negative). Two advantages of frequency shifting are the capabilities it provides to measure flows with high turbulence intensity and to measure with high velocity resolution. While frequency shifts for the low velocities (1 to 7 m/sec) encountered in this research were adequate, they become inadequate at higher velocities. At velocities of 20 m/sec, the system can measure the flow with 0.94 m/sec resolution and turbulence intensities up to 46%. At velocities of 50 m/sec, these numbers change to 11.25 m/sec and 35%. These two figures can be improved by using larger fringe spacing with a longer focal length lens. However, the collecting optics now become the critical factor. If they are kept on the same platform as the focusing lens, the effective measuring volume becomes so large that the LDA no longer makes measurements at a "point". In this case, the effective length would be 2 mm (0.08 in) for a 500 mm focal length focusing lens and 7 mm (0.28 in) for a 1000 mm lens. The effective

measuring volume length can be reduced by larger off-axis collection angles or by keeping the collecting optics close to the test section. However, difficulties arise in keeping the collecting optics aligned with the measuring volume due to the larger distances between the focusing lens and collecting optics. Note: A short effective measuring volume, while important in measuring three-dimensional flows, is not of concern in two-dimensional flows.

AD-A137 019 A STUDY OF ANNULAR DIFFUSER FLOW USING A PHOTON-CORRELATING LASER DOPPLER..(U) AIR FORCE INST OF TECH WRIGHT-PATTERSON AFB OH SCHOOL OF ENGI.. 2/2

UNCLASSIFIED J M DIERKSEN DEC 83 AFIT/GAE/AA/83D-6 F/G 20/4 NL

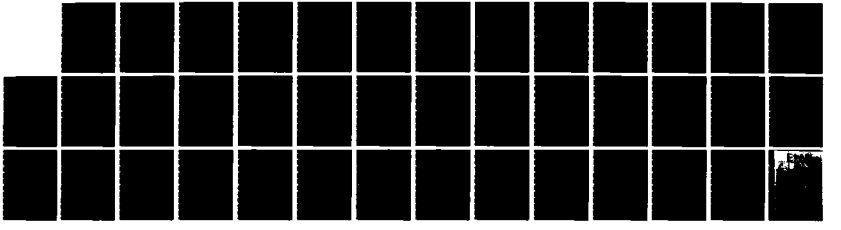

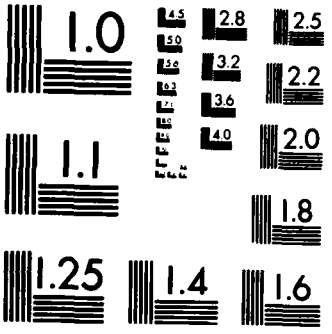

# VI. Conclusions

Well-defined velocity and turbulence intensity profiles for the flow in an annular inlet and diffuser were obtained with a photon-correlating Laser Doppler Anemometer. While the exact point of boundary layer merging cannot be determined, the boundary layers do merge before the flow enters the diffuser. Nevertheless, the flow entering the diffuser is still not fully-developed. Flat plate, turbulent boundary layer predictions over-estimated the actual thickness by approximately 20%. The velocity profiles and static pressure measurements in the diffuser indicate flow which is not separated from the walls.

A non-dimensional velocity may be used to compare profiles of tests which were run at different mass flows. While this method is useful, it does not completely substitute for the comparison of tests at the same mass flow which have the same boundary layer growth rate.

The photon-correlating Laser Doppler Anemometer used in this research is well-suited to study the flow in the ADRF flow handling apparatus. The system, however, has three factors which limit its flexibility in measuring three-dimensional, internal flows. Its limited frequency shifting capability combined with the need to place the collecting optics close to the measuring volume limit it to the measurement of low speed flows. Without a means of filtering the signal caused by background

light, the LDA system is limited to steady flow situations and requires long correlation times for each data point.

## VII. Recommendations

The following recommendations are made for further studies using the ADRF flow handling apparatus:

1) Make flow studies using different diffuser geometries and higher mass flows, within the limitations of the LDA system.
2) Incorporate an active system to control the mass flow of the air supply.
3) Modify the optical platform to allow the PM assembly to be mounted on the opposite side of the focusing lens. This would allow the collecting optics to avoid laser beam reflections in the diffuser to obtain data points closer to the inner wall.
4) Use test section windows which have an anti-reflective coating for the helium-neon laser wavelength.
5) Incorporate a means of filtering the PM assembly signal to reduce or eliminate the effects of background light.
6) Add a computer-controlled traversing mechanism to the optical platform to move it in the radial direction. This would significantly reduce test times compared to tests requiring manual movement of the measuring volume.
7) Increase the range of phase modulator frequency shifting.

8) Investigate the effects on turbulence intensity of the method of flow seeding used in this study.

## Bibliography


1. Kelley, J. V. Design, Fabrication and Testing of an Axisymmetric, Annular, Subsonic Diffuser and Associated Instrumentation Systems. MS Thesis. School of Engineering, Air Force Institute of Technology (AU), Wright-Patterson AFB OH, December 1981.

2. Moore, R. M. Design, Fabrication and Instrumentation of an Annular Diffuser Research Facility. MS Thesis. School of Engineering, Air Force Institute of Technology (AU), Wright-Patterson AFB OH, December 1982.

3. Crawford, M. E. and Kays, W. M. Convective Heat and Mass Transfer. New York: McGraw-Hill Book Company, 1980.

4. Schlichting, H. Boundary-Layer Theory. New York: McGraw-Hill Book Company, 1979.

5. Abbiss, J. B. et al. "Laser Doppler Anemometry," Optics and Laser Technology, 6: 249-261 (December 1974).

6. Malvern Instruments, Ltd., Laser Photon Correlation Velocimeter System: Operating and Installation Manual, Spring Lane Trading Estate, Malvern Link, Worcestershire WR14 1AL, England.

7. TSI LDV-879-23M-2MBRI. Laser Velocimetry Systems. Product Brochure and Technical Summary. Thermo-Systems, Inc., St. Paul MN, 1979.

8. Schulz-DuBois, E. O. "High Resolution Intensity Interferometry by Photon Correlation," Photon Correlation Techniques in Fluid Mechanics, edited by E. O. Schulz-DuBois. New York: Springer-Verlag Berlin Heidelberg, 1983.

9. Birch, A. D. et al. "Photon Correlation Spectroscopy and Its Application to the Measurement of Turbulence Parameters in Fluid Flows," Journal of Physics D: Applied Physics, 8: 438-447 (March 11, 1975).

10. Foord, R. et al. "A Solid-State Electro-optic Phase Modulator for Laser Doppler Anemometry," Journal of Physics D: Applied Physics, 7: L36-L39 (January 21, 1974).

11. Walterick, R. E. An Experimental Investigation of the Near Wake of a Circular Cylinder. MS Thesis. School of Engineering, Air Force Institute of Technology (AU), Wright-Patterson AFB OH, September 1980.

12. Neyland, D. L. Hardware and Software Integration for Concurrent Data Acquisition and Reduction of Photon Correlated Laser Doppler Velocimetry. MS Thesis. School of Engineering, Air Force Institute of Technology (AU), Wright-Patterson AFB OH, December 1981.

13. Stephens, D. G. Turbulence Measurement in an Ejector Wing Flow Field Using Photon Correlated Laser Doppler Velocimetry. MS Thesis. School of Engineering, Air Force Institute of Technology (AU), Wright-Patterson AFB OH, December 1981.

## Appendix A:

## Measuring Volume Size

The actual size of the measuring volume is defined by the $1/e^2$ intensity contour and may be calculated using Eqs (19) and (20)

$$d_m = \frac{2\lambda f}{\pi r_o \cos\left(\frac{\theta}{2}\right)} \tag{19}$$

$$l_m = \frac{2\lambda f}{\pi r_o \sin\left(\frac{\theta}{2}\right)} \tag{20}$$

where $d_m$ is the measuring volume diameter, $l_m$ is the measuring volume length along the major axis of the ellipsoid, and $r_o$ is the unfocused $1/e^2$ beam radius (7:97). The number of fringes in the measuring volume can be calculated using Eq (21).

$$N = \frac{d_m}{d_f} \tag{21}$$

The collecting optics, however, determine the effective measuring volume size because they may only collect scattered light from a portion of the actual measuring volume. The geometry of the collecting optics is shown in Figure 44. This figure shows the collecting optics to be in the same plane as the two laser beams, but this does not have to be the case. The effective measuring volume length can be calculated using Eq (22)

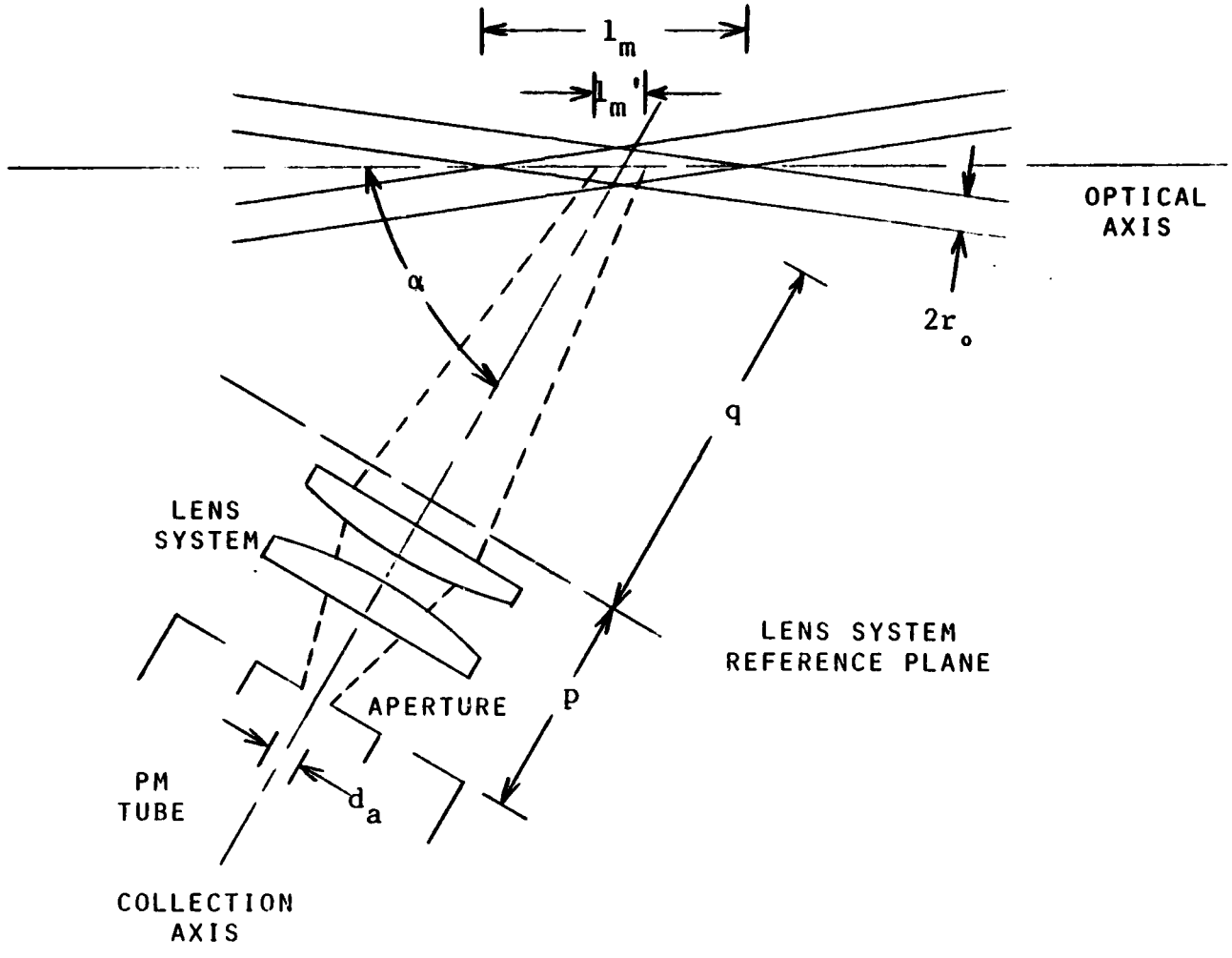


FIG. 44. COLLECTING OPTICS GEOMETRY

$$l_m' = d_a \frac{q}{p \sin \alpha} \tag{22}$$

where $\alpha$ is the angle between the optical axis and the collection axis (7:98). The effective measuring volume length will be the lesser of $l_m$ and $l_m'$ since it can never be larger than $l_m$. A similar method can be used to calculate the effective vertical dimension of the measuring volume by replacing sin $\alpha$ with the cosine of the angle ($\beta$) between the collection axis and the plane of the two intersecting beams.

$$d_m' = d_a \frac{q}{p \cos \beta} \tag{23}$$

Likewise, the effective vertical dimension will be the lesser of $d_m$ and $d_m'$. Lastly, the effective horizontal dimension (perpendicular to the fringe planes) will be the lesser of $d_m$ and $d_m''$ where $d_m''$ is defined by Eq (24).

$$d_m'' = d_a \frac{q}{p \cos \alpha} \tag{24}$$

The following are the applicable dimensions for the optical geometry of the LDA system used in this research.

| | | | |
|---|---|---|---|
| $\lambda$ | = 6328 ($10^{-10}$) m | p | = 205 mm |
| f | = 250 mm | q | = 211 mm |
| $r_o$ | = 0.55 mm | $\alpha$ | = 16.9° |
| $\theta$ | = 4.58° | $\beta$ | = 1.7° |
| $d_m$ | = 183 $\mu$m | $l_m'$ | = 354 $\mu$m |
| $l_m$ | = 4581 $\mu$m | $d_m'$ | = 103 $\mu$m |
| $d_a$ | = 100 $\mu$m | $d_m''$ | = 108 $\mu$m |

## Appendix B:

## LDA Optical Alignment Procedure

The first step in the procedure involves mounting and aligning the laser/beamsplitter and phase modulator on the steel mounting channel. When the laser is on during the alignment procedure, protective goggles should be worn, not only for safety reasons, but because they reduce the reflected laser light from surfaces and give a more accurate indication of the beam center. The beamsplitter is adjusted so the two laser beams are parallel and 20 mm apart. The laser is mounted to the steel mounting channel so the plane of the beams is parallel to the mounting surface and at the correct height for the phase modulator. After the beams and phase modulator are aligned as specified in the system operating manual (reference 6), the final adjustment of the beamsplitter is made to ensure the beams are parallel and 20 mm apart. This is done to correct for any possible flaws in the phase modulator optics which could affect the parallel nature or 20 mm separation of the beams. The laser, beamsplitter, and phase modulator can now be treated as a single unit which can be aligned with the remaining optics using the four adjustable legs on the mounting channel.

The second unit in the alignment process is the optical platform which contains the remainder of the transmitting and collecting optics. The optical platform is mounted on the lab-

oratory bench so it translates in a direction perpendicular to the bench rails and is leveled in the horizontal plane. The beams are then aligned on the lower periscope mirror so as the optical platform is translated, the beams always project to the same points on a screen fixed to the platform. With the beams projecting on a screen attached to the annular inlet test section window, the periscope mirrors are adjusted to keep the beam projections stationary as the platform is translated. The focusing lens is placed in its holder and an alignment mask is inserted into the lens. The mask is an aluminum disk which snugly slides into one side of the lens. It has two 0.75 millimeter (0.03 in) diameter holes, each 10 millimeters (0.39 in) from the center along the same diameter. Scribe marks on the mask are aligned with marks on the lens holder to ensure the alignment holes are horizontal. The focusing lens can then be positioned so the beams pass through the alignment holes. This aligns the center of the lens with the optical axis. As the platform is translated, the beams can be rechecked to ensure they always pass through the alignment mask holes. The beams are then focused on the test section centerbody and the PM assembly positioned so the image is centered and focused on the aperture. Gross focusing adjustments are made by moving the PM assembly on the optical platform while fine focusing is done with the collecting lens. The PM assembly is aligned with the laser beams focused on the test section centerbody to account for the effects of beam refraction through the test section windows. The optical plat-

form is positioned in the vertical direction to place the measuring volume in the horizontal plane passing through the test section centerbody axis. This plane is centered between two IGV blades upstream of the annular inlet test section. Finally, with the beams focused on the centerbody, the laboratory bench is positioned so the beams remain focused as the bench is translated.

## Appendix C:

## LDA Velocity and Turbulence Calculations

The velocity and turbulence measurements of the photon-correlating LDA are based on the intensity autocorrelation function. This function is simply a time correlation of the scattered light intensity which highlights the periodic nature of the signal. The periodicity is due to the ordered motion of the particles transiting the measuring volume. In other words, most particles are moving in the same direction with the same velocity. For these reasons, the time between $\tau = 0$ and the value of $\tau$ where the next peak of the autocorrelation function occurs is a measure of the average time it takes the particles to travel a specified distance. This distance, using the fringe model, is the fringe spacing and the velocity may be calculated with Eq (25)

$$u = \frac{d_f}{(Pk2-3)\ t_s} \tag{25}$$

where Pk2 is the channel number (value of $\tau$) at which the autocorrelation function reaches its first peak after the first valley (see Figure 45) (6:6-5).

Turbulence in the flow is indicated by damping of the correlation function. Due to flow turbulence, the velocity of every particle is a function of time so some of the particles in a fringe at any specified time will not reach the next fringe

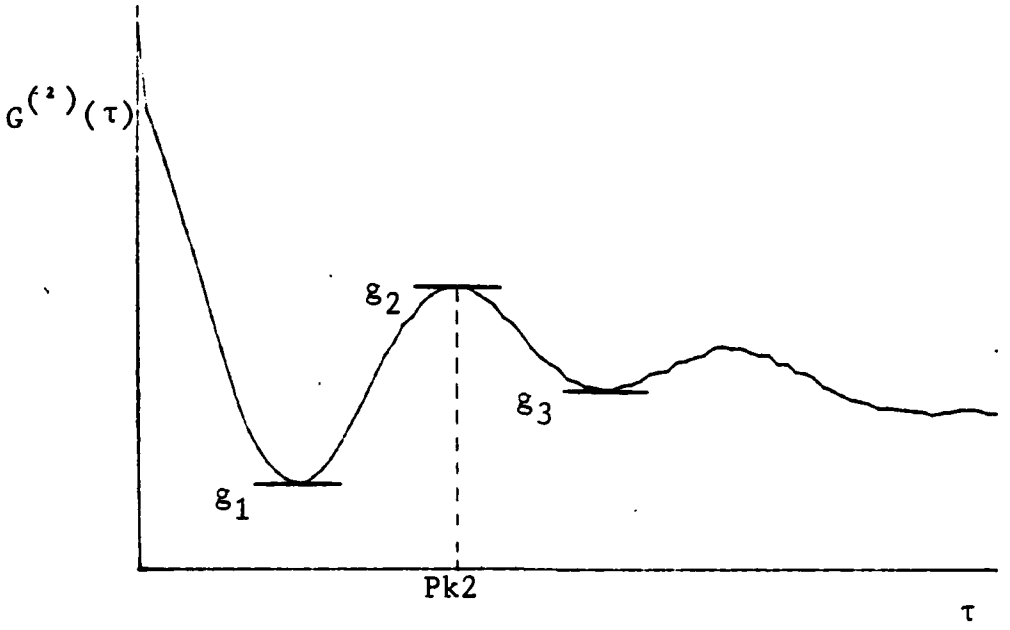


FIG. 45. CORRELATION FUNCTION: VELOCITY AND TURBULENCE INFORMATION

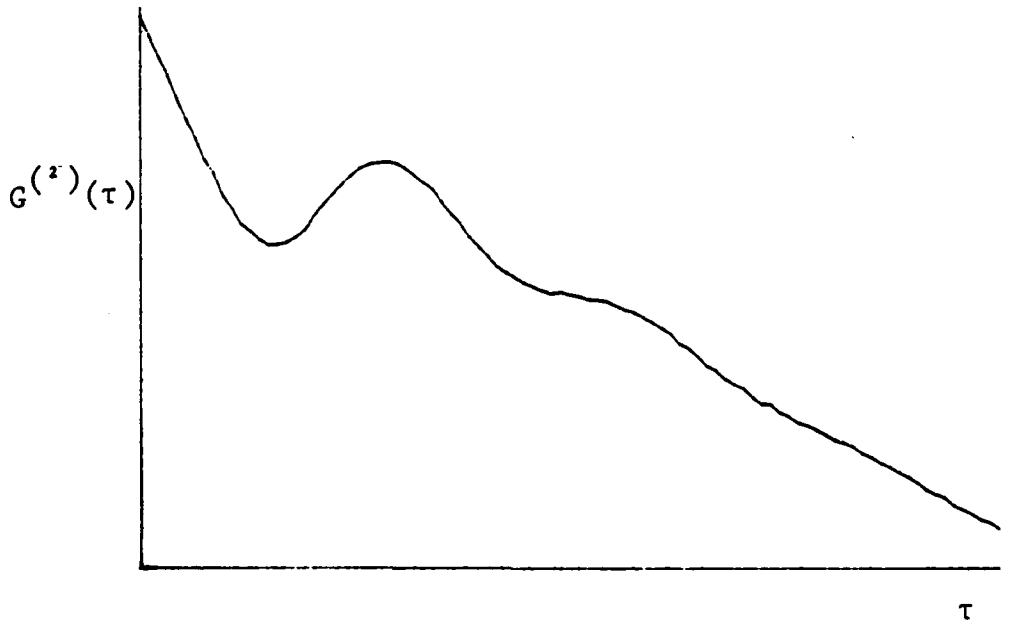


FIG. 46. SKEWED CORRELATION FUNCTION

at the same time in the future as the other particles. This results in less time correlation in the signal for increasing values of $\tau$. The result is a damped autocorrelation function. The turbulence intensity may be calculated from the correlation function using Eqs (26) and (27)

$$R = \frac{g_2 - g_1}{g_2 - g_3} \tag{26}$$

$$\eta = \frac{1}{\pi} \left(\frac{1}{2}(R-1) + \frac{2}{N^2}\right)^{\frac{1}{2}} \tag{27}$$

where $g_1$, $g_2$, and $g_3$ are the values of the correlation function at the first valley, the next peak, and the second valley respectively (see Figure 45) (6:6-6). Also, N is the number of fringes in the $1/e^2$ radius of the measuring volume and $\eta$ is the turbulence intensity.

The correlation function may be skewed due to an insufficient number of fringes in the control volume or the detection of background light (see Figure 46) (13:91). This skewedness must be removed from the correlation function before the information for velocity and turbulence calculations is extracted. The method used to do this is described by Stephens (reference 13). A brief summary is included here.

A mean line from which the correlation function can be unskewed must first be determined. A least-squares polynomial curvefit through the local maxima (peaks) and another curvefit through the local minima (valleys) is determined. A mean line

is then calculated at each correlator channel by averaging the value of the two curves at that channel. The unskewed correlation function is the difference between the skewed function and the mean function. It is from the unskewed correlation function that the values of $g_1$, $g_2$, $g_3$, and Pk2 are taken.

The equations discussed earlier are strictly for use when phase modulation of the laser beams is not employed. They are, however, the basis of the equations used to calculate average velocity and turbulence intensity when phase modulation is in use. Figure 47 shows the effects of phase modulation (frequency shifting) on the correlation function in measuring the same point in a flow. With positive frequency shifting (DRIVE mode), the fringes move in the direction of the flow component being measured. On the other hand, the fringes move in the opposite direction with negative frequency shifting (INVERT mode). Thus, the correlation function contains velocity and turbulence information of the particles with respect to the reference frame of the fringes. To calculate the particle velocity with respect to the laboratory reference frame, Eq (28) is used.

$$u = u^{*} + \Delta F(d_f) \tag{28}$$

In this equation, $u^{*}$ is the velocity of the particle with respect to the fringes and is calculated from the unskewed correlation function. A velocity is first calculated from the unskewed correlation function and then adjusted for frequency shifting.

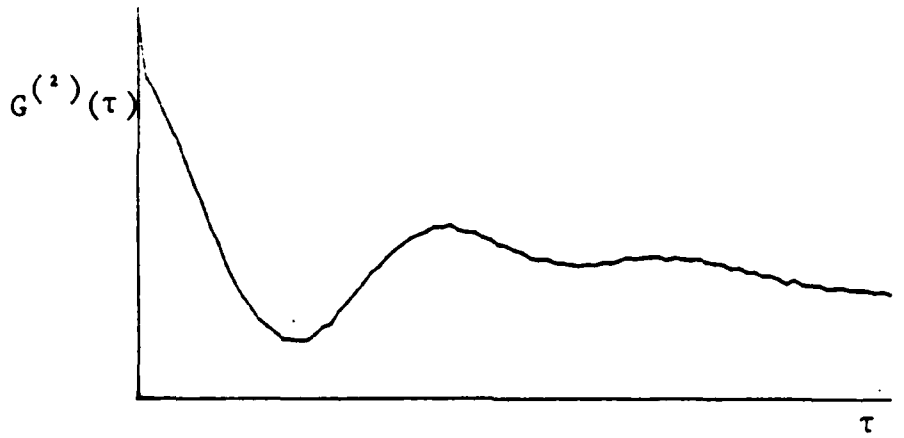


(A) POSITIVE FREQUENCY SHIFTING

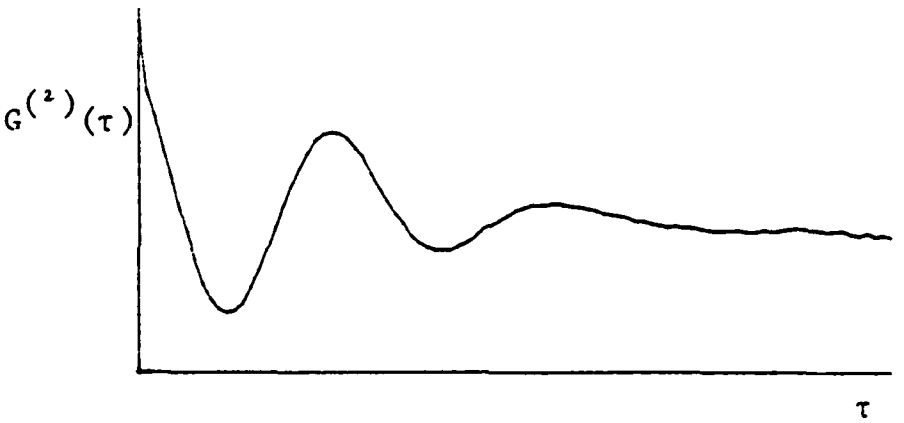


(B) ZERO FREQUENCY SHIFTING

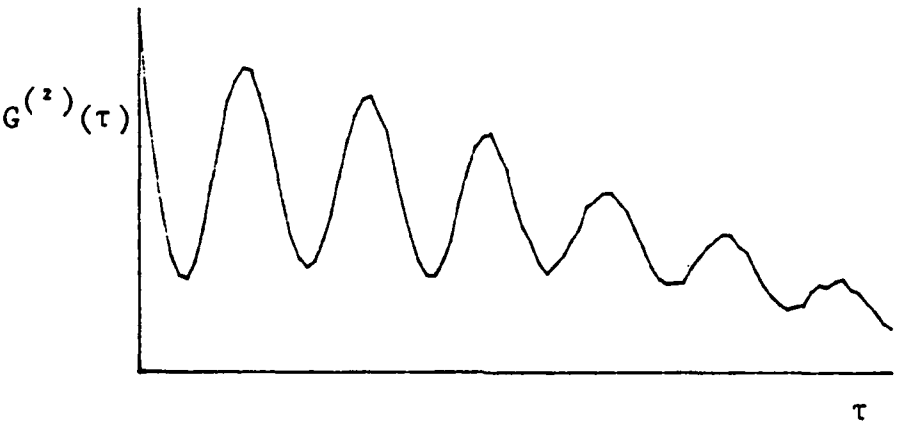


(C) NEGATIVE FREQUENCY SHIFTING

FIG. 47. EFFECTS OF FREQUENCY SHIFTING ON CORRELATION FUNCTION

The equation for calculating the turbulence intensity with frequency shifting is also slightly different than Eq (27) and may be developed in the following way. The turbulence intensity is defined by Eq (29)

$$\eta = \frac{\left(\frac{\sum_{i=1}^{n} (u_i - u)^2}{n}\right)^{\frac{1}{2}}}{u} \tag{29}$$

where $u_i$ is the instantaneous absolute velocity, u is the average absolute velocity, and n is the number of velocity samples taken. Eq (30) may be inferred from Eq (28)

$$u_i = u_i^* + \Delta F(d_f) \tag{30}$$

where $u_i^*$ is the instantaneous velocity of the particle with respect to the fringes. Substituting Eqs (28) and (30) into Eq (29) yields

$$\eta = \frac{\left(\frac{\sum_{i=1}^{n} [u_i^* + \Delta F\, d_f - (u^* + \Delta F\, d_f)]^2}{n}\right)^{\frac{1}{2}}}{u}$$

$$= \frac{\left(\frac{\sum_{i=1}^{n} (u_i^* - u^*)^2}{n}\right)^{\frac{1}{2}}}{u} \tag{31}$$

The turbulence intensity of the particles with respect to the fringes ($\eta^*$) may be defined by Eq (32).

$$\eta^* = \frac{\left(\frac{\sum_{i=1}^{n} (u_i^* - u^*)^2}{n}\right)^{\frac{1}{2}}}{u^*} \qquad (32)$$

Eq (33) results from the combination of Eqs (31) and (32).

$$\eta u = \eta^* u^* \qquad (33)$$

This equation may be rewritten as such

$$\eta = \eta^* \frac{u^*}{u} \qquad (34)$$

Eq (34) is the equation needed to calculate the absolute turbulence intensity of the flow when frequency shifting is used. Note: Eq (25) is used to calculate $u^*$ and Eq (27) is used for $\eta^*$. Without frequency shifting, u equals $u^*$ and hence $\eta$ equals $\eta^*$.

# Appendix D:

# Laser Doppler Anemometer Data

DATE: SEPTEMBER 20,1983 PAGE NO. 1

AXIAL POSITION FROM IGV TRAILING EDGE: 34.3mm

| RADIAL POSITION (mm) | SAMPLE TIME (nsec) | FREQUENCY SHIFT (KHz) | Pk2 | G1 | G2 | G3 | R | TURBULENCE INTENSITY (%) | AVERAGE VELOCITY (m/sec) |
|---|---|---|---|---|---|---|---|---|---|
| -13.0 | 50 | -200.0 | 31 | 129748 | 165486 | 148277 | 2.07671 | 32.5 | 4.07 |
| -12.7 | 50 | -200.0 | 31 | 215147 | 273453 | 242284 | 1.87064 | 29.3 | 4.07 |
| -12.2 | 50 | -200.0 | 29 | 237287 | 301551 | 266624 | 1.83995 | 28.0 | 4.50 |
| -11.7 | 50 | -200.0 | 28 | 415101 | 501179 | 449588 | 1.66848 | 24.7 | 4.75 |
| -11.2 | 50 | +0.0 | 33 | 263109 | 332643 | 294728 | 1.83395 | 20.6 | 5.27 |
| -10.7 | 50 | +0.0 | 32 | 253346 | 332249 | 282937 | 1.60005 | 17.5 | 5.46 |
| -10.2 | 50 | +0.0 | 30 | 256471 | 325068 | 273635 | 1.47734 | 15.7 | 5.86 |
| -9.7 | 50 | +0.0 | 31 | 276040 | 349816 | 296968 | 1.39599 | 14.3 | 5.65 |
| -9.1 | 50 | +200.0 | 39 | 231950 | 295092 | 253006 | 1.50033 | 11.8 | 5.93 |
| -8.6 | 50 | +200.0 | 38 | 253846 | 330069 | 276543 | 1.42404 | 11.0 | 6.10 |
| -8.1 | 50 | +200.0 | 38 | 211493 | 280330 | 230279 | 1.37532 | 10.3 | 6.10 |
| -7.6 | 50 | +200.0 | 37 | 211786 | 282973 | 228568 | 1.30845 | 9.4 | 6.23 |
| -7.1 | 50 | +200.0 | 37 | 198681 | 269164 | 213218 | 1.25985 | 8.7 | 6.23 |
| -6.6 | 50 | +200.0 | 37 | 192882 | 264212 | 206840 | 1.24330 | 8.4 | 6.23 |
| -6.1 | 50 | +200.0 | 37 | 238695 | 323764 | 254422 | 1.22680 | 8.1 | 6.23 |
| -5.6 | 50 | +200.0 | 36 | 232886 | 318001 | 247312 | 1.20407 | 7 8 | 6.38 |
| -5.1 | 50 | +200.0 | 37 | 196597 | 271457 | 208933 | 1.19730 | 7.6 | 6.23 |
| -4.6 | 50 | +200.0 | 36 | 198183 | 272798 | 209791 | 1.18424 | 7.4 | 6.38 |
| -4.1 | 50 | +200.0 | 35 | 223589 | 306047 | 236222 | 1.18092 | 7.4 | 6.53 |
| -3.6 | 50 | +200.0 | 35 | 353269 | 430965 | 366596 | 1.20704 | 7.9 | 6.53 |
| -3.0 | 50 | +200.0 | 35 | 372788 | 454804 | 386105 | 1.19386 | 7.7 | 6.53 |
| -2.5 | 50 | +200.0 | 36 | 337833 | 420565 | 351591 | 1.19947 | 7.7 | 6.38 |
| -2.0 | 50 | +200.0 | 35 | 373119 | 464382 | 387463 | 1.18655 | 7.5 | 6.53 |
| -1.5 | 50 | +200.0 | 36 | 328171 | 418930 | 341067 | 1.16562 | 7.0 | 6.38 |
| -1.0 | 50 | +200.0 | 36 | 299649 | 379733 | 312274 | 1.18715 | 7.5 | 6.38 |
| -.5 | 50 | +200.0 | 35 | 262057 | 337654 | 274958 | 1.20578 | 7.9 | 6 53 |
| 0.0 | 50 | +200.0 | 36 | 243351 | 312691 | 254487 | 1.19132 | 7.5 | 6.38 |

DATE: SEPTEMBER 20,1983 PAGE NO. 2

AXIAL POSITION FROM IGV TRAILING EDGE: 34.3mm

| RADIAL POSITION (mm) | SAMPLE TIME (nsec) | FREQUENCY SHIFT (KHz) | Pk2 | G1 | G2 | G3 | R | TURBULENCE INTENSITY (%) | AVERAGE VELOCITY (m/sec) |
|---|---|---|---|---|---|---|---|---|---|
| .5 | 50 | +200.0 | 36 | 244020 | 316567 | 255535 | 1.18868 | 7.5 | 6.38 |
| 1.0 | 50 | +200.0 | 36 | 238937 | 308357 | 250909 | 1.20841 | 7.9 | 6.38 |
| 1.5 | 50 | +200.0 | 36 | 69728 | 97496 | 74884 | 1.22802 | 8.2 | 6.38 |
| 2.0 | 50 | +200.0 | 36 | 45279 | 77250 | 50500 | 1.19520 | 7.6 | 6.38 |
| 2.5 | 50 | +200.0 | 36 | 44717 | 74615 | 49616 | 1.19596 | 7.6 | 6.38 |
| 3.0 | 50 | +200.0 | 37 | 39903 | 66639 | 44876 | 1.22854 | 8.2 | 6.23 |
| 3.6 | 50 | +200.0 | 36 | 300195 | 393392 | 317276 | 1.22441 | 8.1 | 6.38 |
| 4.1 | 50 | +200.0 | 37 | 252527 | 328254 | 268559 | 1.26855 | 8.8 | 6.23 |
| 4.6 | 50 | +200.0 | 38 | 255219 | 337829 | 272784 | 1.27004 | 8.8 | 6.10 |
| 5.1 | 50 | +200.0 | 38 | 219622 | 286060 | 234830 | 1.29686 | 9.2 | 6.10 |
| 5.6 | 50 | +200.0 | 39 | 219708 | 286222 | 237774 | 1.37288 | 10.2 | 5.98 |
| 6.1 | 50 | +200.0 | 39 | 231086 | 294450 | 250492 | 1.44149 | 11.1 | 5.98 |
| 6.6 | 50 | +200.0 | 39 | 261047 | 329808 | 283969 | 1.50005 | 11.8 | 5.98 |
| 7.1 | 50 | +200.0 | 40 | 188851 | 235587 | 206271 | 1.59423 | 12.7 | 5.86 |
| 7.6 | 50 | +200.0 | 42 | 213723 | 258264 | 233811 | 1.82149 | 14.7 | 5.54 |
| 8.1 | 50 | +200.0 | 44 | 81557 | 104325 | 92862 | 1.98624 | 15.9 | 5.44 |
| 8.6 | 50 | +200.0 | 46 | 92900 | 114492 | 105638 | 2.43851 | 18.9 | 5.26 |
| 9.1 | 50 | +0.0 | 35 | 88708 | 115607 | 103592 | 2.23871 | 25.1 | 4.94 |
| 9.7 | 50 | +0.0 | 37 | 88364 | 109339 | 102074 | 2.88708 | 31.0 | 4.65 |
| 10.2 | 50 | -200.0 | 31 | 107921 | 149297 | 133469 | 2.61408 | 39.8 | 4.07 |
| 10.7 | 50 | -500.0 | 25 | 91543 | 130949 | 106232 | 1.59433 | 38.8 | 3.24 |
| 11.2 | 50 | -500.0 | 26 | 94252 | 137392 | 108809 | 1.50931 | 38.1 | 2.92 |
| 11.7 | 50 | -500.0 | 27 | 106415 | 152904 | 120718 | 1.44438 | 37.8 | 2.64 |
| 12.2 | 50 | -500.0 | 27 | 96924 | 139129 | 109385 | 1.41894 | 36.7 | 2.64 |
| 12.7 | 50 | -500.0 | 28 | 153799 | 193755 | 167865 | 1.54326 | 44.5 | 2.37 |
| 13.2 | 50 | -500.0 | 29 | 208509 | 247161 | 226422 | 1.86375 | 60.0 | 2.13 |

DATE: SEPTEMBER 17,1983 PAGE NO. 1

AXIAL POSITION FROM IGV TRAILING EDGE: 48.8mm

| RADIAL POSITION (mm) | SAMPLE TIME (nsec) | FREQUENCY SHIFT (KHz) | Pk2 | G1 | G2 | G3 | R | TURBULENCE INTENSITY (%) | AVERAGE VELOCITY (m/sec) |
|---|---|---|---|---|---|---|---|---|---|
| -13.5 | 50 | -200.0 | 34 | 294087 | 343771 | 321236 | 2.20471 | 35.9 | 3.52 |
| -13.2 | 50 | -200.0 | 32 | 158763 | 206261 | 179851 | 1.79845 | 28.5 | 3.87 |
| -12.7 | 50 | -200.0 | 30 | 120733 | 165356 | 138338 | 1.65161 | 25.0 | 4.28 |
| -12.2 | 50 | -200.0 | 29 | 138275 | 179444 | 153416 | 1.58174 | 23.3 | 4.50 |
| -11.7 | 50 | -200.0 | 28 | 133691 | 179009 | 149863 | 1.55489 | 22.5 | 4.75 |
| -11.2 | 50 | +0.0 | 35 | 156882 | 212586 | 182285 | 1.83832 | 20.7 | 4.94 |
| -10.7 | 50 | +0.0 | 32 | 190188 | 250260 | 213937 | 1.65384 | 18.3 | 5.46 |
| -10.2 | 50 | +0.0 | 32 | 160884 | 215748 | 180599 | 1.56091 | 17.0 | 5.46 |
| -9.7 | 50 | +0.0 | 31 | 143413 | 199317 | 161069 | 1.46164 | 15.4 | 5.65 |
| -9.1 | 50 | +200.0 | 40 | 132503 | 181906 | 150447 | 1.57040 | 12.5 | 5.56 |
| -8.6 | 50 | +200.0 | 40 | 131580 | 183926 | 147945 | 1.45482 | 11.2 | 5.86 |
| -8.1 | 50 | +200.0 | 38 | 143331 | 202861 | 160219 | 1.39603 | 10.6 | 6.10 |
| -7.6 | 50 | +200.0 | 38 | 174302 | 247147 | 191605 | 1.31152 | 9.4 | 6.10 |
| -7.1 | 50 | +200.0 | 37 | 141384 | 203955 | 155837 | 1.30038 | 9.3 | 6.23 |
| -6.6 | 50 | +200.0 | 37 | 137984 | 200250 | 150894 | 1.26155 | 8.7 | 6.23 |
| -6.1 | 50 | +200.0 | 37 | 134638 | 195466 | 146634 | 1.24565 | 8.5 | 6.23 |
| -5.6 | 50 | +200.0 | 36 | 141454 | 204315 | 153217 | 1.23019 | 8.2 | 6.38 |
| -5.1 | 50 | +200.0 | 36 | 139642 | 197717 | 149235 | 1.19787 | 7.7 | 6.33 |
| -4.6 | 50 | +200.0 | 36 | 118550 | 171912 | 127431 | 1.19964 | 7.7 | 6.38 |
| -4.1 | 50 | +200.0 | 37 | 132134 | 184350 | 140974 | 1.20380 | 7.7 | 6.23 |
| -3.6 | 50 | +200.0 | 36 | 125779 | 182674 | 134696 | 1.18591 | 7.4 | 6.33 |
| -3.0 | 50 | +200.0 | 35 | 124999 | 179480 | 133800 | 1.19268 | 7.6 | 6.53 |
| -2.5 | 50 | +200.0 | 36 | 130904 | 186054 | 139621 | 1.18772 | 7.5 | 6.33 |
| -2.0 | 50 | +200.0 | 35 | 107138 | 154263 | 114954 | 1.19384 | 7.7 | 6.53 |
| -1.5 | 50 | +200.0 | 35 | 124182 | 174995 | 132504 | 1.19536 | 7.7 | 6.53 |
| -1.0 | 50 | +200.0 | 35 | 123838 | 173284 | 131010 | 1.16966 | 7.2 | 6.53 |
| -.5 | 50 | +200.0 | 36 | 115295 | 161952 | 122393 | 1.17960 | 7.3 | 6.38 |
| 0.0 | 50 | +200.0 | 37 | 108655 | 154214 | 115385 | 1.17331 | 7.1 | 6.23 |

DATE: SEPTEMBER 17,1983 PAGE NO. 2
AXIAL POSITION FROM IGV TRAILING EDGE: 48.8mm

| RADIAL POSITION (mm) | SAMPLE TIME (nsec) | FREQUENCY SHIFT (KHz) | Pk2 | G1 | G2 | G3 | R | TURBULENCE INTENSITY (%) | AVERAGE VELOCITY (m/sec) |
|---|---|---|---|---|---|---|---|---|---|
| .5 | 50 | +200.0 | 37 | 115538 | 165107 | 123207 | 1.18303 | 7.3 | 6.23 |
| 1.0 | 50 | +200.0 | 36 | 123634 | 171891 | 130591 | 1.16845 | 7.1 | 6.38 |
| 1.5 | 50 | +200.0 | 37 | 159593 | 214010 | 168741 | 1.20208 | 7.7 | 6.23 |
| 2.0 | 50 | +200.0 | 37 | 133929 | 189796 | 142453 | 1.18005 | 7.3 | 6.23 |
| 2.5 | 50 | +200.0 | 36 | 121426 | 176005 | 129713 | 1.17903 | 7.3 | 6.38 |
| 3.0 | 50 | +200.0 | 36 | 129454 | 187860 | 138898 | 1.19289 | 7.6 | 6.38 |
| 3.6 | 50 | +200.0 | 36 | 109613 | 159951 | 118167 | 1.20472 | 7.8 | 6.38 |
| 4.1 | 50 | +200.0 | 37 | 132046 | 190890 | 142981 | 1.22824 | 8.2 | 6.23 |
| 4.6 | 50 | +200.0 | 36 | 117356 | 169812 | 127552 | 1.24126 | 8.4 | 6.38 |
| 5.1 | 50 | +200.0 | 38 | 113792 | 163249 | 124500 | 1.27636 | 8.9 | 6.10 |
| 5.6 | 50 | +200.0 | 38 | 114362 | 161316 | 126052 | 1.33147 | 9.7 | 6.10 |
| 6.1 | 50 | +200.0 | 39 | 165616 | 205458 | 177609 | 1.43063 | 11.0 | 5.98 |
| 6.6 | 50 | +200.0 | 38 | 37763 | 55603 | 44231 | 1.56873 | 12.7 | 6.10 |
| 7.1 | 50 | +200.0 | 39 | 174138 | 201263 | 188089 | 2.05896 | 17.1 | 5.98 |
| 7.6 | 50 | +200.0 | 39 | 41190 | 56986 | 48397 | 1.83909 | 15.2 | 5.98 |
| 8.1 | 50 | +200.0 | 42 | 236685 | 271007 | 256016 | 2.28948 | 18.4 | 5.84 |
| 8.6 | 50 | +200.0 | 42 | 72908 | 94163 | 85177 | 2.36541 | 19.0 | 5.84 |
| 9.1 | 50 | +0.0 | 34 | 198937 | 250996 | 226537 | 2.12838 | 24.0 | 5.10 |
| 9.7 | 50 | +0.0 | 36 | 287138 | 357833 | 330798 | 2.61495 | 28.7 | 4.79 |
| 10.2 | 50 | -200.0 | 29 | 132135 | 184689 | 154065 | 1.71613 | 25.9 | 4.50 |
| 10.7 | 50 | -200.0 | 30 | 150730 | 212198 | 175931 | 1.69489 | 25.8 | 4.28 |
| 11.2 | 50 | -200.0 | 31 | 63394 | 95230 | 76296 | 1.68143 | 25.9 | 4.07 |
| 11.7 | 50 | -200.0 | 31 | 50439 | 78151 | 60811 | 1.59313 | 24.3 | 4.07 |
| 12.2 | 50 | -200.0 | 33 | 40072 | 64093 | 49655 | 1.66373 | 26.3 | 3.89 |
| 12.7 | 50 | -200.0 | 33 | 47780 | 75879 | 58509 | 1.61769 | 25.4 | 3.89 |
| 13.2 | 50 | -200.0 | 34 | 50303 | 74848 | 61487 | 1.83702 | 30.0 | 3.52 |
| 13.5 | 50 | -200.0 | 38 | 110590 | 138894 | 126876 | 2.35516 | 40.4 | 2.91 |

DATE: SEPTEMBER 20, 1983 PAGE NO. 1
AXIAL POSITION FROM IGV TRAILING EDGE: 110.0mm

| RADIAL POSITION (mm) | SAMPLE TIME (nsec) | FREQUENCY SHIFT (KHz) | Pk2 | G1 | G2 | G3 | R | TURBULENCE INTENSITY (%) | AVERAGE VELOCITY (m/sec) |
|---|---|---|---|---|---|---|---|---|---|
| -13.0 | 50 | -200.0 | 30 | 55026 | 78027 | 62383 | 1.51887 | 22.4 | 4.28 |
| -12.7 | 50 | -200.0 | 29 | 48742 | 71725 | 56193 | 1.47968 | 21.2 | 4.50 |
| -12.2 | 50 | -200.0 | 28 | 45442 | 62027 | 50713 | 1.46588 | 20.6 | 4.75 |
| -11.7 | 50 | -200.0 | 27 | 90641 | 112059 | 97667 | 1.48819 | 20.8 | 5.01 |
| -11.2 | 50 | -200.0 | 27 | 49084 | 73158 | 54941 | 1.32155 | 17.0 | 5.01 |
| -10.7 | 50 | +0.0 | 33 | 49075 | 72937 | 56946 | 1.49222 | 15.9 | 5.27 |
| -10.2 | 50 | +0.0 | 33 | 120324 | 172902 | 135862 | 1.41950 | 14.7 | 5.27 |
| -9.7 | 50 | +0.0 | 32 | 98941 | 151023 | 113589 | 1.39130 | 14.2 | 5.46 |
| -9.1 | 50 | +0.0 | 31 | 161275 | 219151 | 177267 | 1.38182 | 14.0 | 5.55 |
| -8.6 | 50 | +200.0 | 42 | 125993 | 168561 | 143637 | 1.70789 | 13.7 | 5.64 |
| -8.1 | 50 | +200.0 | 41 | 116044 | 159194 | 131913 | 1.58171 | 12.5 | 5.75 |
| -7.6 | 50 | +200.0 | 40 | 112631 | 159897 | 129319 | 1.54576 | 12.2 | 5.86 |
| -7.1 | 50 | +200.0 | 41 | 219119 | 231523 | 238900 | 1.46407 | 11.2 | 5.75 |
| -6.6 | 50 | +200.0 | 39 | 200722 | 266248 | 220461 | 1.43109 | 11.3 | 5.98 |
| -6.1 | 50 | +200.0 | 39 | 185329 | 247633 | 204031 | 1.42892 | 10.9 | 5.98 |
| -5.6 | 50 | +200.0 | 39 | 203964 | 274630 | 222334 | 1.35127 | 9.9 | 5.98 |
| -5.1 | 50 | +200.0 | 38 | 189659 | 259525 | 206752 | 1.32389 | 9.6 | 6.10 |
| -4.6 | 50 | +200.0 | 37 | 188924 | 261559 | 206863 | 1.32796 | 9.7 | 6.23 |
| -4.1 | 50 | +200.0 | 38 | 190269 | 263190 | 207146 | 1.30114 | 9.3 | 6.10 |
| -3.6 | 50 | +200.0 | 38 | 227113 | 315146 | 245860 | 1.27056 | 8.8 | 6.10 |
| -3.0 | 50 | +200.0 | 37 | 188247 | 260878 | 204159 | 1.28055 | 9.0 | 6.23 |
| -2.5 | 50 | +200.0 | 37 | 191431 | 264146 | 206986 | 1.27215 | 8.9 | 6.23 |
| -2.0 | 50 | +200.0 | 37 | 189318 | 267262 | 206165 | 1.27574 | 8.9 | 6.23 |
| -1.5 | 50 | +200.0 | 37 | 181832 | 257908 | 197477 | 1.25388 | 8.7 | 6.23 |
| -1.0 | 50 | +200.0 | 38 | 174879 | 250044 | 190693 | 1.26645 | 8.7 | 6.10 |
| -.5 | 50 | +200.0 | 37 | 173570 | 247225 | 188940 | 1.26370 | 8.7 | 6.23 |
| 0.0 | 50 | +200.0 | 37 | 171656 | 247414 | 188075 | 1.27669 | 9.0 | 6.23 |

DATE: SEPTEMBER 20,1983 PAGE NO. 2

AXIAL POSITION FROM IGV TRAILING EDGE: 110.0mm

| RADIAL POSITION (mm) | SAMPLE TIME (nsec) | FREQUENCY SHIFT (KHz) | Pk2 | G1 | G2 | G3 | R | TURBULENCE INTENSITY (%) | AVERAGE VELOCITY (m/sec) |
|---|---|---|---|---|---|---|---|---|---|
| .5 | 50 | +200.0 | 38 | 170273 | 244047 | 186251 | 1.27645 | 8.9 | 6.10 |
| 1.0 | 50 | +200.0 | 37 | 186109 | 264726 | 203129 | 1.27633 | 8.9 | 6.23 |
| 1.5 | 50 | +200.0 | 38 | 235011 | 310885 | 253016 | 1.31113 | 9.4 | 6.10 |
| 2.0 | 50 | +200.0 | 39 | 178861 | 253695 | 196661 | 1.31210 | 9.4 | 5.98 |
| 2.5 | 50 | +200.0 | 38 | 186430 | 263313 | 205930 | 1.33983 | 9.8 | 6.10 |
| 3.0 | 50 | +200.0 | 40 | 174244 | 246644 | 193591 | 1.36467 | 10.0 | 5.86 |
| 3.6 | 50 | +200.0 | 39 | 169437 | 238577 | 189733 | 1.41555 | 10.8 | 5.98 |
| 4.1 | 50 | +200.0 | 40 | 185436 | 259457 | 208253 | 1.44561 | 11.1 | 5.86 |
| 4.6 | 50 | +200.0 | 41 | 173218 | 242079 | 196126 | 1.49851 | 11.6 | 5.75 |
| 5.1 | 50 | +200.0 | 41 | 179390 | 250186 | 204241 | 1.54086 | 12.1 | 5.75 |
| 5.6 | 50 | +200.0 | 42 | 179616 | 247579 | 205513 | 1.61564 | 12.8 | 5.64 |
| 6.1 | 50 | +200.0 | 42 | 718308 | 793516 | 752605 | 1.83832 | 14.9 | 5.64 |
| 7.1 | 50 | +200.0 | 43 | 168181 | 196567 | 183364 | 2.14997 | 17.3 | 5.54 |
| 7.6 | 50 | +200.0 | 45 | 43617 | 65351 | 53741 | 1.87199 | 14.9 | 5.35 |
| 8.1 | 50 | +0.0 | 33 | 40735 | 69460 | 49373 | 1.43006 | 14.9 | 5.27 |
| 8.6 | 50 | +0.0 | 34 | 83084 | 135695 | 93806 | 1.42620 | 14.8 | 5.10 |
| 9.1 | 50 | +0.0 | 34 | 76669 | 123973 | 91273 | 1.44655 | 15.2 | 5.10 |
| 9.7 | 50 | +0.0 | 34 | 151040 | 217198 | 171944 | 1.46192 | 15.4 | 5.10 |
| 10.2 | 50 | +0.0 | 36 | 116262 | 177865 | 136538 | 1.49060 | 15.9 | 4.79 |
| 10.7 | 50 | +0.0 | 36 | 118002 | 180528 | 139305 | 1.51678 | 16.3 | 4.79 |
| 11.2 | 50 | +0.0 | 38 | 125330 | 187881 | 146538 | 1.51298 | 16.2 | 4.52 |
| 11.7 | 50 | +0.0 | 37 | 132253 | 195969 | 155347 | 1.53809 | 17.4 | 4.35 |
| 12.2 | 50 | -200.0 | 30 | 143511 | 220366 | 165473 | 1.40007 | 19.7 | 4.23 |
| 12.7 | 50 | -200.0 | 31 | 92746 | 141779 | 111043 | 1.59529 | 24.3 | 4.07 |
| 13.2 | 50 | -200.0 | 35 | 157472 | 200360 | 185374 | 2.86178 | 45.3 | 3.36 |

DATE: SEPTEMBER 21,1983 PAGE NO. 1
AXIAL POSITION FROM IGV TRAILING EDGE: 215.4mm

| RADIAL POSITION (mm) | SAMPLE TIME (nsec) | FREQUENCY SHIFT (KHz) | Pk2 | G1 | G2 | G3 | R | TURBULENCE INTENSITY (%) | AVERAGE VELOCITY (m/sec) |
|---|---|---|---|---|---|---|---|---|---|
| -12.7 | 50 | -200.0 | 30 | 718476 | 762962 | 741230 | 2.04708 | 31.7 | 4.26 |
| -12.2 | 50 | -200.0 | 29 | 220309 | 252918 | 231253 | 1.50511 | 21.8 | 4.50 |
| -11.7 | 50 | -200.0 | 28 | 194469 | 228380 | 203530 | 1.36465 | 18.3 | 4.75 |
| -11.2 | 50 | +0.0 | 38 | 268480 | 307560 | 284546 | 1.69812 | 18.9 | 4.52 |
| -10.7 | 50 | +0.0 | 35 | 107658 | 129663 | 115264 | 1.52822 | 16.5 | 4.94 |
| -10.2 | 50 | +0.0 | 36 | 170750 | 204432 | 181616 | 1.47627 | 15.7 | 4.79 |
| -9.7 | 50 | +0.0 | 36 | 173423 | 202506 | 184477 | 1.61315 | 17.7 | 4.79 |
| -9.1 | 50 | +0.0 | 35 | 818010 | 913980 | 848625 | 1.46844 | 15.5 | 4.94 |
| -8.6 | 50 | +0.0 | 35 | 819038 | 916316 | 848147 | 1.42701 | 14.8 | 4.94 |
| -8.1 | 50 | +0.0 | 34 | 1170503 | 1263319 | 1201985 | 1.51327 | 16.2 | 5.10 |
| -7.6 | 50 | +0.0 | 34 | 1201864 | 1300779 | 1232889 | 1.45699 | 15.3 | 5.10 |
| -7.1 | 50 | +0.0 | 33 | 1036022 | 1129870 | 1064776 | 1.44172 | 15.1 | 5.27 |
| -6.6 | 50 | +0.0 | 33 | 769514 | 863705 | 793870 | 1.34877 | 13.4 | 5.27 |
| -6.1 | 50 | +200.0 | 44 | 606165 | 675902 | 631067 | 1.55539 | 12.0 | 5.44 |
| -5.6 | 50 | +200.0 | 44 | 796423 | 897014 | 830304 | 1.50789 | 11.5 | 5.44 |
| -5.1 | 50 | +200.0 | 45 | 762903 | 862942 | 796304 | 1.50123 | 11.3 | 5.35 |
| -4.6 | 50 | +200.0 | 43 | 710311 | 808383 | 739841 | 1.43082 | 10.6 | 5.54 |
| -4.1 | 50 | +200.0 | 43 | 646758 | 737249 | 675110 | 1.45628 | 10.9 | 5.54 |
| -3.6 | 50 | +200.0 | 44 | 859605 | 973902 | 894222 | 1.43446 | 10.6 | 5.44 |
| -3.0 | 50 | +200.0 | 44 | 764314 | 869786 | 795576 | 1.42127 | 10.5 | 5.44 |
| -2.5 | 50 | +200.0 | 43 | 816618 | 927440 | 849924 | 1.42967 | 10.6 | 5.54 |
| -2.0 | 50 | +200.0 | 42 | 803705 | 911383 | 835822 | 1.42505 | 10.6 | 5.54 |
| -1.5 | 50 | +200.0 | 43 | 789746 | 901239 | 822861 | 1.42251 | 10.5 | 5.54 |
| -1.0 | 50 | +200.0 | 43 | 724748 | 826565 | 754346 | 1.40983 | 10.4 | 5.54 |
| -.5 | 50 | +200.0 | 42 | 848258 | 932174 | 884551 | 1.37177 | 10.0 | 5.54 |
| 0.0 | 50 | +200.0 | 44 | 908595 | 1047938 | 949125 | 1.41017 | 10.3 | 5.44 |
| .5 | 50 | +200.0 | 43 | 866117 | 1006716 | 904712 | 1.37836 | 10.0 | 5.54 |
| 1.0 | 50 | +200.0 | 44 | 853094 | 986865 | 891121 | 1.39718 | 10.2 | 5.44 |

DATE: SEPTEMBER 21,1983 PAGE NO. 2

AXIAL POSITION FROM IGV TRAILING EDGE: 215.4mm

| RADIAL POSITION (mm) | SAMPLE TIME (nsec) | FREQUENCY SHIFT (KHz) | Pk2 | G1 | G2 | G3 | R | TURBULENCE INTENSITY (%) | AVERAGE VELOCITY (m/sec) |
|---|---|---|---|---|---|---|---|---|---|
| 1.5 | 50 | +200.0 | 44 | 854754 | 987293 | 893615 | 1.41484 | 10.4 | 5.44 |
| 2.0 | 50 | +200.0 | 44 | 929535 | 1076425 | 973608 | 1.42866 | 10.5 | 5.44 |
| 2.5 | 50 | +200.0 | 44 | 764464 | 887449 | 802375 | 1.44562 | 10.7 | 5.44 |
| 3.0 | 50 | +200.0 | 44 | 855196 | 988724 | 896669 | 1.45053 | 10.8 | 5.44 |
| 3.6 | 50 | +200.0 | 45 | 838651 | 967787 | 881268 | 1.49257 | 11.2 | 5.35 |
| 4.1 | 50 | +200.0 | 46 | 924934 | 1060707 | 968563 | 1.47349 | 10.9 | 5.26 |
| 4.6 | 50 | +200.0 | 45 | 916123 | 1050204 | 963008 | 1.53770 | 11.7 | 5.35 |
| 5.1 | 50 | +200.0 | 47 | 922401 | 1050464 | 969279 | 1.57743 | 12.0 | 5.18 |
| 5.6 | 50 | +200.0 | 46 | 759666 | 872325 | 801867 | 1.59896 | 12.3 | 5.26 |
| 6.1 | 50 | +200.0 | 47 | 752684 | 871258 | 798459 | 1.62877 | 12.5 | 5.18 |
| 6.6 | 50 | +200.0 | 47 | 760889 | 879437 | 807022 | 1.63705 | 12.5 | 5.18 |
| 7.1 | 50 | +200.0 | 47 | 822182 | 951567 | 872712 | 1.64080 | 12.6 | 5.18 |
| 7.6 | 50 | +0.0 | 35 | 746951 | 879520 | 779469 | 1.32503 | 13.0 | 4.94 |
| 8.1 | 50 | +0.0 | 35 | 828524 | 975462 | 867527 | 1.36135 | 13.7 | 4.94 |
| 8.6 | 50 | +0.0 | 36 | 756547 | 892791 | 793781 | 1.37607 | 13.9 | 4.79 |
| 9.1 | 50 | +0.0 | 36 | 738255 | 867969 | 774437 | 1.38685 | 14.1 | 4.79 |
| 9.7 | 50 | +0.0 | 37 | 824351 | 961387 | 862848 | 1.39068 | 14.2 | 4.85 |
| 10.2 | 50 | +0.0 | 37 | 856983 | 1004732 | 902344 | 1.44303 | 15.1 | 4.85 |
| 10.7 | 50 | +0.0 | 38 | 881984 | 1017608 | 924243 | 1.45262 | 15.3 | 4.92 |
| 11.2 | 50 | +0.0 | 38 | 747397 | 872499 | 789775 | 1.51227 | 16.2 | 4.92 |
| 11.7 | 50 | +0.0 | 39 | 695417 | 807527 | 735802 | 1.56304 | 17.0 | 4.99 |
| 12.2 | 50 | +0.0 | 40 | 764416 | 888554 | 811054 | 1.60179 | 17.5 | 4.23 |
| 12.7 | 50 | +0.0 | 40 | 694586 | 808109 | 741000 | 1.69164 | 18.8 | 4.26 |
| 13.2 | 50 | -200.0 | 31 | 681792 | 801545 | 719560 | 1.46066 | 21.4 | 4.07 |
| 13.7 | 50 | -200.0 | 32 | 770057 | 889988 | 816678 | 1.63593 | 25.4 | 3.87 |
| 14.2 | 50 | -200.0 | 34 | 843777 | 940309 | 891569 | 1.98055 | 32.4 | 3.52 |
| 14.7 | 50 | -500.0 | 26 | 359511 | 409768 | 382883 | 1.86933 | 49.6 | 2.92 |

DATE: SEPTEMBER 25,1983 PAGE NO. 1

AXIAL POSITION FROM IGV TRAILING EDGE: 240.0mm

| RADIAL POSITION (mm) | SAMPLE TIME (nsec) | FREQUENCY SHIFT (KHz) | Pk2 | G1 | G2 | G3 | R | TURBULENCE INTENSITY (%) | AVERAGE VELOCITY (m/sec) |
|---|---|---|---|---|---|---|---|---|---|
| -16.8 | 50 | -500.0 | 30 | 733261 | 784044 | 764928 | 2.65662 | 89.3 | 1.90 |
| -15.7 | 50 | -500.0 | 26 | 156083 | 190055 | 167020 | 1.47475 | 36.8 | 2.92 |
| -15.2 | 50 | -200.0 | 35 | 122343 | 153103 | 135939 | 1.79844 | 29.7 | 3.36 |
| -14.7 | 50 | -200.0 | 34 | 261401 | 318026 | 284159 | 1.67198 | 26.9 | 3.52 |
| -14.2 | 50 | -200.0 | 33 | 252430 | 310704 | 273123 | 1.55065 | 24.0 | 3.69 |
| -13.7 | 50 | -200.0 | 33 | 278583 | 346265 | 300788 | 1.48824 | 22.6 | 3.69 |
| -13.2 | 50 | -200.0 | 33 | 282228 | 342899 | 301265 | 1.45727 | 21.9 | 3.69 |
| -12.7 | 50 | -200.0 | 33 | 346753 | 396765 | 363208 | 1.49035 | 22.7 | 3.59 |
| -12.2 | 50 | -200.0 | 31 | 218155 | 266788 | 230792 | 1.35110 | 18.7 | 4.07 |
| -11.7 | 50 | -200.0 | 32 | 159041 | 203426 | 169542 | 1.30992 | 17.9 | 3.87 |
| -11.2 | 50 | -200.0 | 32 | 109911 | 143943 | 116627 | 1.24588 | 16.0 | 3.87 |
| -10.7 | 50 | +0.0 | 42 | 144024 | 184024 | 155891 | 1.42181 | 14.7 | 4.06 |
| -10.2 | 50 | +0.0 | 41 | 409795 | 472980 | 430071 | 1.47255 | 15.6 | 4.16 |
| -9.7 | 50 | +0.0 | 41 | 92191 | 120709 | 99493 | 1.34418 | 13.3 | 4.16 |
| -9.1 | 50 | +0.0 | 40 | 83021 | 109556 | 90303 | 1.37822 | 14.0 | 4.28 |
| -8.6 | 50 | +0.0 | 39 | 124333 | 164207 | 133968 | 1.31865 | 12.9 | 4.39 |
| -8.1 | 50 | +0.0 | 39 | 130938 | 172508 | 140843 | 1.31282 | 12.7 | 4.39 |
| -7.6 | 50 | +0.0 | 38 | 136553 | 179941 | 146671 | 1.30411 | 12.6 | 4.52 |
| -7.1 | 50 | +0.0 | 38 | 203114 | 266271 | 215525 | 1.24459 | 11.3 | 4.52 |
| -6.6 | 50 | +0.0 | 38 | 191839 | 250913 | 203523 | 1.24654 | 11.3 | 4.52 |
| -6.1 | 50 | +0.0 | 38 | 197958 | 259220 | 210610 | 1.26550 | 11.8 | 4.52 |
| -5.6 | 50 | +0.0 | 37 | 172951 | 225334 | 182711 | 1.22897 | 10.9 | 4.65 |
| -5.1 | 50 | +0.0 | 37 | 221644 | 292063 | 234464 | 1.22257 | 10.8 | 4.65 |
| -4.6 | 50 | +0.0 | 37 | 209949 | 279049 | 222533 | 1.22267 | 10.8 | 4.65 |
| -4.1 | 50 | +100.0 | 43 | 193322 | 254049 | 207516 | 1.30504 | 10.5 | 4.75 |

DATE: SEPTEMBER 25,1983 PAGE NO. 2
AXIAL POSITION FROM IGV TRAILING EDGE: 240.0mm

| RADIAL POSITION (mm) | SAMPLE TIME (nsec) | FREQUENCY SHIFT (KHz) | Pk2 | G1 | G2 | G3 | R | TURBULENCE INTENSITY (%) | AVERAGE VELOCITY (m/sec) |
|---|---|---|---|---|---|---|---|---|---|
| -3.5 | 50 | +100.0 | 42 | 193675 | 255042 | 207830 | 1.29982 | 10.4 | 4.85 |
| -3.0 | 50 | +100.0 | 44 | 262383 | 345819 | 280749 | 1.28225 | 10.1 | 4.65 |
| -2.5 | 50 | +100.0 | 44 | 218654 | 289099 | 233648 | 1.27039 | 9.8 | 4.55 |
| -2.0 | 50 | +100.0 | 44 | 239787 | 310095 | 255435 | 1.28628 | 10.1 | 4.65 |
| -1.5 | 50 | +100.0 | 44 | 217687 | 281089 | 231949 | 1.29023 | 10.2 | 4.65 |
| -1.0 | 50 | +100.0 | 43 | 290723 | 378764 | 310423 | 1.28827 | 10.2 | 4.75 |
| -.5 | 50 | +100.0 | 43 | 240672 | 313679 | 256883 | 1.28542 | 10.2 | 4.75 |
| 0.0 | 50 | +100.0 | 43 | 209914 | 274886 | 224828 | 1.29795 | 10.4 | 4.75 |
| .5 | 50 | +100.0 | 44 | 193228 | 254558 | 207263 | 1.29677 | 10.3 | 4.65 |
| 1.0 | 50 | +100.0 | 43 | 182604 | 231974 | 195064 | 1.33756 | 11.0 | 4.75 |
| 1.5 | 50 | +100.0 | 44 | 269440 | 339952 | 287153 | 1.33547 | 10.9 | 4.65 |
| 2.0 | 50 | +100.0 | 44 | 286062 | 363335 | 305382 | 1.33338 | 10.9 | 4.65 |
| 2.5 | 50 | +100.0 | 45 | 286679 | 362246 | 306093 | 1.34585 | 11.1 | 4.56 |
| 3.0 | 50 | +100.0 | 45 | 255268 | 323709 | 273290 | 1.35746 | 11.2 | 4.56 |
| 3.6 | 50 | +100.0 | 44 | 271663 | 345239 | 291543 | 1.37024 | 11.5 | 4.65 |
| 4.1 | 50 | +100.0 | 46 | 233855 | 297829 | 252075 | 1.39822 | 11.8 | 4.47 |
| 4.6 | 50 | +100.0 | 46 | 388815 | 495639 | 420186 | 1.41576 | 12.1 | 4.47 |
| 5.1 | 50 | +100.0 | 45 | 449804 | 564609 | 484958 | 1.44135 | 12.5 | 4.56 |
| 5.6 | 50 | +100.0 | 47 | 348614 | 440988 | 375514 | 1.41086 | 11.9 | 4.39 |
| 6.1 | 50 | +100.0 | 46 | 415635 | 523393 | 448735 | 1.44335 | 12.4 | 4.47 |
| 6.6 | 50 | +100.0 | 47 | 388658 | 491246 | 422534 | 1.49302 | 13.1 | 4.39 |
| 7.1 | 50 | +0.0 | 40 | 385931 | 494483 | 413521 | 1.34078 | 13.3 | 4.23 |
| 7.6 | 50 | +0.0 | 40 | 343279 | 437766 | 369120 | 1.37644 | 13.9 | 4.23 |
| 8.1 | 50 | +0.0 | 42 | 326406 | 417598 | 352045 | 1.39112 | 14.2 | 4.06 |
| 8.6 | 50 | +0.0 | 41 | 315528 | 404731 | 341790 | 1.41724 | 14.7 | 4.16 |

DATE: SEPTEMBER 25,1983



AXIAL POSITION FROM IGV TRAILING EDGE: 240.0mm

| RADIAL POSITION (mm) | SAMPLE TIME (nsec) | FREQUENCY SHIFT (KHz) | Pk2 | G1 | G2 | G3 | R | TURBULENCE INTENSITY (%) | AVERAGE VELOCITY (m/sec) |
|---|---|---|---|---|---|---|---|---|---|
| 9.1 | 50 | +0.0 | 42 | 309989 | 393014 | 335908 | 1.45386 | 15.3 | 4.06 |
| 9.7 | 50 | +0.0 | 41 | 347747 | 443183 | 378188 | 1.46837 | 15.5 | 4.16 |
| 10.2 | 50 | +0.0 | 42 | 311740 | 397121 | 340436 | 1.50623 | 16.1 | 4.06 |
| 10.7 | 50 | +0.0 | 44 | 368796 | 469292 | 403321 | 1.52334 | 16.4 | 3.95 |
| 11.2 | 50 | +0.0 | 45 | 435865 | 548937 | 477182 | 1.57581 | 17.2 | 3.77 |
| 11.7 | 50 | -100.0 | 38 | 366421 | 470039 | 397594 | 1.43030 | 18.1 | 3.73 |
| 12.2 | 50 | -100.0 | 39 | 366212 | 466203 | 400134 | 1.51342 | 19.8 | 3.60 |
| 12.7 | 50 | -100.0 | 40 | 403284 | 505902 | 442197 | 1.61083 | 21.7 | 3.48 |
| 13.2 | 50 | -100.0 | 41 | 393808 | 487673 | 431388 | 1.68262 | 23.1 | 3.37 |
| 13.7 | 50 | -100.0 | 41 | 330030 | 407576 | 365771 | 1.85492 | 25.8 | 3.37 |
| 14.2 | 50 | -200.0 | 37 | 362917 | 448023 | 400501 | 1.79087 | 30.5 | 3.07 |
| 14.7 | 50 | -200.0 | 38 | 231208 | 290487 | 260113 | 1.95166 | 33.9 | 2.94 |
| 15.2 | 50 | -200.0 | 40 | 297443 | 365980 | 335544 | 2.25184 | 40.1 | 2.69 |
| 15.7 | 50 | -500.0 | 28 | 273648 | 351738 | 299013 | 1.48109 | 42.0 | 2.37 |
| 16.3 | 50 | -500.0 | 29 | 292503 | 371450 | 317866 | 1.47334 | 44.0 | 2.15 |
| 16.8 | 50 | -500.0 | 30 | 142840 | 188385 | 157427 | 1.47119 | 47.9 | 1.90 |
| 17.3 | 50 | -500.0 | 31 | 141364 | 184442 | 154678 | 1.44731 | 50.6 | 1.76 |
| 17.8 | 50 | -500.0 | 33 | 225400 | 288468 | 246159 | 1.49065 | 63.5 | 1.32 |
| 18.0 | 50 | -500.0 | 34 | 277883 | 338761 | 301325 | 1.62616 | 79.6 | 1.15 |

DATE: SEPTEMBER 16,1983 PAGE NO. 1

AXIAL POSITION FROM IGV TRAILING EDGE: 262.4mm

| RADIAL POSITION (mm) | SAMPLE TIME (nsec) | FREQUENCY SHIFT (KHz) | Pk2 | G1 | G2 | G3 | R | TURBULENCE INTENSITY (%) | AVERAGE VELOCITY (m/sec) |
|---|---|---|---|---|---|---|---|---|---|
| -18.8 | 50 | -500.0 | 28 | 1333559 | 1386426 | 1359988 | 1.99963 | 60.2 | 2.37 |
| -18.3 | 50 | -500.0 | 28 | 592181 | 638503 | 610874 | 1.67656 | 49.6 | 2.37 |
| -17.8 | 50 | -500.0 | 27 | 176018 | 219994 | 187408 | 1.34955 | 33.6 | 2.64 |
| -17.3 | 50 | -500.0 | 26 | 85611 | 127462 | 94143 | 1.25606 | 27.2 | 2.92 |
| -16.8 | 50 | -200.0 | 35 | 89727 | 132050 | 106745 | 1.67253 | 27.3 | 3.36 |
| -16.3 | 50 | -200.0 | 34 | 746554 | 827380 | 781406 | 1.75807 | 28.5 | 3.52 |
| -15.7 | 50 | -200.0 | 34 | 544087 | 624781 | 575173 | 1.62662 | 26.0 | 3.52 |
| -15.2 | 50 | -200.0 | 34 | 469352 | 533967 | 493698 | 1.60457 | 25.5 | 3.52 |
| -14.7 | 50 | -200.0 | 32 | 274112 | 341040 | 295155 | 1.45863 | 21.6 | 3.67 |
| -14.2 | 50 | -200.0 | 33 | 273736 | 333313 | 290564 | 1.39365 | 20.4 | 3.69 |
| -13.7 | 50 | -200.0 | 32 | 437038 | 496200 | 455683 | 1.46018 | 21.7 | 3.87 |
| -13.2 | 50 | -200.0 | 31 | 316435 | 377710 | 332308 | 1.34959 | 18.7 | 4.07 |
| -12.7 | 50 | +0.0 | 40 | 577690 | 644519 | 605129 | 1.69659 | 18.9 | 4.28 |
| -12.2 | 50 | +0.0 | 41 | 561660 | 623166 | 585370 | 1.62734 | 17.9 | 4.16 |
| -11.7 | 50 | +0.0 | 40 | 496472 | 563100 | 520943 | 1.58050 | 17.3 | 4.28 |
| -11.2 | 50 | +0.0 | 39 | 396438 | 461849 | 417180 | 1.46436 | 15.5 | 4.39 |
| -10.7 | 50 | +0.0 | 39 | 172551 | 228206 | 137530 | 1.36993 | 13.8 | 4.39 |
| -10.2 | 50 | +0.0 | 39 | 162906 | 214370 | 176796 | 1.36965 | 13.8 | 4.39 |
| -9.7 | 50 | +0.0 | 38 | 104851 | 144072 | 114992 | 1.34875 | 13.4 | 4.52 |
| -9.1 | 50 | +0.0 | 38 | 92859 | 129465 | 100997 | 1.28586 | 12.2 | 4.52 |
| -8.6 | 50 | +0.0 | 37 | 106997 | 150107 | 117199 | 1.31004 | 12.7 | 4.65 |
| -8.1 | 50 | +0.0 | 37 | 94768 | 133381 | 103459 | 1.29046 | 12.3 | 4.65 |
| -7.6 | 50 | +0.0 | 37 | 147343 | 198867 | 158661 | 1.28148 | 12.1 | 4.65 |
| -7.1 | 50 | +0.0 | 36 | 109764 | 164750 | 121106 | 1.25988 | 11.6 | 4.79 |
| -6.6 | 50 | +0.0 | 36 | 94067 | 147429 | 103035 | 1.22683 | 10.9 | 4.79 |
| -6.1 | 50 | +100.0 | 42 | 76379 | 116818 | 86468 | 1.31596 | 10.7 | 4.65 |

DATE: SEPTEMBER 16,1983 PAGE NO. 2

AXIAL POSITION FROM IGV TRAILING EDGE: 262.4mm

| RADIAL POSITION (mm) | SAMPLE TIME (nsec) | FREQUENCY SHIFT (KHz) | Pk2 | G1 | G2 | G3 | R | TURBULENCE INTENSITY (%) | AVERAGE VELOCITY (m/sec) |
|---|---|---|---|---|---|---|---|---|---|
| -5.6 | 50 | +100.0 | 42 | 69501 | 107989 | 78399 | 1.30071 | 10.5 | 4.85 |
| -5.1 | 50 | +100.0 | 42 | 68571 | 109385 | 77768 | 1.29090 | 10.3 | 4.85 |
| -4.6 | 50 | +100.0 | 42 | 75044 | 119550 | 84777 | 1.27990 | 10.1 | 4.85 |
| -4.1 | 50 | +100.0 | 41 | 72230 | 115190 | 81232 | 1.26510 | 9.9 | 4.95 |
| -3.6 | 50 | +100.0 | 41 | 69457 | 114105 | 79077 | 1.27464 | 10.0 | 4.95 |
| -3.0 | 50 | +100.0 | 42 | 69136 | 112447 | 78892 | 1.29072 | 10.3 | 4.85 |
| -2.5 | 50 | +100.0 | 41 | 68005 | 111707 | 77500 | 1.27757 | 10.1 | 4.95 |
| -2.0 | 50 | +100.0 | 42 | 116273 | 178197 | 130086 | 1.28712 | 10.2 | 4.85 |
| -1.5 | 50 | +100.0 | 42 | 110776 | 170038 | 123842 | 1.28284 | 10.1 | 4.85 |
| -1.0 | 50 | +100.0 | 42 | 118908 | 181499 | 132724 | 1.28326 | 10.2 | 4.85 |
| -.5 | 50 | +100.0 | 42 | 111939 | 174370 | 125966 | 1.28981 | 10.3 | 4.85 |
| 0.0 | 50 | +100.0 | 43 | 106749 | 166169 | 119786 | 1.28109 | 10.1 | 4.75 |
| .5 | 50 | +100.0 | 43 | 100222 | 154844 | 113742 | 1.32895 | 10.9 | 4.75 |
| 1.0 | 50 | +100.0 | 44 | 96528 | 149187 | 109865 | 1.33917 | 11.0 | 4.65 |
| 1.5 | 50 | +100.0 | 44 | 87882 | 136267 | 100651 | 1.35851 | 11.3 | 4.65 |
| 2.0 | 50 | +100.0 | 43 | 84663 | 130170 | 97082 | 1.37534 | 11.6 | 4.75 |
| 2.5 | 50 | +100.0 | 44 | 112726 | 172481 | 129100 | 1.37744 | 11.6 | 4.65 |
| 3.0 | 50 | +100.0 | 45 | 125270 | 187856 | 143568 | 1.41317 | 12.1 | 4.56 |
| 3.6 | 50 | +100.0 | 45 | 104581 | 157740 | 120881 | 1.44221 | 12.5 | 4.56 |
| 4.1 | 50 | +100.0 | 46 | 94595 | 142149 | 110491 | 1.50214 | 13.2 | 4.47 |
| 4.6 | 50 | +100.0 | 47 | 85396 | 128241 | 99452 | 1.48823 | 13.0 | 4.39 |
| 5.1 | 50 | +100.0 | 47 | 111330 | 166218 | 130460 | 1.53496 | 13.6 | 4.39 |
| 5.6 | 50 | +100.0 | 47 | 102699 | 152669 | 120670 | 1.56162 | 13.9 | 4.39 |
| 6.1 | 50 | +100.0 | 47 | 96412 | 142823 | 113823 | 1.60067 | 14.4 | 4.39 |
| 6.6 | 50 | +0.0 | 41 | 85165 | 134612 | 99132 | 1.39367 | 14.3 | 4.16 |
| 7.1 | 50 | +0.0 | 42 | 104221 | 161941 | 121850 | 1.43972 | 15.1 | 4.06 |

DATE: SEPTEMBER 16,1983 PAGE NO. 3
AXIAL POSITION FROM IGV TRAILING EDGE: 262.4mm

| RADIAL POSITION (mm) | SAMPLE TIME (nsec) | FREQUENCY SHIFT (KHz) | Pk2 | G1 | G2 | G3 | R | TURBULENCE INTENSITY (%) | AVERAGE VELOCITY (m/sec) |
|---|---|---|---|---|---|---|---|---|---|
| 7.6 | 50 | +0.0 | 41 | 85184 | 131808 | 100075 | 1.46924 | 15.5 | 4.16 |
| 7.6 | 50 | +0.0 | 42 | 83495 | 129536 | 97651 | 1.44396 | 15.1 | 4.06 |
| 8.1 | 50 | +0.0 | 41 | 79622 | 124606 | 93302 | 1.43702 | 15.0 | 4.16 |
| 8.6 | 50 | +0.0 | 43 | 79457 | 122268 | 93656 | 1.49630 | 16.0 | 3.96 |
| 9.1 | 50 | -100.0 | 36 | 81819 | 130618 | 95446 | 1.38743 | 16.9 | 4.00 |
| 9.7 | 50 | -100.0 | 37 | 80905 | 125530 | 94070 | 1.41847 | 17.7 | 3.86 |
| 10.2 | 50 | -100.0 | 37 | 79375 | 123970 | 92225 | 1.40475 | 17.4 | 3.86 |
| 10.7 | 50 | -100.0 | 39 | 84554 | 131605 | 100163 | 1.49644 | 19.5 | 3.60 |
| 11.2 | 50 | -100.0 | 39 | 81427 | 123700 | 96913 | 1.57809 | 21.0 | 3.60 |
| 11.7 | 50 | -100.0 | 40 | 77166 | 114448 | 91755 | 1.64289 | 22.3 | 3.48 |
| 12.2 | 50 | -100.0 | 40 | 77515 | 114132 | 93400 | 1.76623 | 24.3 | 3.48 |
| 12.7 | 50 | -100.0 | 41 | 77481 | 111889 | 93179 | 1.83908 | 25.6 | 3.37 |
| 13.2 | 50 | -100.0 | 41 | 84730 | 122230 | 101656 | 1.82270 | 25.3 | 3.37 |
| 13.7 | 50 | -200.0 | 37 | 63100 | 94082 | 76617 | 1.77395 | 30.1 | 3.07 |
| 14.2 | 50 | -200.0 | 38 | 80925 | 117586 | 97083 | 1.78806 | 30.9 | 2.94 |
| 14.7 | 50 | -200.0 | 39 | 86036 | 123696 | 104619 | 1.97417 | 34.8 | 2.81 |
| 15.2 | 50 | -200.0 | 39 | 56949 | 83235 | 69634 | 1.93259 | 34.1 | 2.81 |
| 15.7 | 50 | -200.0 | 42 | 45919 | 66792 | 56978 | 2.12675 | 39.3 | 2.47 |
| 16.3 | 50 | -500.0 | 29 | 49695 | 74471 | 56294 | 1.36308 | 39.1 | 2.13 |
| 16.8 | 50 | -500.0 | 30 | 54944 | 83664 | 63125 | 1.39833 | 44.1 | 1.90 |
| 17.3 | 50 | -500.0 | 30 | 22366 | 33701 | 25560 | 1.39228 | 43.8 | 1.90 |
| 17.8 | 50 | -500.0 | 30 | 12998 | 19188 | 14442 | 1.30424 | 38.7 | 1.90 |
| 18.3 | 50 | -500.0 | 30 | 13390 | 19887 | 15243 | 1.39897 | 44.2 | 1.90 |
| 18.8 | 50 | -500.0 | 31 | 15811 | 23558 | 17922 | 1.37442 | 46.4 | 1.70 |
| 19.3 | 50 | -500.0 | 32 | 5418 | 7880 | 6225 | 1.48782 | 57.6 | 1.50 |
| 19.8 | 50 | -500.0 | 34 | 6833 | 9697 | 7757 | 1.47632 | 69.6 | 1.15 |

## Appendix E:

## Velocity Resolution of Photon-correlating LDA Measurements

The autocorrelation function determined by a digital correlator, such as the Malvern Type K7023, is defined only at discrete values of $\tau$, the correlator time delay. These values of $\tau$ are represented by the correlator channels. Since the velocity measurements are a function of the peak channel number, Pk2, and since Pk2 has discrete values, the velocity will also have discrete values. In comparing a continuous correlation function with its digital representation, it is evident that a peak of the continuous function may occur anywhere within a $\pm\frac{1}{2}$ channel interval of the peak of its digital form. While the value of $\tau$ at which a peak occurs can be estimated from a digital correlation function (i.e. estimating fractional channels), the estimated peak will vary among experimenters so that the $\pm\frac{1}{2}$ channel interval is still a useful means of determining the range of velocities represented by a photon-correlating LDA measurement.

The absolute velocity can be calculated using Eq (35).

$$u = \frac{d_f}{(Pk2-3)t_s} + \Delta F\, d_f \qquad (35)$$

The rate of change in velocity with respect to a change in the peak channel number, Pk2, is given by Eq (36).

$$\frac{du}{d(Pk2)} = \frac{-d_f}{(Pk2-3)^2 t_s} \tag{36}$$

Two more useful forms of Eq (36) are Eqs (37) and (38).

$$\frac{du}{d(Pk2)} = \frac{-(u^*)^2 t_s}{d_f} \tag{37}$$

$$\frac{du}{d(Pk2)} = \frac{-(u - \Delta F d_f)^2 t_s}{d_f} \tag{38}$$

The absolute value of du/d(Pk2) is the velocity resolution of the LDA system in measuring a given flow. Bear in mind that u, $\Delta F$, $t_s$ and $d_f$ cannot assume any combination of values because the correlator is limited by the number of channels used to represent the correlation function. The value of Pk2 is limited to the range of 5 to 99 by the Malvern K7023; however, in practical applications, it should be limited to the range of 10 to 95. Thus, combinations of the variables in Eqs (37) and (38) may be checked for reasonableness by using Eq (35) and the above limitation on Pk2.

The value of du/d(Pk2) is also a measure of the accuracy of the digital representation of the correlation function. Since an actual peak of the function occurs within a ±½ channel interval of the digital representation's peak, the accuracy of the measurement will be ±½|du/d(Pk2)|.

# VITA

Jeffrey M. Dierksen was born on September 13, 1955 in Alameda, California. He graduated from Proviso West High School in Hillside, Illinois in 1973 and continued his education at the United States Air Force Academy in Colorado Springs, Colorado. Upon graduation in 1977, he received a Bachelor of Science degree in aeronautical engineering and a commission as a Second Lieutenant. His first assignment in the Air Force was as a Minuteman ICBM Missile Launch Officer at Francis E. Warren AFB in Cheyenne, Wyoming. He also served there as an Emergency War Order Instructor. He entered the Air Force Institute of Technology, School of Engineering in June of 1982.

Permanent Address: 1700 Pinto Lane
Cheyenne, Wyoming 82007

# REPORT DOCUMENTATION PAGE

| | |
|---|---|
| 1a. REPORT SECURITY CLASSIFICATION: Unclassified | 1b. RESTRICTIVE MARKINGS |
| 2a. SECURITY CLASSIFICATION AUTHORITY | 3. DISTRIBUTION/AVAILABILITY OF REPORT: Approved for public release; distribution unlimited. |
| 2b. DECLASSIFICATION/DOWNGRADING SCHEDULE | |
| 4. PERFORMING ORGANIZATION REPORT NUMBER(S): AFIT/GAE/AA/83D-6 | 5. MONITORING ORGANIZATION REPORT NUMBER(S) |
| 6a. NAME OF PERFORMING ORGANIZATION: School of Engineering, Air Force Institute of Technology; 6b. OFFICE SYMBOL (If applicable): AFIT/EN | 7a. NAME OF MONITORING ORGANIZATION |
| 6c. ADDRESS (City, State and ZIP Code): Wright-Patterson AFB, Ohio 45433 | 7b. ADDRESS (City, State and ZIP Code) |
| 8a. NAME OF FUNDING/SPONSORING ORGANIZATION: Air Force Aero-Propulsion Laboratory; 8b. OFFICE SYMBOL (If applicable): AFWAL/POTC | 9. PROCUREMENT INSTRUMENT IDENTIFICATION NUMBER |
| 8c. ADDRESS (City, State and ZIP Code): Wright-Patterson AFB, Ohio 45433 | 10. SOURCE OF FUNDING NOS. — PROGRAM ELEMENT NO. / PROJECT NO. / TASK NO. / WORK UNIT NO. |
| 11. TITLE (Include Security Classification): See Box 19 | |
| 12. PERSONAL AUTHOR(S): Jeffrey M. Dierksen,Capt,USAF | |
| 13a. TYPE OF REPORT: MS Thesis; 13b. TIME COVERED: FROM _____ TO _____ | 14. DATE OF REPORT (Yr., Mo., Day): 1983 December; 15. PAGE COUNT: 131 |
| 16. SUPPLEMENTARY NOTATION: Approved for public release: IAW AFR 190-17. LYNN E. WOLAVER, Dean for Research and Professional Development, Air Force Institute of Technology (AIC), Wright-Patterson AFB, OH 45433 | |

| 17. COSATI CODES | | |
|---|---|---|
| FIELD | GROUP | SUB. GR. |
| 21 | 1 | |
| | | |

18. SUBJECT TERMS (Continue on reverse if necessary and identify by block number): Diffusers; Lasers; Doppler Systems; Velocimeters

19. ABSTRACT (Continue on reverse if necessary and identify by block number)

TITLE: A STUDY OF ANNULAR DIFFUSER FLOW USING A PHOTON-CORRELATING LASER DOPPLER ANEMOMETER

THESIS CHAIRMAN: Dr. William C. Elrod

| | |
|---|---|
| 20. DISTRIBUTION/AVAILABILITY OF ABSTRACT: UNCLASSIFIED/UNLIMITED ☒ SAME AS RPT. ☐ DTIC USERS ☐ | 21. ABSTRACT SECURITY CLASSIFICATION: Unclassified |
| 22a. NAME OF RESPONSIBLE INDIVIDUAL: Dr. William C. Elrod | 22b. TELEPHONE NUMBER (Include Area Code): 513-255-3517; 22c. OFFICE SYMBOL: AFIT/ENY |

An experimental investigation of air flow in an annular inlet and diffuser was conducted using a photon-correlating Laser Doppler Anemometer. The inlet has an inside wall radius of 22.9 centimeters (9.0 in) and a cross-sectional area of 0.0426 sq meters (0.4583 sq ft). The diffuser walls have a divergence half-angle of seven degrees. Flow rates in the vicinity of 0.25 kg/sec (0.55 lbm/sec) were studied. The Reynolds number in the annular inlet was 18,300. The flow in the annulus was turbulent and the boundary layer growth was approximately 20% less than that predicted using flat plate boundary layer assumptions, The laser anemometer measurements are compared to hot film anemometer measurements. Good comparison was obtained except in the annular inlet. The difference is probably due to the differing boundary layer growth rates between the laser and hot film anemometer tests since they were conducted with different mass flow rates. The photon-correlating Laser Doppler Anemometer is evaluated in this application. The flexibility of a laser anemometer system in measuring three-dimensional, internal flows is determined by two factors: the system's frequency shifting capability and the geometry of its optics. Reflected background light is inherent in measuring internal flows. Without a means of reducing the signal caused by this light, long measurement times are necessary for each data point.

END

FILMED

2-84

DTIC